

# NanoCare

Health related Aspects of Nanomaterials

Final Scientific Report



**NanoCare**  
**Health related Aspects of Nanomaterials**  
**Final Scientific Report**



**DECHEMA e.V.**

**in cooperation with**

**NanoCare Project Consortium  
Germany**

**Editors:**

**T.A.J. Kuhlbusch, IUTA, Duisburg, Germany**

**H.F. Krug, Empa, St. Gallen, Switzerland**

**K. Nau, Forschungszentrum Karlsruhe, Germany**

**Authors:**

NanoCare Project Partners (see page 102)

This book was carefully produced. Nevertheless, the authors do not warrant the information contained therein to be free of errors. Readers are advised to keep in mind that data, illustrations, procedural details or other items may inadvertently be inaccurate.

Published in cooperation with

the NanoCare Project Consortium

funded by Bundesministerium für Bildung und Forschung (BMBF) /

Federal Ministry of Education and Research, Germany

1<sup>st</sup> Edition July 2009

ISBN: 978-3-89746-108-6

© DECHEMA e.V.,  
D-60486 Frankfurt am Main  
Germany, 2009

Registered names, trademarks, etc. used in this book, even when not specifically marked as such, are not to be considered unprotected by law.

## Index

1. Introduction.....	1
1.1 Aims of NanoCare.....	2
1.2 NanoCare Structure .....	4
2. Communication .....	6
2.1 Internal Communication – Database for Laboratory Assay Documentation.....	6
2.2 Integrated external Communication – Focus Groups Interviews, WebSite, Public Dialogue Meetings .....	6
3. Particle Synthesis and Characterisation.....	9
3.1 Identification and Synthesis of Suitable Nanomaterials .....	9
3.2 Standardisation, Particle Characterisation and Nanomaterials.....	11
3.3 Dispersion of the NanoCare Materials in Cell Culture Media – A Challenge.....	16
3.3.1 Development of Protocols for Nanomaterial Dispersion in Physiological Media ....	16
3.3.2 Dispersion and Examination of the NanoCare Nanomaterials.....	17
3.3.3 Stability of Agglomerates .....	19
3.4. Conclusions for the Characterisation of Nanomaterials .....	21
4. Toxicological Studies.....	22
4.1. Particle Cell Exposure Model.....	22
4.2 Particle Mobility .....	25
4.2.1 Transport of Metal Oxide Nanoparticles through Cell Monolayers.....	25
4.2.2 Particles on Cells .....	26
4.3 In vitro Test Systems .....	29
4.3.1 Method Development and Standardisation.....	29
4.3.2 In vitro Testing.....	36
4.4. In vivo Test Systems.....	48
4.4.1 Intratracheal Instillation Study.....	48
4.4.2 Standard Short-Term Inhalation Test for Nanomaterials .....	51
4.4.3 28-Day Inhalation Study.....	62
4.4.4 Conclusion to Chapter 4.4.....	66
4.5. Comparison of in vitro and in vivo Findings.....	68
4.5.1 Objectives .....	68
4.5.2 Data Overview.....	68
4.5.3 Comparative Analysis of Selected Nanomaterials .....	69
4.5.4 Correlation of Data from Vector Model Investigations and Intratracheal Instillation .....	71
4.5.5 Predictive Value of Cell Culture Experiments on Cell Lines.....	72
4.5.6 Conclusions.....	73

5. Exposure to Nanoparticles: Measurement, Modelling and Agglomerate Stability.....	74
5.1 Objectives -----	74
5.2 Measurement Technology -----	74
5.3 Measurement Strategy for Nanoparticles in Workplaces and Validation -----	77
5.4 Modelling of Spatial Variability of Exposure Levels Following Accidental NP Release	79
5.5 Agglomerate Stability and Material Properties-----	82
5.5.1 Release of Nanoparticles during Manual Handling of the Nanostructured Materials (“Stability under Weak Shear Forces”) .....	82
5.5.2 Stability under Strong Shear Forces .....	85
5.5.3 Conclusions.....	88
6. Conclusions.....	89
References .....	93
Glossary .....	98
NanoCare Partners .....	102
Annex A: Nano Material Data Sheets.....	103
Annex B: In vitro Data Summary .....	151

# 1. Introduction

---

T.A.J. Kuhlbusch, H.F. Krug, K. Nau

---

Nanotechnology has developed into a key technology of the 21st century. Exploitation of effects on the nanoscale enables new applications like scratch resistant or self-cleaning coatings. The number of nanotechnological products has received an enormous boost over the recent years, however, its concept dates back to a dinner talk at the annual meeting of the American Physical Society in 1959 by R. Feynman<sup>1</sup>.

Quote: I would like to describe a field, in which little has been done, but in which an enormous amount can be done in principle. This field is not quite the same as the others in that it will not tell us much of fundamental physics (in the sense of "What are the strange particles?") but it is more like solid-state physics in the sense that it might tell us much of great interest about the strange phenomena that occur in complex situations. Furthermore, a point that is most important is that it would have an enormous number of technical applications.

What I want to talk about is the problem of manipulating and controlling things on a small scale.

.....

*Why cannot we write the entire 24 volumes of the Encyclopaedia Britannica on the head of a pin?*

The next steps towards today's nanotechnology in publication are a paper by Taniguchi (1974) introducing the term 'nano-technology', the first book on nanotechnology by Drexler (1987), followed by the first journal called 'Nanotechnology' in 1990.

The perception of possible risks going along with the development of nanotechnology started in the late 1990's with the first safety guidelines published in 1999 (Foresight). The first studies related to exposure towards engineered nanoparticles were by Kuhlbusch et al. (2004) and Brower et al. (2004) while first studies related to the toxicology of nanoscale particles date back to 1992 (e.g. Oberdörster et al., 1992)

Looking at this timeframe it becomes evident that the first ideas related to the project NanoCare in 2003 were in a very early stage of the development of Nanotechnology. 13 partners from university, industry and research institutes subsequently developed a research plan related to the safety of nanotechnology. This project NanoCare finally started in March 2006 and the scientific results of the effort are summarised in this report.

---

<sup>1</sup> February 1960 issue of Caltech's [Engineering and Science](http://www.foresight.org/nano/history.html), based on information on <http://www.foresight.org/nano/history.html>

## 1.1 Aims of NanoCare

NanoCare aims at combining the innovation in material sciences with specific focus on nanostructured materials and the identification of possible exposure and hazard to enable a sustainable development of nanotechnology. Sustainability relates to economy and to the possibility of human or ecological hazard. The latter may significantly influence the economical future of nanotechnology by influencing the public perception and hence acceptance. NanoCare tackled the sustainability of nanotechnology with three major pillars:

- Knowledge generation
- Knowledge management
- Knowledge transfer and communication

The focus of the research (*knowledge generation*) of NanoCare was based on the identification and assessment of possible exposure and hazard of nanostructured materials on human health with regard to possible risks.

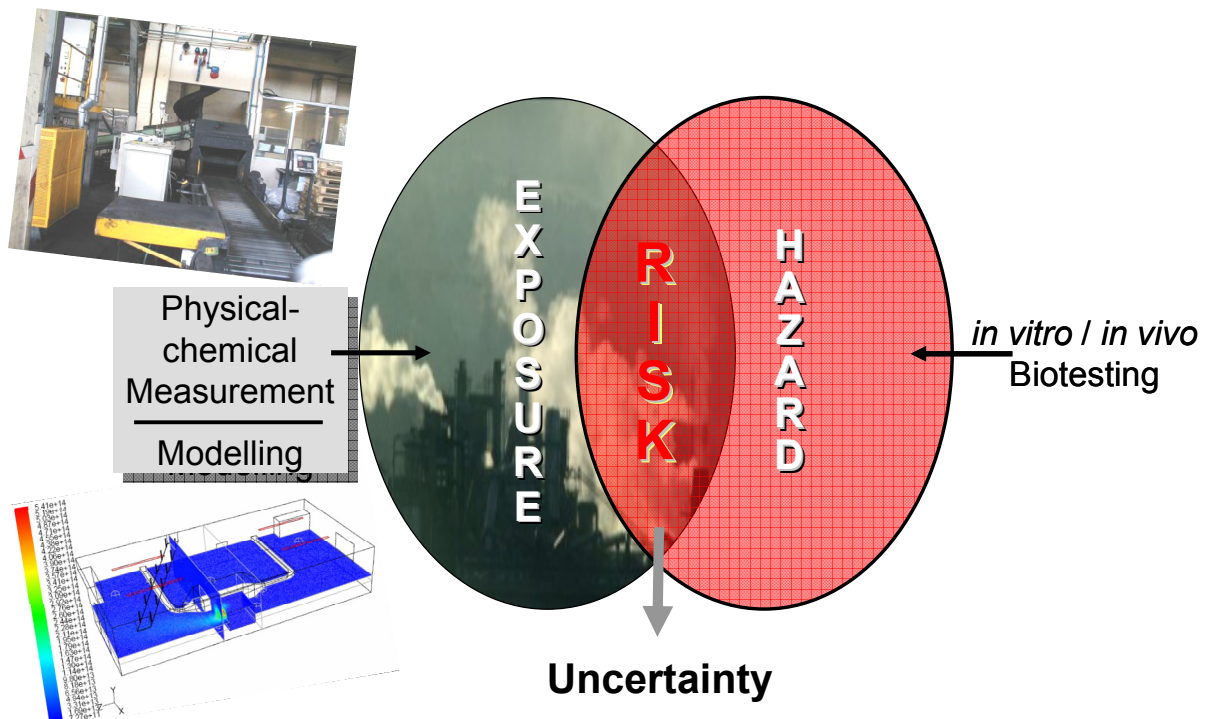


**Figure 1.1** The need to assess Exposure and Hazard to allow the assessment of Risk (adopted from H. Krug)

A risk may only arise if both are present, a) possible hazard of nanostructured materials and b) internal exposure thereto. Hence the two basic research topics of NanoCare were related to exposure (external and internal) and to the toxicology of nanostructured materials.

The specific aims of the *exposure related research* were directed towards the questions:

- How stable are agglomerates of nanostructured materials during normal handling and during stress conditions?
- How do airborne nanostructured materials behave after an accidental release and which processes determine their mobility?
- How can exposure, especially in relation to nanoparticles and nanostructured materials, be assessed?
- Is there a possible exposure to nanostructured materials? And if yes, what is their size distribution?
- How can exposure assessment related information be made comparable and standardised?
- How can the possible toxicology of nanoparticles be directly assessed at a workplace?

The specific aims of the *toxicology related research* were directed towards the questions:

- How does the uptake of nanomaterials occur by inhalation and where do they remain?
- How do nanomaterials behave in biological fluids? Is there a likeliness to deagglomerate?
- How can the toxicological testing be standardised?
- Is there a no-effect-level or lower-effect level detectable in in-vivo studies for different nanomaterials?
- Can a toxic effect be detected in in-vitro studies at a concentration likely for workplace exposure or slightly higher?
- Is it possible to link the results of in-vitro studies to those obtained from in-vivo studies?

An overarching aim of NanoCare was to test whether specific material properties and exposure characteristics may possibly be linked to toxicological effects. Therefore eleven different materials in several variations were produced in the framework of NanoCare. All NanoCare materials were extensively characterised according to standardised protocols.

The second pillar "*knowledge management*" was based on literature studies as well as the research work conducted within NanoCare. These data were all combined in an internal and partially public database which allowed all NanoCare participants to interact and combine their information. This data tool in itself leads to the creation of new knowledge by facilitating the exchange of information and discussions.

The last pillar related to “*knowledge transfer and communication*” was unique to the ‘nano’ projects of the BMBF in so far that this pillar was responsible to facilitate direct exchange of information between scientists and the public via specific workshops, dialogues and an internet based information system ([www.nanopartikel.info](http://www.nanopartikel.info)).

## 1.2 NanoCare Structure

A specific structure was needed for NanoCare to combine the three pillars (see Figure 1.2). This figure depicts that the basis of the knowledge management and the communication is the knowledge from the basis, either from the literature or created within NanoCare.

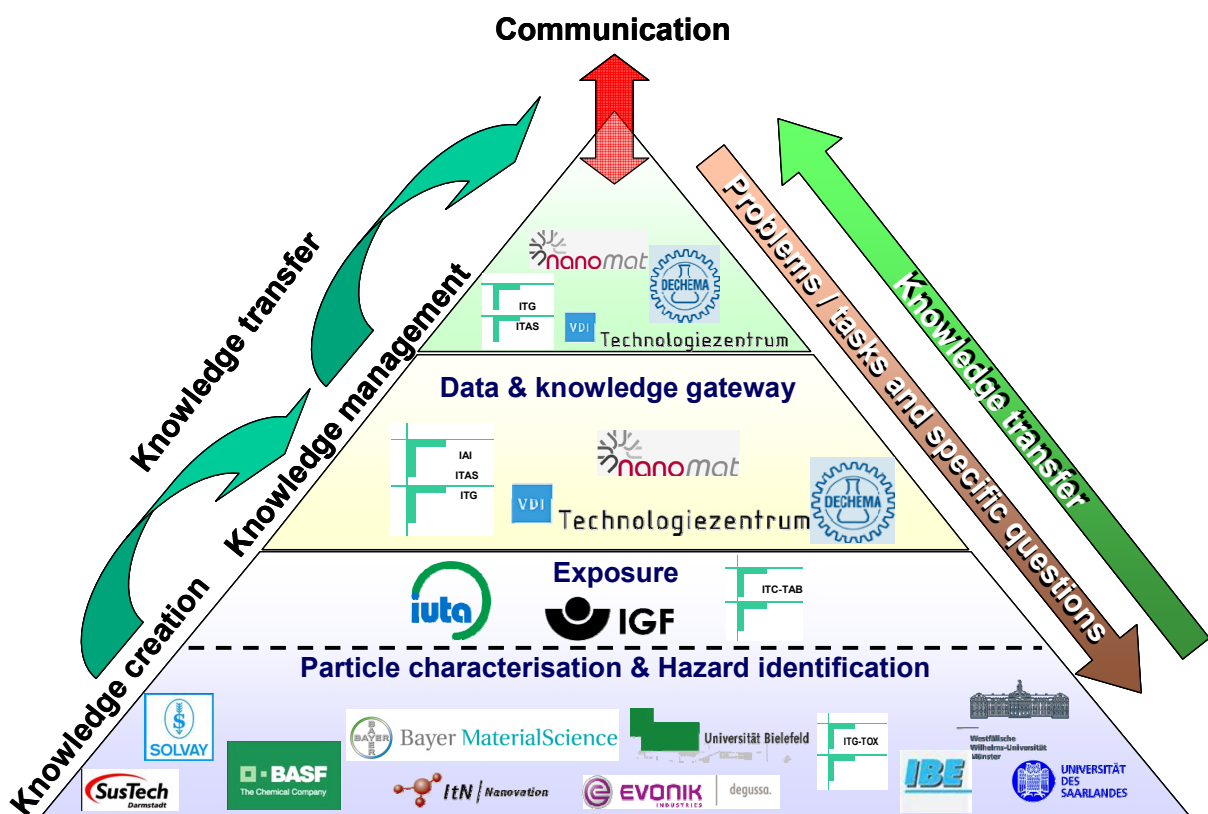
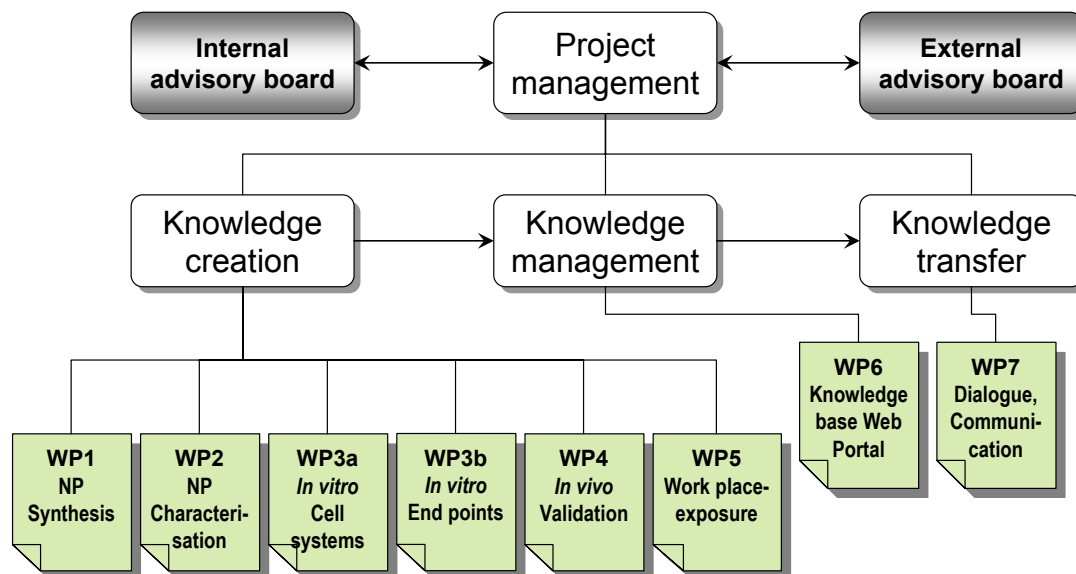


Figure 1.2 General structure of NanoCare

Figure 1.2 also shows the involvement of the various partners in the three pillars. Still, it is important to note that the participants in the discussions and the presentations given were all involved in research related to nanomaterial production, characterisation, hazard identification and exposure assessment.



**Figure 1.3** Specific structure and work packages of NanoCare

Figure 1.3 depicts the specific structure of NanoCare. Five of the seven work packages are related to the creation of knowledge while one work package each is responsible for the knowledge management and the knowledge transfer and communication.

The basis to derive a common information base for the two later pillars “knowledge management” and “knowledge transfer and communication” was achieved by focussing the hazard and exposure related research on a common set of nanostructured materials specifically produced and extensively characterised as the powder or in dispersion (WP1 and WP2). These materials were then used in the various in-vitro and in-vivo toxicological studies as well as in the exposure related research. The combined information on basic nanomaterial characteristics, their mobility and behaviour in air and liquids, the possible exposure and their toxicity build a unique data set which is presented and explored in detail in this scientific report.

In this report, Chapter 3 focuses on the production and characterisation of nanomaterials in NanoCare with the next chapter summarising the findings related to in-vivo and in-vitro toxicological studies. A separate section focuses here on the comparability of these two study types since in-vivo studies should be kept to a minimum in the future. Chapter 5 gives an overview of the findings related to exposure relevant characterization methods and nanomaterial exposure. The synthesis and conclusions of NanoCare are then presented in chapter 6.

## 2. Communication

---

S. Dierig, T. Fleischer, A. Förster, O. Kusche, N. Malanowski,  
K. Nau, C. Steinbach

---

Communication was one major pillar of NanoCare which covered both internal but also especially external communication.

### 2.1 Internal Communication – Database for Laboratory Assay Documentation

Research work on the physicochemical properties to characterise a given nanomaterial, combined to studies on the behaviour in biological test systems represents the intellectual aim of the NanoCare initiative. During the course of the project, various activities such as physical characterisation and biological testing have been conducted. To support the documentation and scientific evaluation of these activities, a web based tool was developed, offering comfortable data acquisition similar to a laboratory information management system (LIMS) in order to document the complete lifecycle of the nanoscaled materials investigated within the project. This system is designed to enable users distributed over various organizations to jointly document their activities, yielding a database that allows for the reproducibility of the entire life cycle of any given specimen. As requirements and activities were constantly evolving throughout the course of the project, whereas the application had to be ready quite early in the project, the concept is focused on an approach where activities can be documented in a flexible fashion using ad-hoc workflows. The application has been designed as a general purpose tool that can be configured according to individual needs, not limited to an application in a nanomaterials context, but allowing re-use in a wide range of applications.

### 2.2 Integrated external Communication – Focus Groups Interviews, WebSite, Public Dialogue Meetings

In the last few years a growing number of academic organisations, but also governmental institutions and NGOs, have been experimenting with and implementing participatory methods, enabling a better interaction between the public, stakeholders, experts and policy-makers in the process of shaping a technology and its regulatory framework. The most prominent methods for the inclusion of the general public in discussions about future developments in science and technology are, for instance, focus groups, citizens' juries and citizens' and stakeholder dialogues.

#### Focus Groups Interviews

Based on this background, social scientists who were involved in the NanoCare project concentrated on the attitudes of laypeople, experts and multipliers towards synthetic nanoparticles and nanotechnology in general and investigated the information needs especially of the lay public. These information needs were later on taken into account for the set up of the project website. The participants of the lay focus groups mostly had only little

knowledge about nanotechnology, but were nevertheless interested in learning more about the technology itself and its applications. Though most interviewees were positive about nanotechnology, they would not accept products that had not been tested thoroughly before being introduced to the market. They demanded independent control of research and transparent declaration of products containing nanoparticles as fundamental prerequisites of public trust. Furthermore, the participants asked for more information and clarification especially on the topic of risk assessment of the various nanotechnology applications, and for more discussion of new scientific outcomes with the public. Only then, they argued, can nanotechnology in general be successfully introduced into a huge number of fields in our lives.

### Website

The project website [www.nanopartikel.info](http://www.nanopartikel.info) aims at informing the general public about the project and its results as well as providing some general information about safety issues related to nanomaterials. Besides a general introduction, the scope, goals, funding, partners, and the structure (work packages) of the project are presented as well as the scientific publications and Standard Operation Procedures (SOPs) that originated from NanoCare. Furthermore, dates and details about dialog events, hyperlinks to press coverage, a frequently asked questions (FAQ) section and a facility to direct questions to the project team are provided. Furthermore a so-called "Knowledge Platform" has been integrated. It serves as the major entry point to a collection of images and texts written by the NanoCare consortium.



Figure 2.1 Website NanoCare [www.nanopartikel.info](http://www.nanopartikel.info)

Following the advice given by the focus groups interviews mentioned above, the site primarily addresses lay readers. It provides core information on single nanomaterials and gives insights into the current knowledge about their behaviour in biological systems. In its

current state, the knowledge platform introduces readers to topics related to those nanomaterials investigated by NanoCare research groups. For the use of science journal literature as a textual resource for web publishing a criteria catalogue has been developed in order to ensure the quality standards of research publication to the websites contents. The website [www.nanopartikel.info](http://www.nanopartikel.info), especially the knowledge base, will be continued and provided in German and in English by a new BMBF funded project called DaNa (Cooperative project: Acquisition, evaluation and broad-based illustration of societal relevant data and findings of nanomaterials).

### Public Dialogue Meetings

The special aim of the public dialogue meetings was on the one hand to present results of NanoCare research in a generally understandable way to interested citizens. On the other hand, the citizens participating had the opportunity to raise questions and also concerns about nanomaterials relevant to their point of view. These dialogues not only focused on health and safety aspects of nanomaterials, but also on current environmental and consumer related aspects. In this sense very concrete examples were discussed between nanotechnology experts from industry, science, politics and NGOs and interested citizens. Dialogues with societal groups and citizens took place in Düsseldorf Hamburg, Munich, Dresden and Berlin between 2007/09. In October 2007 a stakeholder-dialogue between professional representatives of business, politics, science and society was very much focused on pros and cons of the design of NanoCare-research on health and safety aspects. This dialogue had around 120 participants. Around 60 interested citizens participated in the citizens' dialogues later on. In June 2009 another stakeholder-dialogue with around 100 participants took place in Berlin. It focused on two major questions: 1) What do we learn from the scientific results of the project NanoCare? 2) What could be done next? The dialogues were chaired by science journalists. After the event the participants had the opportunity to answer a questionnaire concerning the value of the dialogue from their point of view. According to the results of this survey the participants were either "very satisfied" or "satisfied" with the dialogue. Besides this, quite a number of participants asked for additional events of these kinds of dialogues on nanomaterials. The results of the public dialogue meetings will be documented in a separate publication by VDI Technologiezentrum (<http://zukuenftigetechologien.de>).



**Figure 2.2** Citizens' Dialogue on Nanotechnology (Dresden 2008).

## 3. Particle Synthesis and Characterisation

---

C. Goebbert, F. Hardinghaus, K.H. Kampmann, M. Kroell, C.-M. Lehr, U.F. Schäfer, C. Schultze-Isfort, C. Schultze, M. Voetz, W. Wohlleben

---

Nanomaterials have been produced, examined, characterised and used in many different applications for decades. Some examples are titanium dioxide and carbon black. Industrial produced nanomaterials usually consist of particles in the micrometer range, agglomerates or aggregates, primarily assembled by nanometer-sized particles. The methodical examination of the mechanical strength and stability of such agglomerates and aggregates is an important and basic approach for the assessment of a potential health risk of nanomaterials.

The basis for NanoCare and the objective of this report is the identification, production and characterisation of suitable nanomaterials and to ensure the comparability and reproducibility of the follow-up in-vitro and in-vivo toxicological testing, dustiness behaviour and workplace concentration measurements. For this reason, Standard Operation Procedures (SOPs) as well as the right and most suitable characterisation methods have been defined. Special attention has been given to the agglomeration and aggregation behaviour and particle stability.

### 3.1 Identification and Synthesis of Suitable Nanomaterials

For this project, suitable nanomaterials were identified, produced and characterised. The selected materials were specifically synthesised and modified with regard to particle size, surface coating (i.e. hydrophobic or hydrophilic), surface charge and surface chemistry.

To eliminate toxicological relevant findings caused by the material itself and not by the nanoscaled size or surface modification, the materials used had to fulfil the following requirements:

- Stable & chemically non-toxic materials
- Insoluble in water

The summary of the selected nanomaterials is shown in table 3.1:

**Table 3.1** List of Nanomaterials produced and tested in the NanoCare project.

No	Materials	Available form (Dispersion / Powder)		Primary Particle size [nm]	Remarks	Provider
		D	P			
<b>1</b>	<b>TiO<sub>2</sub></b>	D	P			
1.1	TiO <sub>2</sub>	D (pH 3-4)	P	17	Organic molecules on the surface	ITN
1.2	TiO <sub>2</sub>	D (pH 3-4)	P	25	Reference material	Evonik
1.3	TiO <sub>2</sub> -40		P	40	-	Evonik
1.4	TiO <sub>2</sub> -70		P	30	-	Evonik
1.5	TiO <sub>2</sub> -120		P	10	-	Evonik
<b>2</b>	<b>Carbon Black</b>	-	P	14	Reference material	Evonik
<b>3</b>	<b>CeO<sub>2</sub></b>		P	10-20, 40-50	-	-
3.1	CeO <sub>2</sub> -A		P	14	pH 6.2	Evonik
3.2	CeO <sub>2</sub> -B		P	20	pH 5.4	Evonik
3.3	CeO <sub>2</sub> -C		P	23	pH 3.4	Evonik
3.4	CeO <sub>2</sub> -D		P	14	pH 3.4	Evonik
3.5	CeO <sub>2</sub>		P	70	-	BASF
<b>4</b>	<b>Doped CeO<sub>2</sub></b>		P	10-20, 40-50	-	-
4.1	3 % Li-CeO <sub>2</sub>		P		-	Evonik
4.2	1 % Li-CeO <sub>2</sub>		P		-	Evonik
4.3	1 % Ti-CeO <sub>2</sub>		P		-	Evonik
4.4	5 % Al-CeO <sub>2</sub>		P		-	Evonik
4.5	1 % Al- CeO <sub>2</sub>		P		-	Evonik
<b>5</b>	<b>AlOOH, (Boehmite)</b>		P		-	
5.1	AlOOH, (Boehmite I)		P	40	-	BMS
5.2	AlOOH, (Boehmite II)		P	>40	-	BMS
<b>6</b>	<b>Ti-Zr-Mixed oxide</b>		P		-	
6.1	Ti-Zr-Mixed oxide		P	30	-	Evonik
6.2	Ti-Zr-Mixed oxide		P	35	-	Evonik
6.3	Ti-Zr-Mixed oxide		P	35	-	Evonik

<b>7</b>	<b>Ti-Al-Zr Mixed oxide</b>		P		-	
7.1	Ti-Al-Zr Mixed oxide		P	25	-	Evonik
7.2	Ti-Al-Zr Mixed oxide		P	30	-	Evonik
7.3	Ti-Al-Zr Mixed oxide		P	35	-	Evonik
<b>8</b>	<b>ZrO<sub>2</sub></b>	D			Organic molecules on the surface	
8.1	ZrO <sub>2</sub>	D		37	pH 4	ITN
8.2	ZrO <sub>2</sub>	D		31	pH 3,7	ITN
8.3	ZrO <sub>2</sub>	D		461	pH 8-10, strongly agglomerated	ITN
<b>9</b>	<b>ZnO</b>		P	150	-	BASF
<b>10</b>	<b>BaSO<sub>4</sub></b>		P	38	Strongly agglomerated	SOLVAY
<b>11</b>	<b>SrCO<sub>3</sub></b>		P		-	
11.1	SrCO <sub>3</sub>		hydrophilic	19	strongly agglomerated	SOLVAY
11.2	SrCO <sub>3</sub>		hydrophobic	17	strongly agglomerated	SOLVAY

Some materials in this table represent commercially available nanomaterials; others are produced at least on large laboratory scale. For further examinations, the above-mentioned materials were sent to the partners for in vitro and in vivo testing and for working place relevant dustiness measurements.

All toxicological and working place relevant measurement results of these materials are described in the corresponding chapters.

### 3.2 Standardisation, Particle Characterisation and Nanomaterials

The accurate and thorough analysis and characterisation are important parts to understand how nanomaterials may interact with living organisms and tissues. Measurements had to follow rigid standard operational procedures and were performed by the same project partners to ensure reproducible and comparable results.

NanoCare in co-operation with other international projects and initiatives came to a mutual consent which properties have to be characterized at a minimum level to be able to compare and evaluate the results of toxicological findings and tests (Powers et al., 2007; Murdock et al., 2008; Schulze et al., 2008; Landsiedel et al., 2008; Warheit, 2008; Tiede et al., 2008; Valsami-Jones et al., 2008).

The characterisation parameters investigated within NanoCare are the size and form of the primary particles, the aggregates/agglomerates, specific surface area, chemical composition and impurities, crystallinity and crystal phase, organic surface modification and isoelectrical point in water. The solubility of the materials is determined by atomic spectroscopy after the

standard operation procedure for the dispersion of nanomaterials in solvent (this procedure has already been published in <http://www.nanopartikel.info/methoden.html>).

The nanomaterials were characterised in suspension and powder form. The following characterisation methods were used (full names of the methods can be found at the end of this report):

**Table 3.2a** Characterisation methods used for nanomaterials (*powder form*) in the project NanoCare.

<i>Information</i>	<i>Method</i>
Particle form (for primary particles, aggregates/agglomerates)	TEM
	AFM
Particle size distribution (primary particles, aggregates/agglomerates) Dustiness behaviour	SMPS
	FFF, AUC (in solution only), TEM
	LS
	Down pipe
	PCS
Chemical composition (surface, bulk, purity, exact analysis of the org. modification / stabilisation)	TOF-SIMS
	XPS
	ICP-MS
	AAS, elementary analysis
Specific surface area Density	BET
	Pycnometry
Crystallinity/crystal phase	XRD, EDX (TEM) electron diffraction
Solubility in relevant solvents	ICP-MS
Bulk density	

**Table 3.2b** Characterisation methods used for nanomaterials (*dispersion form*) in the project

<i>Information</i>	<i>Method</i>
Particle form (for primary particles, aggregates/agglomerates)	Cryo-TEM, Cryo-SEM, (FCS)
Crystallinity/crystal phase	XRD
Particle size distribution (primary particles, aggregates/agglomerates, density, molecular weight)	AUC, HDF; Cryo-TEM
Particle size distribution, diffusion velocity	DLS, PCS
Surface potential	Zeta-Pot.

The results of the characterisation were entered into an internet-based database together with a specific lot number for accurate traceability. A summary of the basic data are given in Annex A with data sheets for each nanomaterial variation.

### Boehmite

**Boehmite** is a mineral, which belongs chemically to Aluminium Oxy-Hydroxides (AlO(OH)). Boehmite and other aluminium oxides are used as catalyst carriers in the petro-chemical industry because of their thermal resistance. In the colour and polymer industries, they are applied as thickening agent, and filler material, to lower the stickiness and enhance the scratch resistance. These materials also have a positive effect on the colour brilliance. Further application fields can be found in the ceramic industry (high scratch and thermal

resistance), the paper industry (anti-sticking agent in the paper processing), as artificial gemstones (sapphire, yttrium-aluminium garnet for high energy laser) and as carriers for luminescent substances.

The Boehmite used in the NanoCare project is a powder with agglomerates in the  $\mu\text{m}$  range. Primary particles are of nanoscale.

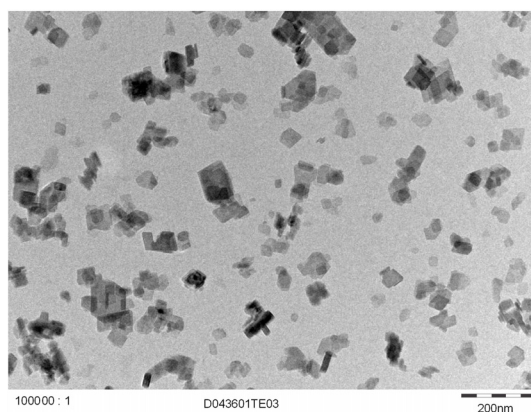
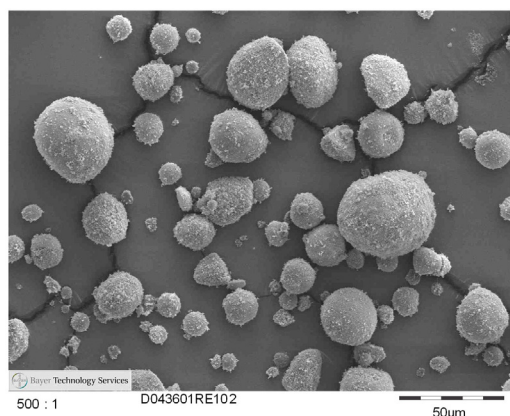


**Figure 3.1a** SEM picture of boehmite agglomerates      **Figure 3.1b** TEM picture of (with ultrasound) dispersed Boehmite primary particles

Boehmite has been used to examine mass transport through cell membrane, inhalation studies as well as exposure related measurements during industrial processing. The results are described in the corresponding chapters.

### Barium sulphate & Strontium carbonate

**Barium sulphate** is negligible soluble in water and ideally fulfils one of the material requirements of the project. Strontium Carbonate, which was produced with 2 different surface modifications is equally negligible soluble in water. During the synthesis of these nanomaterials, organic modifiers have been used.

The relevant characteristics of the supplied materials are described below in detail:

**BaSO<sub>4</sub>** (No. 10) has crystalline primary particles with a mean particle size of 47 nm (TEM) and 37.5 nm (X-ray diffraction), respectively. The powder is strongly agglomerated; the particle size of the agglomerates has a  $d_{90}$  value of 35  $\mu\text{m}$  and a  $d_{50}$  value of 17  $\mu\text{m}$ . It has a bulk density of 1.03 kg/litre. The solubility in water is 138 mg Barium per litre (internal method of producer) and 6 mg Barium per litre (NanoCare internal method). The zeta potential is -33 mV in 15 % aqueous suspension and has the isoelectrical point at pH 4. The specific surface area is 41.4  $\text{m}^2/\text{g}$ .

SrCO<sub>3</sub> has been synthesised in 2 different product varieties with different surface properties.

**SrCO<sub>3</sub>** with hydrophilic surface (No. 11.1) has crystalline primary particles with a mean particle size of 18.5 nm (X-ray diffraction). The powder is strongly agglomerated; the particle size of the agglomerates has a  $d_{90}$  value of 23.7  $\mu\text{m}$  and a  $d_{50}$  value of 5.9  $\mu\text{m}$ . It has a bulk density of 0.45 kg/litre. The solubility in water (NanoCare internal method) is 28 mg Strontium per litre. The zeta potential is -10 mV in 15 % aqueous suspension and has the isoelectrical point at a pH lower than 7 (the point could not specifically be determined under acidic conditions). The specific surface area is 33  $\text{m}^2/\text{g}$ .

**SrCO<sub>3</sub>** with hydrophobic surface (No. 11.2) has crystalline primary particles with a mean particle size of 17.0 nm (X-ray diffraction). The powder is strongly agglomerated; the particle size of the agglomerates has a d<sub>90</sub> value of 18.6 μm and a d<sub>50</sub> value of 5.9 μm. It has a bulk density of 0.66 kg/litre. The solubility in water (NanoCare internal method) is 53 mg Strontium per litre. The zeta potential is -66 mV in 15 % aqueous suspension and has the isoelectrical point at a pH lower than 7 (the point could not specifically be determined under acidic conditions). The specific surface area is 8.9 m<sup>2</sup>/g.

All three powders were sent for further examinations to the partners for in-vitro and in-vivo testing and for working place relevant dustiness measurements.

All toxicological and working place relevant measurement results with these materials are described in the corresponding chapters.

### Zinc Oxide

**Zinc oxide** is an excellent UV-absorber that is used both for technical purposes (light fastness of plastics) and for cosmetics. The later application is especially sensitive to product safety, because an emulsion containing the nanoparticles comes into contact with the skin of consumers. Especially sun screens with high sun protection factors >15 require inorganic UV-absorbers such as TiO<sub>2</sub> or ZnO particles

### Cerium Oxide

Several varieties of fumed cerium oxide particles were produced by introducing suitable precursor systems into a flame. Through carefully adjusting process parameters such as flame temperature, residence time, cooling rate and precursor concentration the physicochemical properties of the ceria could be controlled. Thus, ceria particles with high and low BET surface areas, with isoelectric points at high and low pH values and with different surface chemistries were produced. Moreover, several doped ceria particles were developed. The dopants include titanium, lithium, potassium and aluminium. Doping with the aforementioned materials also leads to different physico-chemical properties of the ceria. Samples of the different ceria varieties were given to other partners for toxicological studies. Attempts to produce hydrophobic ceria failed. Typically, fumed particles, which are hydrophilic in nature, can be hydrophobised by post-treatment with suitable silanes. Due to the high catalytic activity of the ceria, conventional post-treatment methods failed. Thus, it was not possible to provide the above-mentioned ceria varieties in a hydrophobised form.

### Zirconium Dioxide

**Zirconium dioxide** (ZrO<sub>2</sub>), also known as zirconia, is a white crystalline oxide of zirconium. Its most naturally occurring form, with a monoclinic crystalline structure, is the rare mineral, baddeleyite. The high temperature cubic crystalline form, called 'cubic zirconia', is synthesised in various colours for use as gemstones.

Pure ZrO<sub>2</sub> has a monoclinic crystal structure at room temperature and transitions to tetragonal and cubic at increasing temperatures. Several different oxides of Y, Mg, Ca, Ce are added to zirconia to stabilise the tetragonal and/or cubic phases. The ZrO<sub>2</sub> used in the project has a mixed tetragonal and cubic phase.

Wet-chemically synthesised ZrO<sub>2</sub> prepared with different surface modifications (acid (No. 8.1) and base stabilised (No. 8.3) shows a clear change in the zeta potential (see figure 3.2):

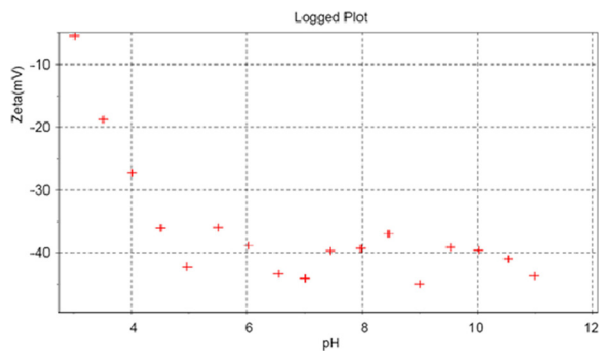


**Figure 3.2a** Zeta potential of acid stabilised  $ZrO_2$

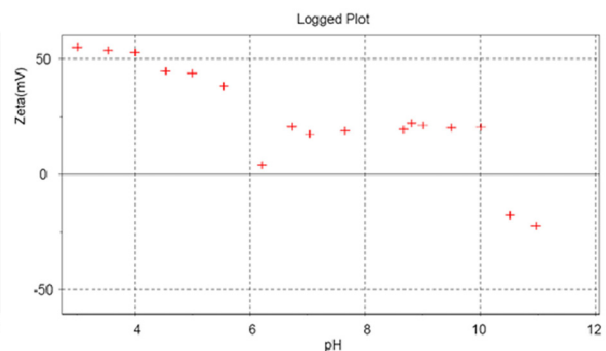


**Figure 3.2b** Zeta potential of base stabilised  $ZrO_2$ , IEP at pH 10,89

The analysis shows that the acid stabilised  $ZrO_2$  (No. 8.3) is stable in aqueous solutions in a pH range of 3 - 5.5; the base stabilised  $ZrO_2$  (No. 8.1) is stable in a broad pH range. This has an important influence on the penetration abilities in biological systems and tissues. The primary particle size for both stabilised form is about 15 nm, however, the base stabilised version is largely agglomerated.

### Titanium Dioxide

**Pyrogenic titania** ( $TiO_2$ , No. 1.2) consists of a aggregate/agglomerate structure, has an average primary particle size of about 21 nm, a specific surface area of about  $50 \text{ m}^2/\text{g}$  and has a crystalline structure which comprises of the anatase and rutile phase. The ratio between anatase and rutile phase of  $TiO_2$  (No. 1.2) is approximately 80:20. The pyrogenic titania differs significantly from pigmentary  $TiO_2$  produced in substantial quantities through precipitation processes. The average particle diameter of precipitated titania is about  $0.3 \mu\text{m}$  with surface areas in the range of  $10 \text{ m}^2/\text{g}$ . The precipitation route leads to the thermodynamically stable rutile modification. On the contrary, in pyrogenic  $TiO_2$  the thermodynamically metastable anatase phase is the dominant modification (about 80 %). The lattice transformation towards higher amounts of rutile is observed at temperatures above  $700^\circ\text{C}$  and associated with a decrease in the specific surface area. A variety of fumed titania, zirconia-titania and alumina-titania-zirconia mixed oxides could be produced.

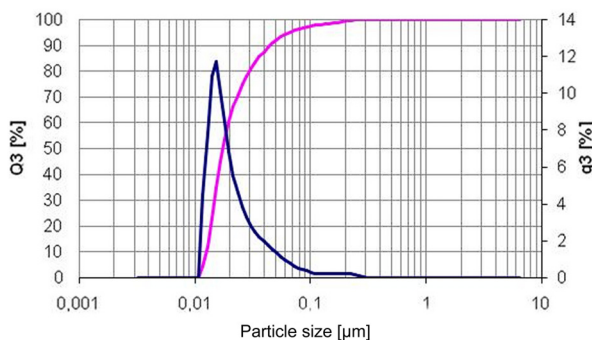


**Figure 3.3a** Particle size distribution Titanium dioxide, rutile.

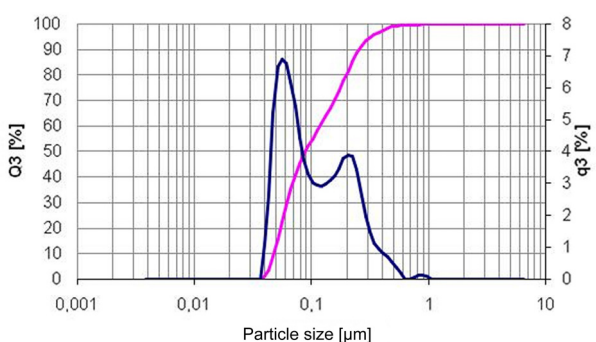


**Figure 3.3b** Particle size distribution Titanium dioxide, anatase.

A second material which has been supplied to the project was a wet-chemically synthesised and surface modified Titanium dioxide (No. 1.1) in the 2 modifications rutile and anatase. Though both have the same surface modification, the particles behave very differently.

### 3.3 Dispersion of the NanoCare Materials in Cell Culture Media – A Challenge

Cell culture media and isotonic buffer solutions for physiological conditions contain more than 30 components with 11 mg/ml of different ionic salts, 4.5 mg/ml sugar (glucose), 1.5 mg/ml amino acids and 0.3 mg/ml proteins. Serum (blood) also contains more than 70 mg/ml of surface active substances and proteins. With 0.1 mg/ml, the usually used concentration of nanomaterials in cell culture media is very low and thus, presents a strong challenge for the analysis of them in biological media. In addition, surface active substances can be absorbed on the surface of the particles and thus significantly change the surface properties.

#### 3.3.1 Development of Protocols for Nanomaterial Dispersion in Physiological Media

In order to perform cell based toxicologically relevant assays, it is necessary to disperse the nanoparticles of interest in physiological media. However, physiological media contain many ions which influence the  $\zeta$ -potential (zeta potential) and thus may destabilize the dispersion resulting in agglomeration of the primary nanoparticles. This alters the effective particle size and hence this biases the test result. Therefore, we investigated the influence of various dispersion media on dispersity and  $\zeta$ -potential, first with model particles of polystyrene (Fluoresbrite carboxylated nanoparticles from Polysciences,  $\varnothing$ 50 nm). As can be seen in Figure 3.4a, the size of the particles varies from 50-70 nm in (isotonic) Phosphate Buffer (PB), whereas large agglomerates occur in Krebs-Ringer-Buffer (KRB). Dispersed in KRB with 1 % of Bovine Serum Albumin, the particles are well dispersed again. Linear complexity of the dispersion medium results in a decrease of  $\zeta$ -potential (Figure 3.4b). These results support that the protein is adsorbing onto the particles and thus stabilizing them. The stabilization mode of the dispersion switches from originally electrostatic to sterical. These results were obtained independently by using Dynamic Light Scattering (DLS) measurements and Analytical Ultracentrifugation.

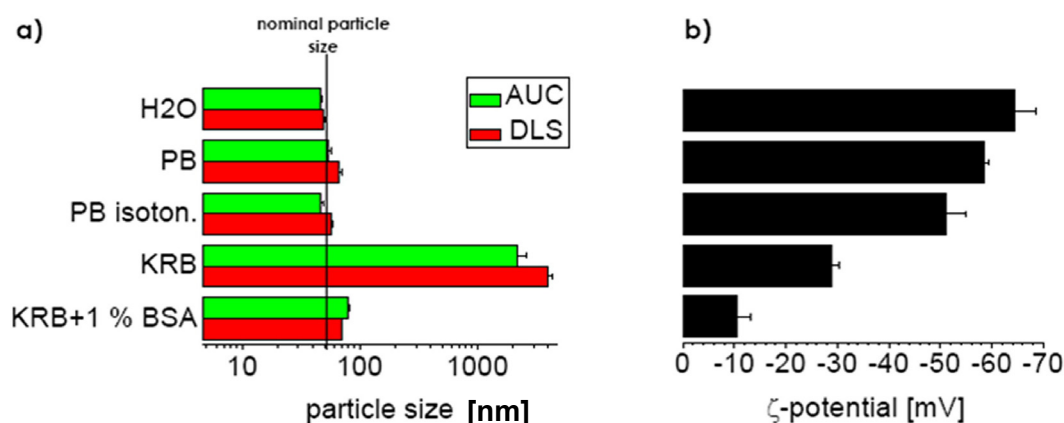


**Figure 3.4** Sizes and  $\zeta$ -potentials of polystyrene c50 NPs in different dispersion media. a) hydrodynamic diameters of the c50 NPs, measured via Dynamic Light Scattering (DLS; red bars) and Analytical Ultracentrifugation (AUC; green bars); the black line corresponds to the nominal particle size. In Milipore water and both phosphate buffers (PB and PB isoton.), the sizes ranged from around 50-70 nm. In KRB, large agglomerates occurred, which were not present when dispersing the particles with KRB containing 1 % of BSA. b)  $\zeta$ -potentials of the particles: with increasing complexity of the dispersion medium, the  $\zeta$ -potential decreases.

To transfer these results to some metal oxide particles from NanoCare partners,  $\text{TiO}_2$  (1.2),  $\text{ZrO}_2$  (8.1) and  $\text{CeO}_2$  (3.5) were characterized by Dynamic Light Scattering, but this technique failed due to fast sedimentation. As described previously, the  $\zeta$ -potentials all switched to slightly negative values (data not shown) (Limbach et al., 2005). However, experiments by means of Analytical Ultracentrifugation clearly showed that the addition of proteins led to a concentration-dependant decrease in particle size.

These results combined with other findings lead to a catalogue of aspects that have to be considered for in-vitro cell based assays and were published 2008 in 'Nanotoxicology' (Schulze et al., 2008).

The data were used to develop a SOP for nanomaterial dispersion in biological media. This SOP and a corresponding SOP for nanomaterial dispersion in surfactant were used for all assays in the project.

### 3.3.2 Dispersion and Examination of the NanoCare Nanomaterials

Nanomaterials are covered by absorbed proteins and thus influence i.e. transport processes. With increasing protein concentration the inorganic nanomaterials show a decreasing particle size. The dispersion has been carried out according to the NanoCare SOP without the use of ultrasound, stirred in small vessels at 900 rpm for 24 hours (Schulze et al., 2008).

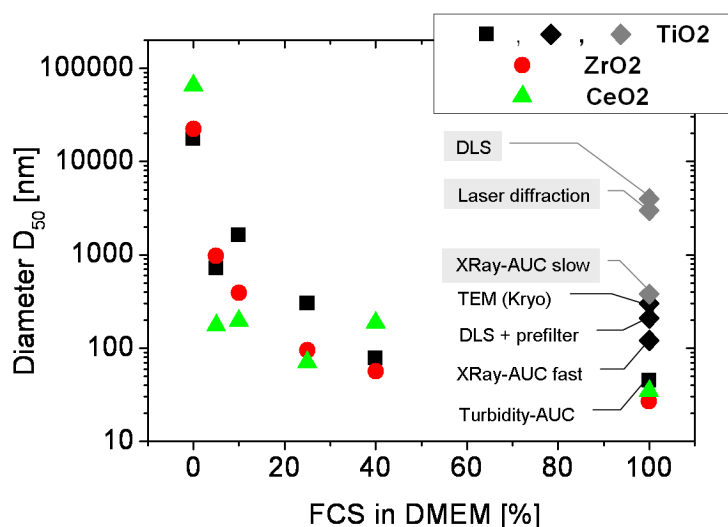


**Figure 3.5** Agglomeration level dependant on the protein concentration for  $\text{TiO}_2$  (black squares) (No. 1.2), organic stabilised  $\text{ZrO}_2$  (No. 8.1) (red dots) and  $\text{CeO}_2$  (No. 3.5) (green triangles).  $d_{50}$  values acquired by analytical ultracentrifugation represents the mean (mass) size of agglomerates with variance of  $\pm 30\%$ . Diamond shaped symbols show alternative measuring methods for  $\text{TiO}_2$  in 100% FCS.

It can clearly be seen that the mean particle size decreases on a large scale, if the dispersion media are changed from DMEM to 100% FCS. In DMEM the particles are strongly agglomerated by the ionic interaction, in FCS the analysis shows significantly smaller fractions. It is important to know that different measuring methods show significantly different results.  $\text{TiO}_2$  in 100 % FCS (diamond shaped symbols in Figure 3.5) has been used as an example to compare different measuring methods.

Well known and as valid regarded methods like Dynamic Light Scattering (DLS), Analytical Ultracentrifugation (AUC), X-ray AUC, Transmission Electron Microscopy (TEM), Cryo-TEM,

Energy Dispersive X-ray (EDX) Nanoanalysis in a Field Emission TEM (FE-TEM) and, finally fractionized optical ultra-centrifugation (black diamond shaped symbols in Figure 3.5) agrees only within a factor of 4 due to the different physical measurement principles and sample preparations. Pure optical methods fail.

Therefore, complementary Small Angle Neutron Scattering (SANS) experiments at the Geesthacht Neutron Facility (GeNF) have been performed to get a conclusive answer regarding the characterisation of the size distribution and the particle morphology of the aggregates to cross check particle sizes and compositions.

In these SANS experiments a titanium dioxide (No. 1.2) with a specific surface area of about 50 m<sup>2</sup>/g and a primary particle size of about 21 nm was examined. Goal of the experiments was to determine the size and the shape of aggregates in the presence of proteins and lipids under physiological conditions. Additionally, by differentiating between the scattering contribution of inorganic and organic matter of similar size one should be able to determine the adsorption of biological material onto the surface of the aggregates or any other interaction of the two.

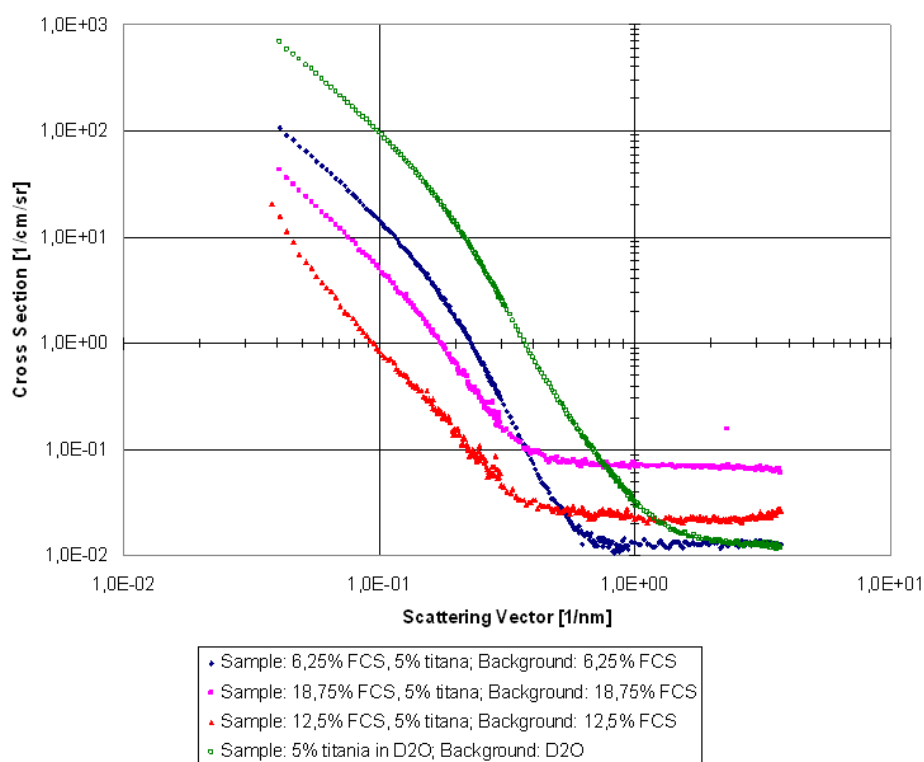


**Figure 3.6** Scattering vector in dependence of the FCS concentration.

The SANS measurements were carried out with the SANS-2 instrument at the Geesthacht Neutron Facility (GeNF). Dispersions of TiO<sub>2</sub> in foetal Calf Serum (FCS), Dulbecco's Modified Eagles's Medium (DMEM) and D<sub>2</sub>O were studied as in vitro experiments. A rotating sample rack was used to avoid settling of the dispersed material. All measurements were performed at ambient temperature. The biologically sensitive samples were prepared under sterile conditions directly before the experiments. No aging effects were recognized during the measurements.

The general goal of the experiments is to examine the interaction between the organic (enzymes, lipids) and inorganic ( $\text{TiO}_2$ , No. 1.2) matter. Therefore the first milestone of the experiments was the successful contrast matching of  $\text{TiO}_2$ . The contrast point was found at 42.8 %  $\text{D}_2\text{O}$  in an aqueous solution.

First qualitative results show that the size of the  $\text{TiO}_2$  particles decreases, when it is dispersed in a biological medium containing proteins, lipids and salts.

In addition to the SANS experiments, Cryo-TEM shows the presence of additional small particles, which do not consist of  $\text{TiO}_2$ . These additional small particles are not inorganic particles, since they show degradation in the electron beam (see red circles in figure 3.7).

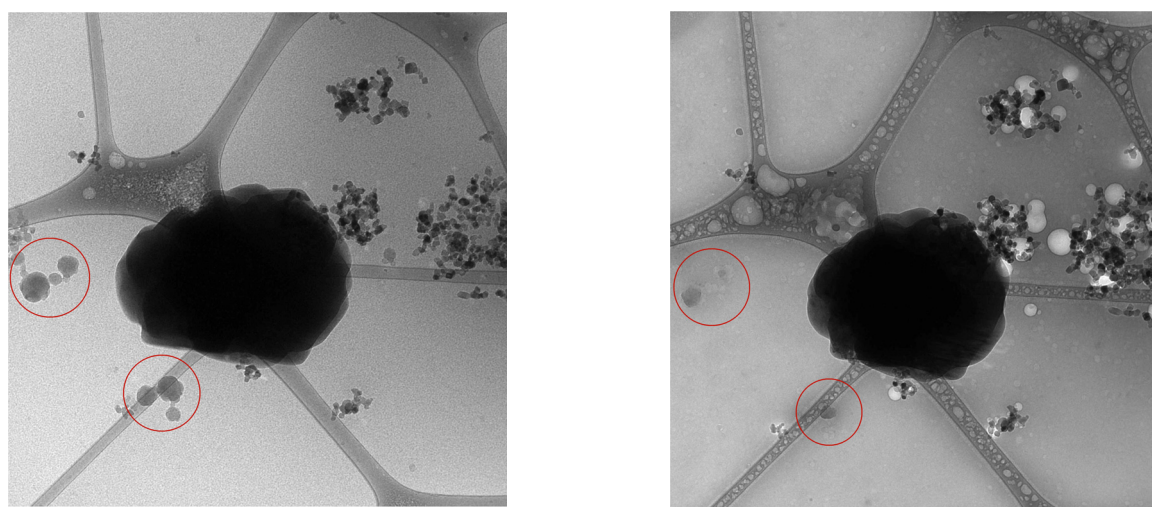


**Figure 3.7** Cryo-TEM picture before (left) and after (right) 6 minutes electron bombardment.

The effect of proteins on the dispersion process has been the subject of recent investigations. In other projects, a deagglomeration of metal oxides (metal carbides) in cell culture media or water with Albumins or serum has been reported (Nepal and Geckeler, 2007; Yokel et al., 2008; especially in the projects INOS (Richter et al., 2007); NanoCare (Schulze et al., 2008); NANOSH (Bihari et al., 2008)).

### 3.3.3 Stability of Agglomerates

The level of agglomeration of a series of 9 NanoCare materials was examined: Carbon Black (No. 2), Boehmite (No. 5),  $\text{TiO}_2$ -powder (No. 1.2 – 1.5) and  $\text{TiO}_2$ -dispersion (No. 1.1),  $\text{BaSO}_4$  (No. 10),  $\text{CeO}_2$  (No. 3.5),  $\text{CeO}_2$ -A (No. 3.1) and  $\text{CeO}_2$ -B (No. 3.2). A double comparison has been done, i.e., on one hand, the particles were compared among themselves; on the other hand, they were compared with the dispersion of the particles in serum or in lung lavage (porcine broncho alveolare Lavage Fluid, pBALF). As measurement method, analytical ultra-centrifugation with optical-interference detection was used to get a signal which is linear with the concentration. Figures 3.8 and 3.9 show the resulting particle size distributions.

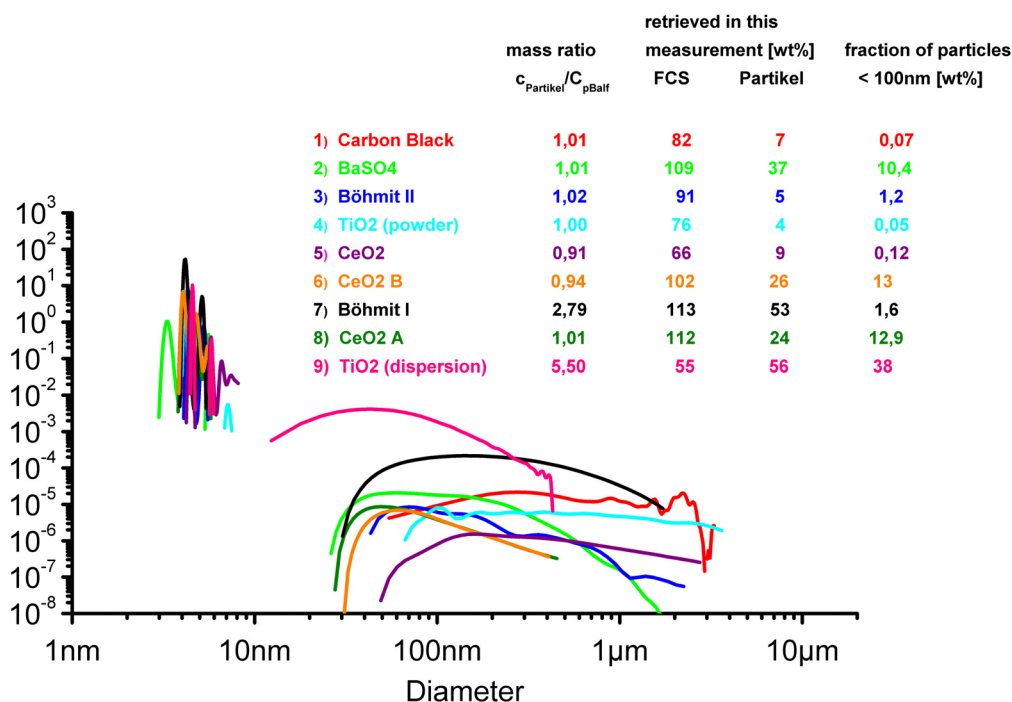


**Figure 3.8** Particle size distribution after dispersion (using the NanoCare-SOP) in diluted serum using analytical ultra-centrifugation (y axis = mass weight signal). The table shows the initial weight ratio and the protein and particle concentrations found as well as the resultant ultra fine fraction of the particle suspension.

The signal of the particle suspension in diluted serum (Figure 3.8) is dominated by the monomer and dimer peaks of BSA at 5 nm. For some of the examined materials like stabilised TiO<sub>2</sub> (No. 1.1), cerium oxide A (No. 3.1) and B (No. 3.2) and BaSO<sub>4</sub> (No. 10), ultrafine particles could be found. Other materials like CeO<sub>2</sub> (No. 3.5) and TiO<sub>2</sub> (No. 1.2), which have a significantly smaller particle size in pure serum, are mainly agglomerated in BSA within the used concentration.

The protein signal of the particle suspensions in diluted lung lavage (Figure 3.9) is shifted to larger molar masses (diameter of approximately 10 nm) since the surfactant proteins exist as oligomer; as expected no BSA signal could be detected at 66 kDa (4.5 nm). The nanomaterials are all strongly agglomerated, except for a small part (typically smaller than 1 wt. %) which is ultrafine dispersed. Only stabilized TiO<sub>2</sub> (No. 1.2, 29.7 wt. %, smaller than 100 nm) and BaSO<sub>4</sub> (No. 10, 6.2 wt. %, smaller than 100 nm) show a significant fraction in the ultra fine particle size region.

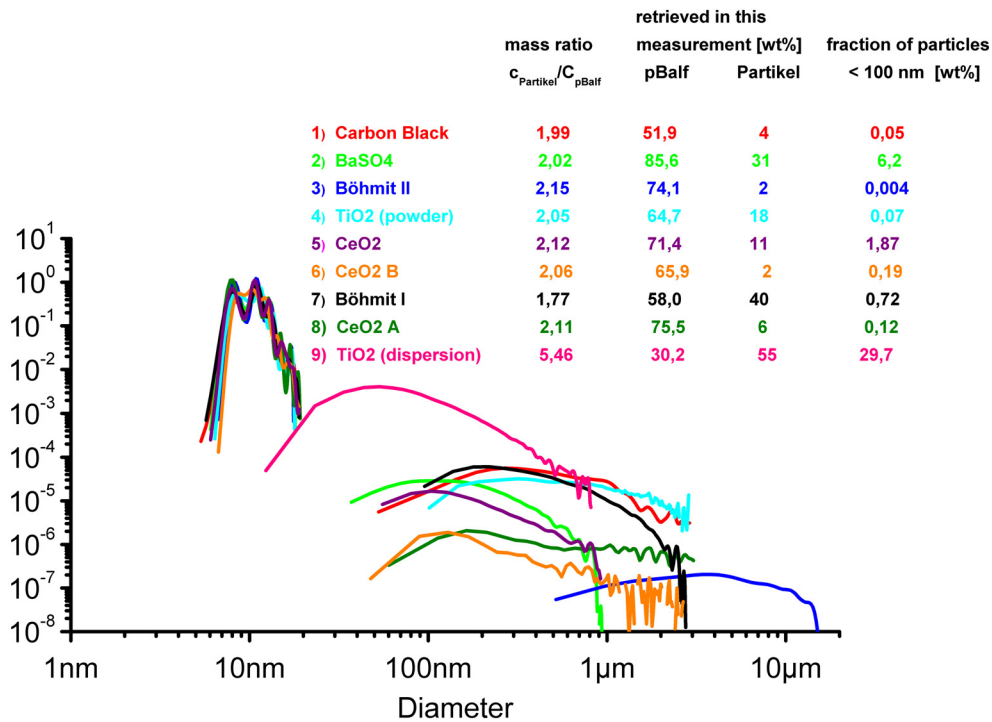


**Figure 3.9** Particle size distribution after dispersion (using the NanoCare-SOP) in diluted pBALF using analytical ultra-centrifugation (y axis = mass weight signal). The table shows the initial weight ratio and the protein and particle concentrations found as well as the resultant ultra fine fraction of the particle suspension.

All above-mentioned materials were distributed as powders and suspensions for further examinations for in-vitro and in-vivo and for working place relevant dust measurements.

### 3.4. Conclusions for the Characterisation of Nanomaterials

In agreement with other projects a list of recommendations has been developed for the reproducible and comparable characterization of nanomaterials in physiological suspensions. For future investigations, the following points have to be known:

- Suitable dispersion procedure,
- Agglomeration level and the size of the agglomerates,
- Zeta potential,
- Wettability and the change of agglomeration/de-agglomeration by the absorption of suspension components,
- Absorption of suspension components with possible influences on passivation, solubility and molecular recognition.

## 4. Toxicological Studies

---

J. Schnekenburger, R. Landsiedel, M. Wiemann  
 S. Brill, J. Bruch, D. Geiger, D. Hahn, A. Kroll, H.F. Krug, C.-M. Lehr,  
 L. Ma-Hock, S. Mülhopt, K. Nau, J. Pauluhn, H-R. Paur, M.H. Pillukat, J. Ragot,  
 U.F. Schäfer, C. Schulze, K. Tönsing, D. Wesner, K. Wiench, W. Wohlleben,  
 S. Zünkeler

---

Potential adverse effects of nanoparticles were studied in newly developed standardised in vitro and in vivo models. Since validated methodologies for the toxicological assessment of nanoparticles are currently not available NanoCare has established first reliable testing strategies. Nanoparticles display unique physico-chemical properties that differ significantly from bulk materials of the same chemical composition and evidence is accumulating that classical cytotoxicity assays may not be appropriate for nanotoxicity testing (for review see Oberdörster et al., 2005a&b, Kroll et al., 2008, Lewinski et al., 2008). Consequently, nanoparticle properties, such as their cell penetrating potential, their interactions with cells as well as with biological media and possible interference with test components were characterised and appropriate test systems selected to obtain a reliable risk assessment strategy and SOP for in vitro testing methods.

Possible toxic effects of NanoCare materials were analysed and compared using a broad set of established cell lines, primary rat alveolar macrophages bridging the in vitro and in vivo systems and rat inhalation models. Testing identical materials with standardized methods allowed an evaluation of particle toxic effects, in vitro test systems, the value of in vitro assays and a correlation of in vitro and in vivo assays.

Additionally, the toxicity testing was supported by mechanistic studies of particle cell interactions and transport across epithelial barriers.

### 4.1. Particle Cell Exposure Model

Exposure of in vitro cell systems to nanoparticles is restricted by the need of dispersion in biological media. To overcome these technical limits and to allow a direct dose-response measurement a new system for the exposure of in vitro cell systems under in vivo conditions has been developed.

The task was the development of new exposure methods for a nearly realistic in vitro testing of the lung toxicity. Inhaling particles and deposition on lung epithelial cells in the lower lung takes place at the air liquid interface. This is simulated with a previously developed Cell Exposure System (Figure 4.1 left) (Paur et al., 2008).

This system consists of a sampling unit to collect the aerosol from the nanoparticle loaded atmosphere. Particles larger than 1 µm are removed by passing a size selective inlet. In the next step the aerosol is humidified up to 85 %. Then the aerosol flow of 100 ml/min is directed into VITROCELL exposure modules, which contain three Transwell inserts with human lung cells on the microporous membrane. The aerosol flows perpendicular onto the surface of the cell culture (Figure 4.2). The responses of the cells were analysed by

measuring the viability (LDH, AlamarBlue) as well as the release of Interleukin-8 (IL-8) as a marker for pro-inflammatory changes.



**Figure 4.1** Right: Scheme of the Cell Exposure System with the (1) size selective inlet, (2) the water vapour dosage for humidification (3), the conditioning reactor for a constant aerosol with 37°C and 85% r.h., (4) the VITROCELL® exposure chambers containing the Transwell® membrane inserts and the sensor of the (5) quartz crystal microbalance. Left: photograph of the fully automated and temperature controlled prototype during an outside measurement of environmental aerosols.

In this study, the system was built up for the measurement at nanoparticle exposed workplaces to directly determine the toxicity of a special workplace atmosphere. A prototype (Figure 4.1 right) was built up and characterised for its performance dependent on different parameters.

For the determination of the dose response relationship the accurate knowledge of the dose is an essential question. A newly developed method is installed at the *Cell Exposure System*: for the online monitoring of particle dose the sensor of a quartz crystal microbalance is placed in an exposure chamber instead of the Transwell membrane insert and exposed to the aerosol in the same way as the cell cultures. The deposited mass per area unit is monitored as a function of exposure time showing a linear relationship for a constant aerosol flow with defined particle concentration (Mülhopt et al., 2008).

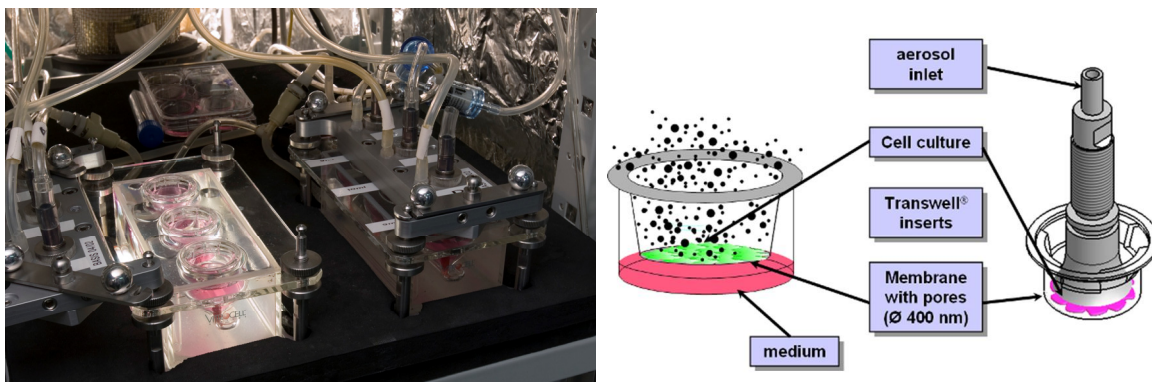


**Figure 4.2** Left: opened and closed VITROCELL® exposure chambers with water temperature control and medium for supplying the cell cultures with nutrients. Right: scheme of the exposure of a cell culture towards aerosol at the air liquid interface consisting of the aerosol inlet, the cell culture insert and the medium container.

For the testing of the system different nanoparticles were suspended in clean air. For reproducible aerosol generation two methods of particle suspending were tested: dry suspension by a rotating brush aerosol generator and wet dispersion by spraying a water suspension of the particles via a two phase nozzle in a heated air stream. For titanium oxide (No 1.2) the wet dispersion shows reproducible results with an agglomerate size mode of 150 nm and a geometric standard deviation  $\sigma_g$  of 2, the dry dispersion was unsuitable for titanium oxide.

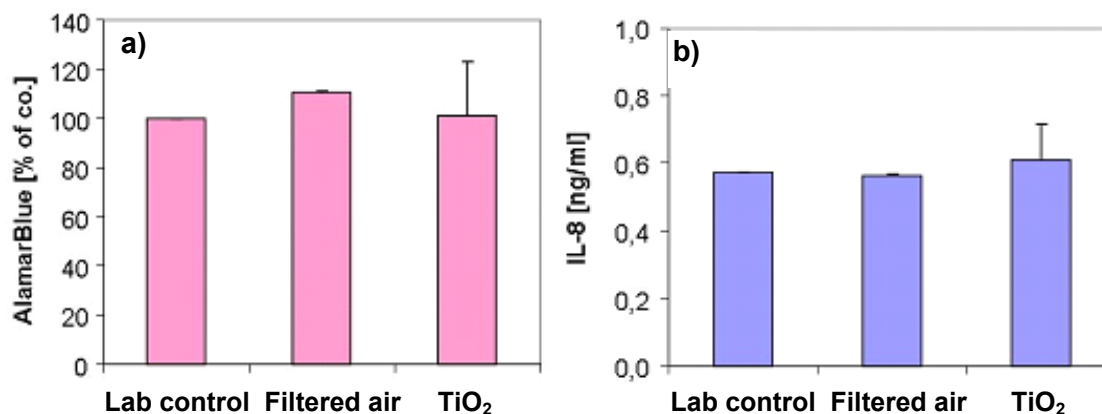


**Figure 4.3** a) Viability (Alamar Blue test, left) and b) inflammatory response (IL-8 ELISA, right) of A549 cells after 2 hours exposure towards TiO<sub>2</sub> (1.2) aerosol and filtered air in comparison with a lab control. Flow rate: 100 ml/min.

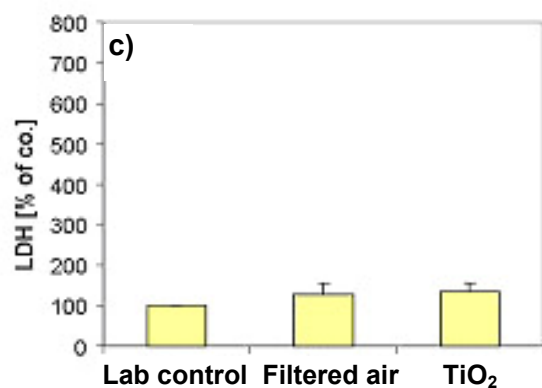


**Figure 4.3** c) Cell death (measured by LDH activity of A549 after 2 hours exposure towards TiO<sub>2</sub> aerosol and filtered air in comparison with a lab control. Flow rate: 100 ml/min).

Exposure experiments were carried out with human lung epithelial cells (A549) for 2 hours and 4 hours. After exposure to TiO<sub>2</sub> (No 1.2) no significant response in viability could be observed, no evidence of acute cytotoxicity could be found (Figure 4.3). Exposure experiments with Carbon Black (No 2) delivered no reproducible results up to now (unpublished results). The results of the Cell Exposure System are preliminary and have to be complemented by further studies.

## 4.2 Particle Mobility

### 4.2.1 Transport of Metal Oxide Nanoparticles through Cell Monolayers

To estimate the toxicological characteristics of nanoparticles, their potential of entering the body must be investigated. Therefore the potential to permeate physiological barriers, such as the air-blood barrier of the lung is especially of interest. For this type of studies, we have established cell culture models consisting of airway borne epithelial cells (Calu-3 cells) grown on Transwell systems (Corning, cat-nr. 3462; Figure 4.4), building a tight cell layer.

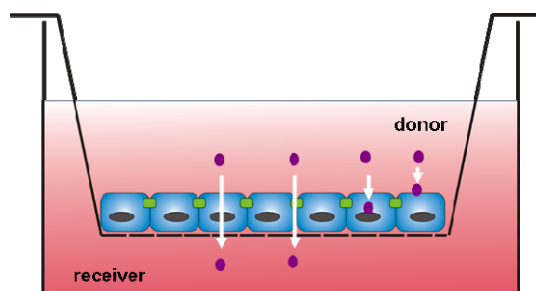


**Figure 4.4** The Transwell system: Epithelial cells (blue squares) separate the apical (donor) from the basolateral (receiver) compartment. Intercellular and intracellular transport of particles can be investigated as well as the uptake into or the adhesion of particles onto the cells.

For investigation of ion and drug permeation, the Calu-3 cell culture model is well established (Mathias et al., 1996; Forbes, 2000; Forbes and Ehrhardt, 2005; Lehr et al., 2006). To being able to perform particle-based transport assays, the setup had to be adapted. Normally filters with a pore size of 0.4  $\mu\text{m}$  are used within the Transwell system, but as shown in Figure 4.5, this filter material even used without cell layer provides a significant barrier to particles up to 200 nm. Hence, filters with a pore size of 3  $\mu\text{m}$  were tested. As shown in Figure 4.5, this change revealed a permeation of up to 100 % after an incubation period of 5 hours, which is a prerequisite for further studies with cell layers and is in good correlation with the literature (Geys et al., 2006).

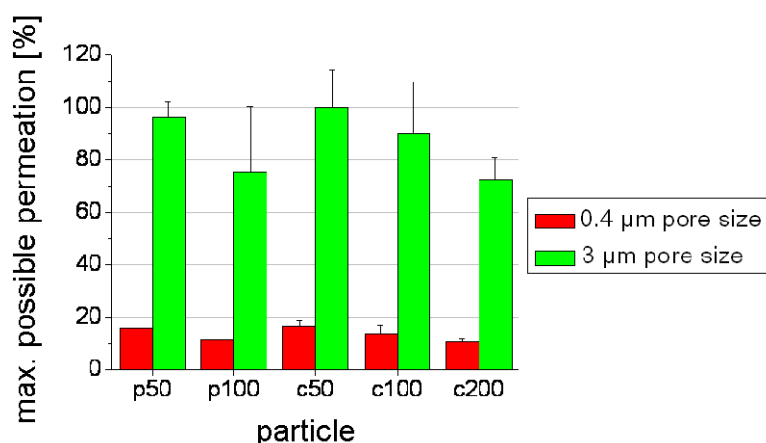


**Figure 4.5** Permeation of model particles through filters with different pore sizes: After 5 hours of incubation, up to 100 % of the particles permeated through the filter with the large pores, whereas a pore size of 0.4  $\mu\text{m}$  was a significant barrier for particle permeation (c=carboxylated; p=plain; the number corresponds to the particle size).

Based on these findings cell growth on 3 µm filter was evaluated and resulted in tight cell layers presenting a transepithelial resistance above 800 Ωcm<sup>2</sup> after optimisation (data not shown).

The transport assays with metal oxide nanoparticles from the industrial partners were performed with a particle concentration of 100 µg/cm<sup>2</sup> (=224 µg/ml) for 6 and 24 hours of incubation under sterile conditions. The quantification was done via Inductively Coupled Plasma - Mass Spectrometry (ICP-MS). The results are summarised in Table 4.1. All of the particles tested permeated through the naked filter, but no transport of particles through the cell monolayer could be detected. In case of ZrO<sub>2</sub> (8.1), 2.7 ± 2.6 % of nanoparticles were taken up, adherent on the cell surface or been transported and stuck in the filter. A particle adhesion could not be confirmed with X-ray Photoelectron Spectroscopy (XPS; also Electron Spectroscopy for Chemical Analysis, ESCA).

**Table 4.1** Summary of transport assays performed with metal oxide nanoparticles; no transport could be detected for any particle tested

Nano-particle	Permeation through naked filter after 24 hours [%]	Transport across cells after 24 hours [%]	Cellular uptake & filter washout [%]
ZrO <sub>2</sub> (8.1)	35 ± 4.5	0	2.7 ± 2.6
TiO <sub>2</sub> (1.2)	34.8 ± 4.1	0	0
AlOOH (5.1)	46.7 ± 19.1	0	0

Although the recovery of metal oxide nanoparticles, except AlOOH (5.1), was with 70-150 % beyond limits it was clearly found that no nanoparticles can be determined in the basolateral receiver compartment within the analytical detection limits.

Hence, with this lung barrier model, no permeation of metal oxide nanoparticles could be detected (Schulze et al. (1), 2009)

#### 4.2.2 Particles on Cells

The initial step of the interaction of nanoparticles and cells is the binding of nanoparticles to the cellular surface. Relevant aspects are the state of aggregation of nanoparticles bound to the cell, the position and distribution on the cellular surface and the binding-force between particles and cells. To investigate this binding-process atomic force microscopy (AFM) and force spectroscopy (FS) have been used. By scanning the sample topographic images of whole cells and magnified areas of the surface were obtained showing protrusions of approximately 100 nm to 250 nm (fixed RLE-6TN cells in liquid). Cells incubated with nanoparticles (CeO<sub>2</sub>, 3.2) show a higher number and increased height (up to 500 nm and more) of the protrusions. This indicates that nanoparticles aggregates with a diameter of several hundred nm are bound on the cellular surface. These protrusions can be found on the whole surface of the cell indicating an even distribution of the binding capability on a macroscopic scale.

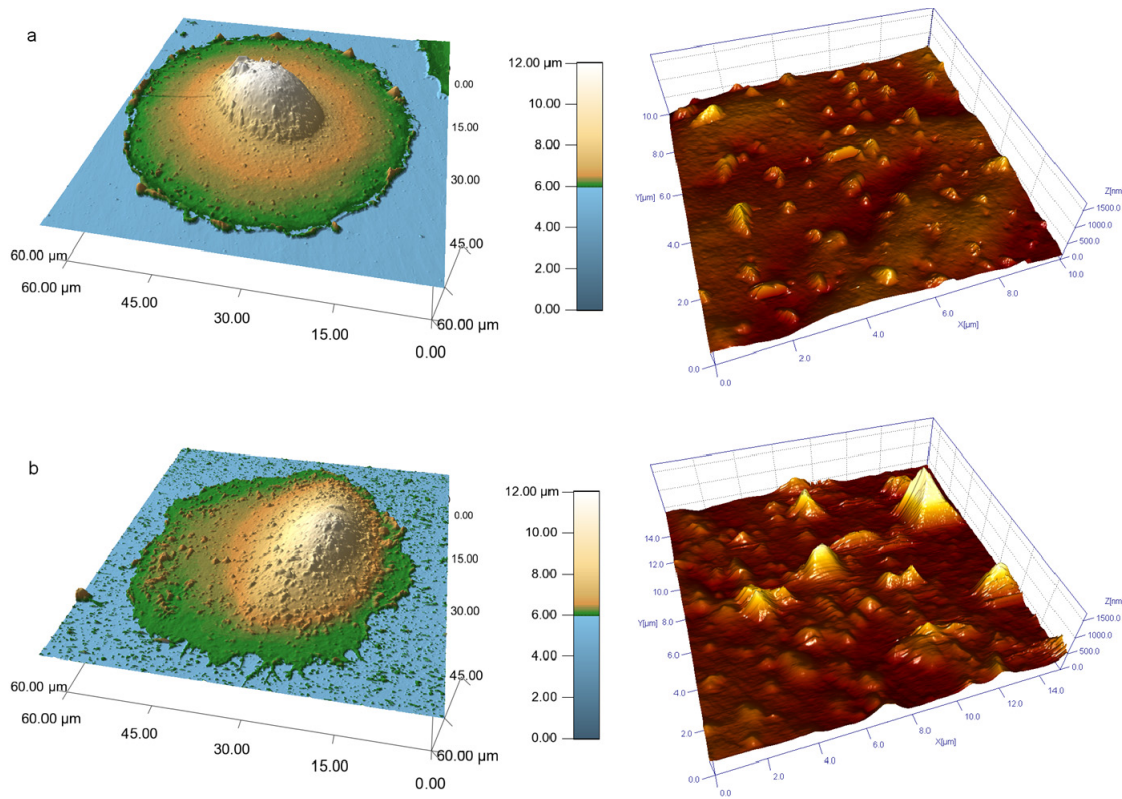


**Figure 4.6** Topographic AFM-images of a whole RLE-6TN-cell (left) and magnified parts of the cell surface (right). Untreated cells (a.) and incubated with CeO<sub>2</sub>-nanoparticles 3.2 (b.). The cells are fixed and imaged in buffer solution. Magnified images a: 10 μm, b: 15 μm scan size.

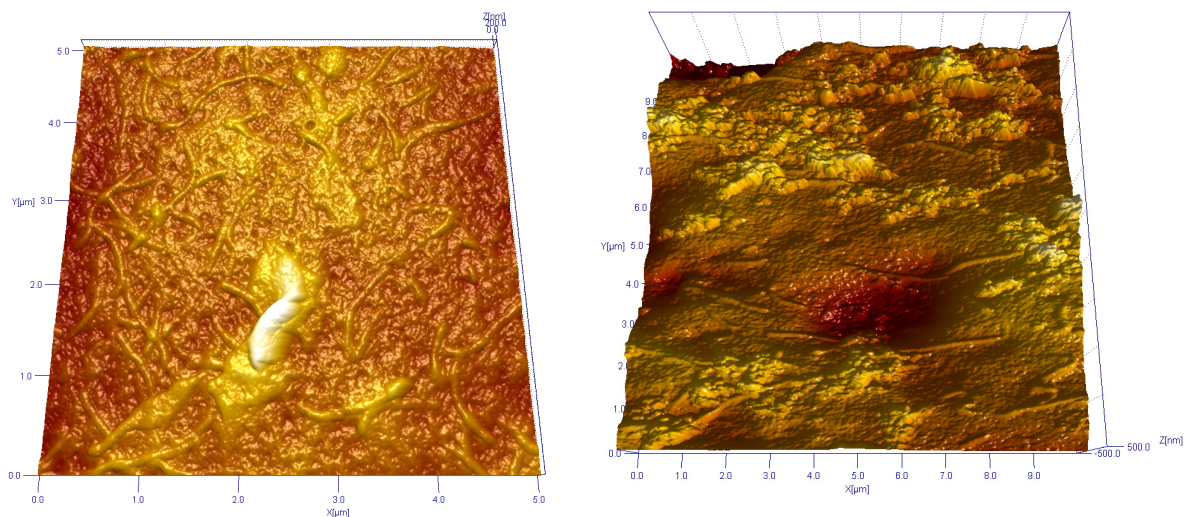


**Figure 4.7** AFM-topography of fixed and dehydrated RLE-6TN-cells. Untreated cell (left, scan size 5 μm) and incubated with nanoparticles CeO<sub>2</sub> 3.2 (right, scan size 10 μm).

To improve the resolution of the images the cells were dried making them more rigid and reducing deformations of the soft cells by the tip. The corresponding images show microvilli (35-80 nm diameters, 1-2 μm length) on a rough surface. These microvilli might appear as

the mentioned protrusions when imaging cells in liquid. Cells incubated with nanoparticles ( $\text{CeO}_2$ , 3.2) reveal areas covered with agglomerated structures (individual height approx. 25-50 nm) comparable to images of pure nanoparticles. These aggregates have lateral dimensions of several hundred nanometers to a few microns and are thought to be composed of nanoparticles. In some cases small aggregates seem to be associated with microvilli but it is not yet clear if this is a specific interaction. Larger aggregates are bound on the cellular surface with no obvious local preferences.

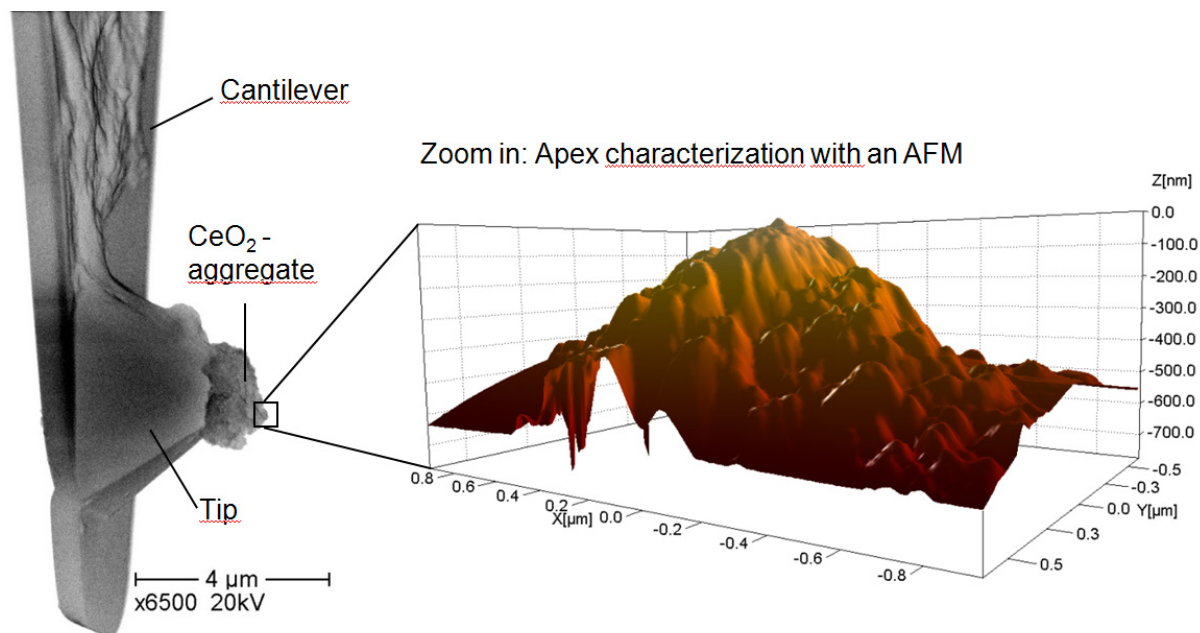


**Figure 4.8** Coated AFM-tip ( $\text{CeO}_2$ , 3.4) mapped with an electron microscope (left) and an AFM image of the reconstructed apex (right).

To analyse the interactions and binding forces between nanoparticles and the cell membrane force distance measurements on living cells using AFM probe tips coated with nanoparticles were performed. The immobilisation of nanoparticles at the cantilevers apex was achieved by an epoxy adhesive. In most cases one primary particle builds the cantilevers apex and therefore allows force measurements between nanoparticles and cells (Figure 4.8).

Taking into account that the cellular uptake processes need a period of time force-distance-curves have been recorded for different dwell times (Figure 4.9).

Furthermore, the binding forces in different cell regions have been analysed with force volume measurements on whole cells ( $\text{CeO}_2$ , 3.2, 3.3, 3.4 area of the nucleus,  $\text{TiO}_2$  1.2 and  $\text{Si}_3\text{N}_4$ -tips additionally on the whole surface). It has been shown that the height signal can be used to identify the cells shape and the nucleus to localise the binding events. The measured binding forces are independent of the position on the cellular surface confirming the assumption of a homogeneous distribution of the affinity of the cell membrane to the nanoparticles as shown in the images (Figure 4.6b).

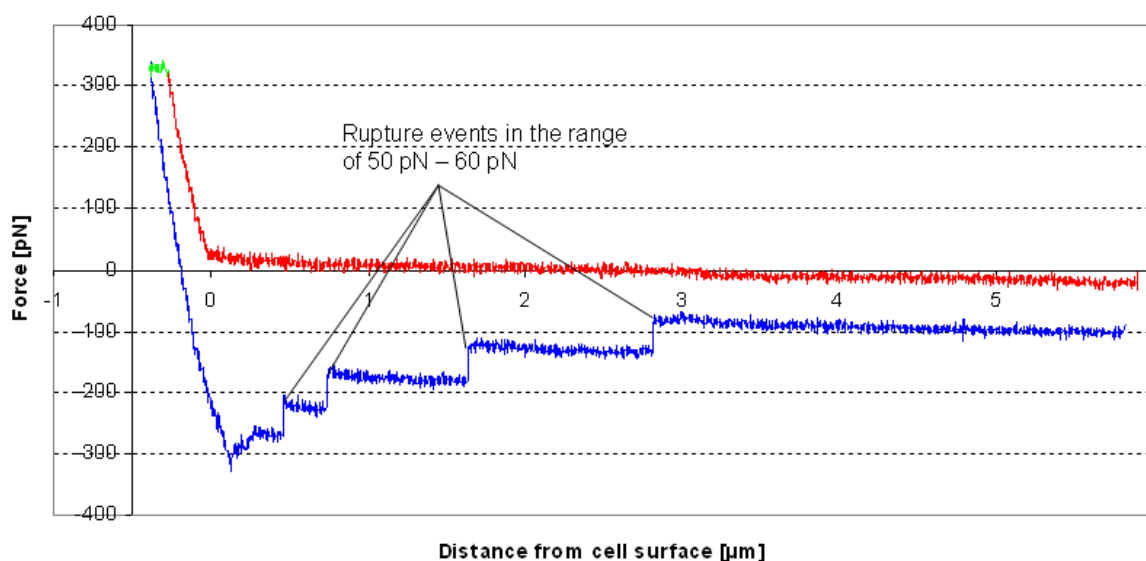


**Figure 4.9** Typical force distance curve for a coated AFM-tip ( $\text{CeO}_2$  3.2) on a living cell with a dwell-time of 30 s. The red curve shows the approach, the green one the tips movement during the contact (dwell-time) and the blue one describes the retraction.

The initial binding of nanoparticles to the cellular surface has been investigated by imaging and force spectroscopy using AFM. The results indicate that the binding-affinity for nanoparticle aggregates is homogeneously distributed on the surface of the cells investigated. To assess if certain cell membrane components bind specifically to the NP used it was necessary to analyse the adhesion force between these particles and whole cells. Force volume measurements offer the possibility to visualise the contours of the cell but in comparison to this height signal the calculated adhesion shows a homogenous distribution. That means that further studies concerning NP-cell-interactions are not restricted to certain areas of the cell and it seems that the measured rupture forces which have comparable values (@ 50 pN) for all investigated NP are membrane and not particle specific. Different results are achieved by the attachment of the adhesion protein fibronectin to a cantilever which leads to significantly larger rupture forces (@ 1 nN). In comparison to known biological membrane interactions the binding of NP to cell surface structures is relatively weak especially concerning the large contact area. This may be important for the binding of agglomerated / aggregated primary NP in solution.

### 4.3 In vitro Test Systems

In this study, the responses of a set of cell lines and coculture systems after exposure to different engineered nanoparticles were determined in vitro. Different widely used endpoints such as cell membrane integrity, the intracellular formation of reactive oxygen species (ROS), cellular metabolic activity and the release of the pro-inflammatory mediator IL-8 were addressed. For standardisation, currently available in vitro toxicity methods were carefully evaluated and SOPs were developed. An overview of the in vitro experiments is given in Annex B.

#### 4.3.1 Method Development and Standardisation

A variety of nanoparticles have recently been shown to interfere with classical in vitro toxicity assays thereby heavily influencing the assay outcome (for review see Kroll et al., 2008;

Lewinski et al., 2008). An appropriate nanoparticle risk assessment will thus require a careful validation of in vitro methods for each material. In this study, the nanoparticles have been characterised in advance regarding their dispersion and interactions in physiological media, their sterility, their endotoxin concentration, and their possible interference with the test systems.

### Adsorption of Lung Surfactant Proteins onto Nanoparticles

As shown in chapter 3, nanoparticles can interact and can be coated with proteins. This coating may influence the reaction of cells onto those particles twofold: on the one hand, particles typically occurring as agglomerates can deagglomerate and can be dispersed down to primary particle size (Schulze et al., 2008). On the other hand, such a protein corona could mask the particle properties, maybe leading to a stealth effect. Both events can lead to an altered cytotoxic pattern of the particles and must be considered in risk assessment of particles entering biological systems.

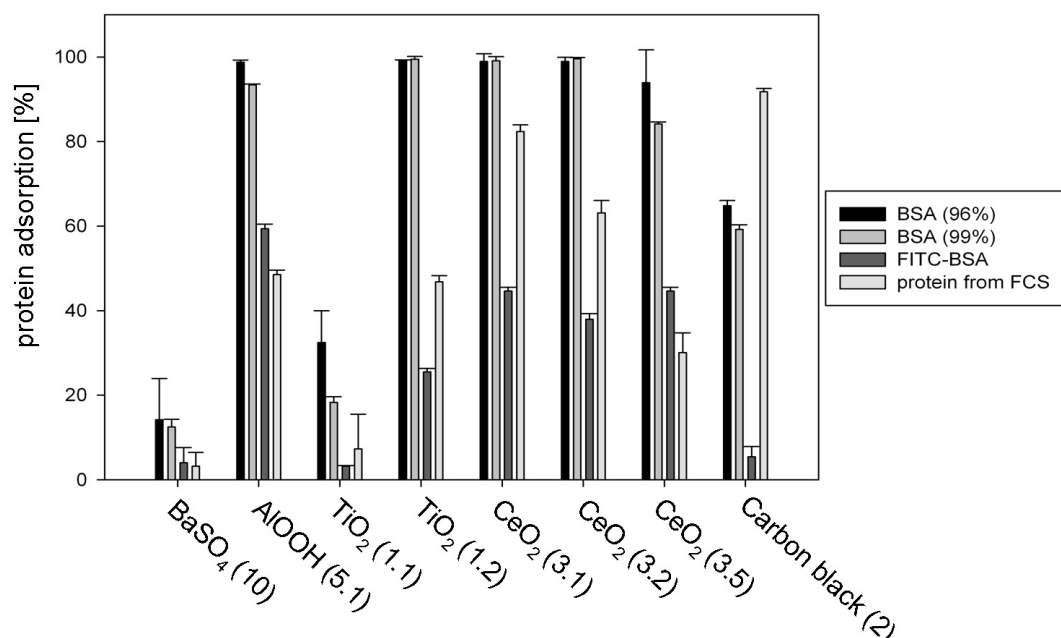


**Figure 4.10** Protein adsorption of different nanoparticles and Protein solutions relative to negative controls (spun off protein solution without nanoparticles) at a nanoparticles:protein relation of 10:1 (w/w): Clearly, the particles reveal different adsorption patterns. Also, the protein affinity to one particle is varying. The adsorption of BSA labelled with a fluorescent dye (FITC-BSA) is decreased (mean + standard deviation).

To address the metal oxide particle-protein interaction, experiments by means of Ultrasound Resonator Technology (in cooperation with TF Instruments), Microcalorimetry and Surface Plasmon Resonance technique were carried out (Cedervall et al., 2007a&b). However, due to sedimentation during measurement these techniques failed. Therefore we provided an indirect proof of these interactions based on BCA assay experiments (Bicinchoninic acid Kit, Sigma-Aldrich). With this test, the protein amount remaining in the supernatant can be determined after dispersing particles in protein solution and spinning them off again.

In the first experiments Bovine Serum Albumine (BSA, different degrees of purity) was used as model protein. Clearly, different particles reveal different protein adsorption (see Figure 4.10). BaSO<sub>4</sub> (10) and TiO<sub>2</sub> (1.1) are adsorbing much less BSA than the rest of the particles

tested. Moreover, no differences are found between the two degrees of purity. For analytical reasons FITC-labelled BSA was tested, too. As shown in Figure 4.10, the adsorption pattern is decreased, whereas the relation of labelled to unlabelled BSA is varying. Additional experiments using protein from Foetal Calf Serum (FCS) further confirmed that protein adsorption clearly depends on the type of protein applied. Within these series different types of CeO<sub>2</sub> showed different affinity to the FCS proteins.

The most prominent pathway for body nanoparticle interaction is via the respiratory tract. Within the lung first contact of nanoparticle systems will occur with the Alveolar Lining Fluid, containing 4 different proteins: surfactant protein A, B, C, and D (SP-A, SP-B, SP-C, and SP-D) (Bissinger and Carlson, 2006). These proteins have special functions: e.g. Sp-A is involved in immunological procedures and in the reabsorption of the Alveolar Lining Fluid into the lung cells (Hartshorn et al., 1998; Hickling et al., 2004; Kishore et al., 2005; Salvador-Morales et al., 2007). Inhaled particles could be dispersed in this thin fluid layer and be coated with these proteins, altering their toxicological qualities. This process was already proven for carbon nanotubes (Salvador-Morales et al., 2006 & 2007). To evaluate these interactions, nanoparticles were incubated with porcine Bronchoalveolar Lavage Fluid (pBALF) in a first step. Again, a different protein adsorption pattern was detected (Figure 4.11, Schulze et al. (2), 2009).

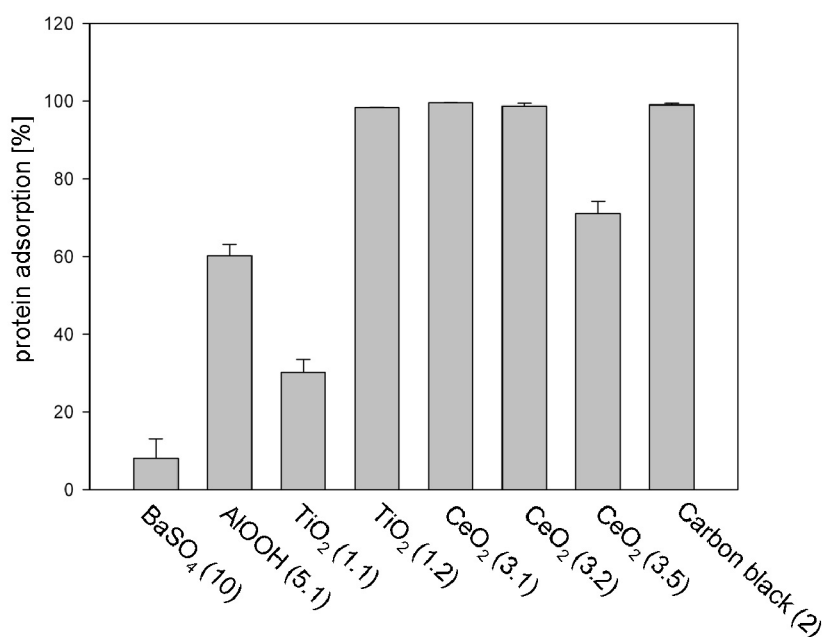


**Figure 4.11** Adsorption of proteins derived from pBALF relative to the negative control (centrifuged pBALF without Nanoparticles) at a nanoparticle:protein relation of 10:1 (w/w): The particles show different adsorption patterns of pBALF-proteins (mean + standard deviation).

To investigate the adsorption of SP-A onto nanoparticles, particles were dispersed in pBALF. After an incubation period of 1 hour the nanoparticles were separated by centrifugation and SP-A was determined in the supernatant and in the pellet. Protein analysis was performed by SDS-PAGE followed by immunoblotting. Figure 4.12 shows the immunoblots of the supernatants and particle pellets.

The adsorption pattern of Sp-A can be divided in 4 subgroups:

**Subgroup 1:** CeO<sub>2</sub> (3.5) and TiO<sub>2</sub> (1.1) (red boxes figure 4.12). Sp-A is found in both supernatant and particle pellet indicating that Sp-A adsorbs partially (weak interaction between SP-A and particle).

**Subgroup 2:** AlOOH (5.1) and BaSO<sub>4</sub> (10) (purple boxes, figure 4.12). Sp-A is totally adsorbed. No more Sp-A can be detected in the supernatant indicating a medium SP-A particle interaction.

**Subgroup 3:** CeO<sub>2</sub> (3.1), CeO<sub>2</sub> (3.2) and TiO<sub>2</sub> (1.2) (light blue boxes, figure 4.12). No Sp-A is found in the supernatant and the Sp-A signal is much lower than for BaSO<sub>4</sub> (10) and AlOOH (5.1). The reason may be that the denaturation procedure prior to SDS-PAGE seems insufficient to detach all the protein adsorbed. Therefore, a strong SP-A particle interaction can be assumed.

**Subgroup 4:** Carbon black (2) (dark blue box, figure 4.12). No Sp-A could be detected neither by the supernatant nor the pellet. The reason may be that Sp-A-particle interaction for carbon black is so strong that the protein is adsorbed totally, but the denaturation procedure does not lead to desorption at all. This indicates a very strong SP-A particle interaction.

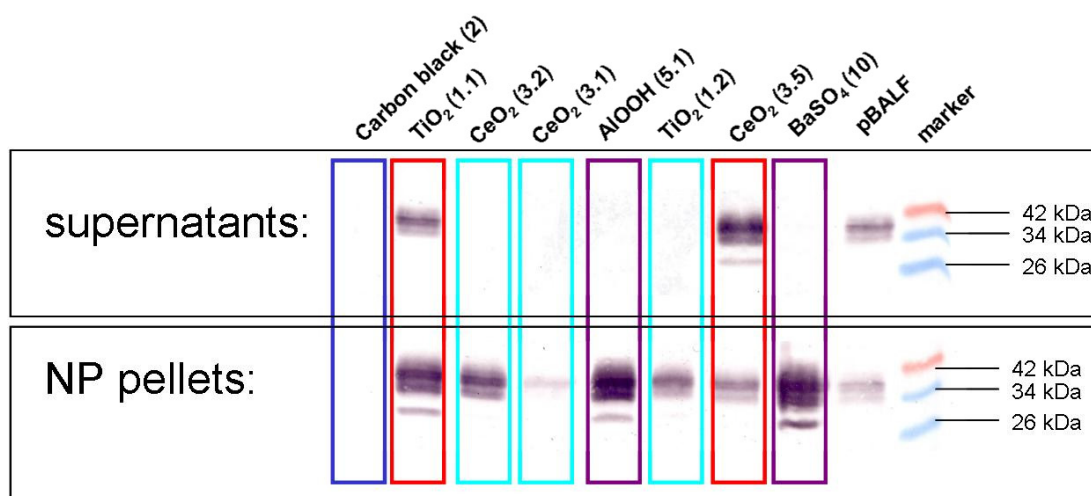


**Figure 4.12** Immunoblot of Sp-A: The adsorption pattern of Sp-A can be divided in 4 subgroups: Subgroup1: weak interaction; CeO<sub>2</sub> (3.5) and TiO<sub>2</sub> (1.1) (red boxes). Subgroup 2: medium interaction; AlOOH (5.1) and BaSO<sub>4</sub> (10) (purple boxes). Subgroup 3: strong interaction; CeO<sub>2</sub> (3.1), CeO<sub>2</sub> (3.2) and TiO<sub>2</sub> (1.2) (light blue boxes). Subgroup 4: very strong interaction; carbon black (2) (dark blue box). pBALF was used as control and was diluted 1:10 relative to the samples.

Further investigations are needed to complete the understanding of protein nanoparticle interaction, in particular also addressing the other lung surfactant proteins and the mechanisms of protein adsorption / desorption, as well as its impact on the interaction between nanoparticles and cells.

## Dispersion of Nanoparticles in Physiological Media

### a) Nanoparticle Dispersions for the Exposure of Standardised Adherent Cell Lines

A detailed description of the dispersion of nanoparticles for the exposure of standardised adherent cell lines is provided in Chapter 3.4 (Dispersion of the NanoCare materials in cell culture media – a challenge).

These results lead to a catalogue of aspects that have to be considered for in vitro cell based assays and were published by Schulze et al. (2008).

The data were used to develop a SOP for nanoparticle dispersion in biological media. The above described SOP and the following SOP for nanoparticle dispersion in surfactant were used for all assays in the project (SOP, see [www.nanopartikel.info](http://www.nanopartikel.info)).

### b) Nanoparticle Dispersions for the Exposure of Acutely Isolated Alveolar Macrophages

Acutely isolated alveolar macrophages (AM) from guinea pigs were used in addition to the work on cell lines (see section 4.3.2). However, to study nanoparticles some adaptations of a published protocol were made which concerned the use of cell culture additives and appropriate particle loading.

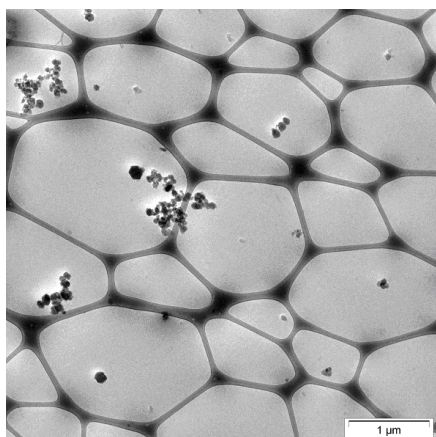


**Figure 4.13** Single particles and small agglomerates of BaSO<sub>4</sub> viewed in a suspension which was allowed to rest for 24 hours (CryoTEM preparation).

As already shown in this section, proteins stabilise nanoparticles in biological fluids, i.e., they partly prevent agglomeration, at least in high concentration. However, inhaled particles inside intact lung alveoli are not primarily in contact with serum proteins. Instead they most likely contact and/or adsorb components of the lung surfactant layer, the most frequent molecules of which are phospholipids. Thus, initial work focussed on whether or not phosphatidylcholine (PC), as an amphiphilic molecule, could be used to stabilize nanoparticles. By means of fluorescent PC (BODIPY-PC) and further binding studies it could be shown that PC binds to suspended particles (Wiemann et al., 2009). Biological tests furthermore showed that a concentration of 0.025 mg PC/ml cell culture neither interfered nor masked the cytotoxic effect of quartz DQ12 particles. Use of PC was therefore incorporated into a standard operation procedure (SOP) to prepare particle suspension for experiments on macrophages. This SOP includes ultrasonic treatment and additional work was carried out to describe suspensions of nanostructured materials by various techniques (dynamic light scattering, SEM, kryo-TEM, and Analytical Ultracentrifugation). In general, brief ultrasonic treatment (10 s) was necessary to suspend nanoparticle powders in cell culture medium but did not

decompose aggregated testing materials into nanoparticles. Nevertheless some nanoparticles (especially from BaSO<sub>4</sub> and CeO<sub>2</sub>) remained suspended in the cell culture supernatant when particle suspensions were allowed to stand for 24 hours (Figure 4.13).

According to this characterisation, in vitro experiments on macrophages were conducted with a major fraction of nanostructured agglomerated materials able to sediment onto cultured cells and a minor fraction of suspended nanoparticles. It should be pointed out that all NanoCare materials, when tested in an air-borne state were found to be largely aggregated and agglomerated (see section 5). In the light of these results together with the knowledge of uptake and distribution of TiO<sub>2</sub> and AlOOH inside lungs (sections 4.4.2 and 4.4.3) application of agglomerated particles appeared highly justified to measure cytotoxic effects of nanostructured materials on lung macrophages.

In the next step an appropriate and meaningful dosage of these particles for in vitro experiments had to be found. It is well known that a healthy, non-particle-laden rat lung contains a total of 10x10<sup>6</sup> to 13x10<sup>6</sup> alveolar macrophages (Rehn et al., 1991). It may thus be calculated that a lung burden of e.g. 1.2 mg particles corresponds to a mean cellular dose of 92-120 pg/alveolar macrophage (AM). These assumptions are pretty much in line with the major findings outlined in section 4.4.3: alveolar macrophages lavaged from rat lungs after inhalation of AlOOH (5.1) and AlOOH (5.2) contained 60 and 92 pg/AM, respectively, while cumulative lung burdens amounted to 1.7 and 2.7 mg. As this concentration evoked inflammatory effects (see section 4.4.3), comparative in vitro studies on AM were carried out in the range of 15-120 pg/AM. Further experiments such as time lapse video microscopy accompanied by quantitative chemical analyses of ingested material were carried out to verify that particle doses applied were indeed taken up by AM.

Taken together, an in vitro method was developed for the application of nanostructured materials to alveolar macrophages. The method quantitatively and qualitatively paralleled the loading of lung macrophages seen after inhalation exposure to TiO<sub>2</sub> or AlOOH (see section 4.4.2) and was designed to compare biological activities of NanoCare particles in vitro and in vivo (see section 4.5).

#### Preparation of Nanoparticles for Biological Testing

First, different methods for material sterilisation (antibiotics, NaN<sub>3</sub>, autoclaving, γ irradiation) were tested since engineered nanoparticles are not produced for sterile cell culture conditions (Schulze et al., 2008). The contamination with gram-negative bacteria leads to the enrichment of endotoxin, a component of the cell wall of these micro-organisms. Therefore, the concentration of endotoxin was determined in the 24 nanoparticle powders and dispersions that were selected for toxicity assessment.

None of the samples contained detectable amounts of endotoxin; however, some surface modifiers as well as zinc oxide nanoparticles interfered with the enzymatic endotoxin detection reaction.

#### Reliability of in vitro Assays for Nanoparticle Toxicity Evaluation

All types of nanoparticles were tested for a possible interference with the in vitro toxicity test systems. Furthermore, the in vitro toxicity assays performed in microplate formats were also tested for their suitability to study biological effects in all cell lines selected for this study. Dispersions of Carbon Black at concentrations of 50 µg/cm<sup>2</sup> were shown to interfere with optical detections in LDH, ROS and MTT assays (Kroll and Schnekenburger, manuscript in preparation). The MTT test was found to be generally inapplicable to Carbon Black as the particles may not be sufficiently removed from the test system and alter the read out of the

colour based test. Therefore, cell viability tests with Carbon Black were performed using WST as a substrate. The detection of calcium influx and the formation of nitrogen monoxide were abandoned, as both could not be reproducibly realised with all cell lines.

### Characterisation of Cell Lines

**Table 4.2** Cell lines and Culture media

Cell line	Species	Origin	Provider	Catalogue number	Culture medium
A549	<i>H. sapiens</i>	Lung adenocarcinoma, alveolar epithelium, type II pneumocyte like	ATCC	CCL-185	DMEM 10 % FCS Gold 4 mM L-glutamine
CaCo-2	<i>H. sapiens</i>	Colon carcinoma, Colon epithelium like	ATCC	HTB-37™	DMEM 20 % FCS Gold 4 mM L-glutamine
CaLu3	<i>H. sapiens</i>	Lung adenocarcinoma	ATCC	HTB-55	RPMI 10 % FCS Gold 2 mM L-glutamine 1 mM sodiumpyrovate
HaCaT	<i>H. sapiens</i>	Skin, keratinocytes	CLS	-	DMEM 10 % FCS Gold 4 mM L-glutamine
MDCK (NBL-2)	<i>C. familiaris</i>	Kidney, epithelium like	ATCC	CCL-34	RPMI 10 % FCS Gold 2 mM L-glutamine 1 mM sodiumpyrovate
MDCK II	<i>C. familiaris</i>	Kidney, epithelium like	ECACC	00062107	MEM 5 % FCS Gold 2 mM L-glutamine
NIH-3T3	<i>M. musculus</i>	Embryo, fibroblasts	DSMZ	ACC 59	DMEM (without L-Glutamine) 10 % FCS Gold
NRK-52E	<i>R. norvegicus</i>	Kidney, epithelium like	DSMZ	ACC 199	DMEM 10 % FCS Gold 4 mM L-glutamine
RAW 264.7	<i>R. norvegicus</i>	Macrophages, AML virus transformed	ATCC	TIB-71	DMEM 10 % FCS Gold 4 mM L-glutamine
RLE-6TN	<i>R. norvegicus</i>	Lung, alveolar epithelium like	ATCC	CRL-2300	RPMI 10 % FCS Gold 2 mM L-glutamine 1 mM sodiumpyrovate
T84	<i>H. sapiens</i>	Colon carcinoma, colon epithelium like	ATCC	CCL-248	DMEM:F12 10 % FCS Gold 2.5 mM L-glutamine
MonoMac6	<i>H. sapiens</i>	monocyte-macrophage-like leucaemia cells	DSMZ	ACC 124	RPMI 10 % FCS Gold 2 mM L-glutamine 1 mM sodiumpyrovate Insulin-Transferrin-Selenium (Gibco)

In this project, cell lines representing different routes of exposure were selected (Table 4.2). The human cell lines were typed by the DSMZ (German Collection of Micro-organisms and Cell Cultures) to confirm their identity. Cell lines were freshly ordered, expanded, and deep frozen in aliquots to serve as standardised stock for the duration of the project. All cells in culture were regularly checked for infection with different mycoplasma species. Cells were maintained at 37°C with 5% CO<sub>2</sub> in a humidified incubator.

The identity of all cell human lines was confirmed by the DSMZ and the cell lines used were free of mycoplasma.

### 4.3.2 In vitro Testing

#### In vitro Testing of Engineered Nanoparticles Using two Different Cell Lines and Multiple Cytotoxicity Assays

Cell lines A549 and RAW 264.7 were used in experiments with a set of different nanoparticles at 0.5, 5, 25 and 50 µg/cm<sup>2</sup> for 24, 48 and 72 hours (from 1 hour up to 72 hours). The results of the studies are summarised in Table 4.3.

**Table 4.3** Biological effects of the tested nanoparticles in vitro. Used material with reference No (see also Table 3.1), measured biological effects (↓: decrease, ↑: increase), cell lines, low effect level (LOEL) of particle exposure, and time of exposure.

Material	No	Biological effects	Cell line	LOEL	time
TiO <sub>2</sub> (reference material)	1.2	metabolic activity ↓	A549	25 µg/cm <sup>2</sup>	24, 48, 72 h
		LDH release	A549	50 µg/cm <sup>2</sup>	24, 48, 72 h
		ROS	A549	1,5 µg/cm <sup>2</sup>	1 h
		Glutathion ↓	A549	25 µg/cm <sup>2</sup>	6 h
		HO-1 Expression ↑	RAW 264.7	1 µg/cm <sup>2</sup>	6 h
		COX-2 Expression ↑	RAW 264.7	0,1 µg/cm <sup>2</sup>	6 h
		Secretion of IL-8	A549	25 µg/cm <sup>2</sup>	24, 48, 72 h
TiO <sub>2</sub> -40	1.3	metabolic activity ↓	A549	no effect	24 h
		LDH release		25 µg/cm <sup>2</sup>	
		Secretion of IL-8		25 µg/cm <sup>2</sup>	
TiO <sub>2</sub> -70	1.4	metabolic activity ↓	A549	no effect	24 h
		LDH release		50 µg/cm <sup>2</sup>	
		Secretion of IL-8		25 µg/cm <sup>2</sup>	
TiO <sub>2</sub> -120	1.5	metabolic activity ↓	A549	50 µg/cm <sup>2</sup>	24 h
		LDH release		25 µg/cm <sup>2</sup>	24 h
		Secretion of IL-8		25 µg/cm <sup>2</sup>	24 h
Carbon Black (reference material)	2	metabolic activity ↓	A549	25 µg/cm <sup>2</sup>	24, 48, 72 h
		LDH- release	A549	25 µg/cm <sup>2</sup>	24, 48, 72 h
		ROS	A549	0,5 µg/cm <sup>2</sup>	1 h
		Glutathion ↓	A549	5 µg/cm <sup>2</sup>	6 h
		HO-1 Expression ↑	RAW 264.7	1 µg/cm <sup>2</sup>	6 h
		COX-2 Expression ↑	RAW 264.7	0,1 µg/cm <sup>2</sup>	6 h
		Secretion of IL-8	A549	50 µg/cm <sup>2</sup>	24 h
				5 µg/cm <sup>2</sup>	48,72 h

Material	No	Biological effects	Cell line	LOEL	time
CeO <sub>2</sub> -A	3.1	metabolic activity ↓	A549	25 µg/cm <sup>2</sup>	72 h
		LDH release	A549	25 µg/cm <sup>2</sup>	72 h
		ROS	A549	6,25 µg/cm <sup>2</sup>	1 h
		Glutathion ↓	A549	25 µg/cm <sup>2</sup>	6 h
		HO-1 Expression ↑	RAW 264.7	1 µg/cm <sup>2</sup>	6 h
		COX-2 Expression ↑	RAW 264.7	1 µg/cm <sup>2</sup>	6 h
		Secretion of IL-8	A549	25 µg/cm <sup>2</sup>	72 h
CeO <sub>2</sub> -B	3.2	metabolic activity ↓	A549	25 µg/cm <sup>2</sup>	72 h
		LDH release	A549	25 µg/cm <sup>2</sup>	72 h
		ROS	A549	25 µg/cm <sup>2</sup>	1 h
		Glutathion ↓	A549	5 µg/cm <sup>2</sup>	6 h
		HO-1 Expression ↑	RAW 264.7	0,1 µg/cm <sup>2</sup>	6 h
		COX-2 Expression ↑	RAW 264.7	0,1 µg/cm <sup>2</sup>	6 h
		Secretion of IL-8	A549	25 µg/cm <sup>2</sup>	48 h
				5 µg/cm <sup>2</sup>	72 h
CeO <sub>2</sub> -C	3.3	metabolic activity ↓	A549	25 µg/cm <sup>2</sup>	72 h
		LDH release	A549	25 µg/cm <sup>2</sup>	72 h
		ROS	A549	25 µg/cm <sup>2</sup>	1 h
		Glutathion ↓	A549	25 µg/cm <sup>2</sup>	6 h
		COX-2 Expression ↑	RAW 264.7	10 µg/cm <sup>2</sup>	6 h
		Secretion of IL-8	A549	25 µg/cm <sup>2</sup>	48 h
CeO <sub>2</sub> -D	3.4	metabolic activity ↓		25 µg/cm <sup>2</sup>	24 h
				50 µg/cm <sup>2</sup>	48 h
				5 µg/cm <sup>2</sup>	72 h
		LDH release	A549	25 µg/cm <sup>2</sup>	72 h
		ROS		25 µg/cm <sup>2</sup>	1 h
		Glutathion ↓		25 µg/cm <sup>2</sup>	1 h
		Secretion of IL-8		25 µg/cm <sup>2</sup>	48 h
CeO <sub>2</sub>	3.5	LDH release	A549	50µg/cm <sup>2</sup> (<10%)	48, 72 h
		Glutathion ↓	A549	25 µg/cm <sup>2</sup>	6 h
		HO-1 Expression ↑	RAW 264.7	1 µg/cm <sup>2</sup>	6 h
		COX-2 Expression ↑	RAW 264.7	1 µg/cm <sup>2</sup>	6 h
		Secretion of IL-8	A549	50 µg/cm <sup>2</sup>	48, 72 h
AlOOH (Boehmite I)	5.1	LDH release		50 µg/cm <sup>2</sup>	72 h
		Glutathion ↓	A549	5 µg/cm <sup>2</sup>	6 h
		Secretion of IL-8		50 µg/cm <sup>2</sup>	24, 48, 72 h
AlOOH (Boehmite II)	5.2	metabolic activity ↓	A549	25 µg/cm <sup>2</sup>	24, 48, 72 h
		LDH release	A549	50µg/cm <sup>2</sup> (<10%)	72 h
		HO-1 Expression ↑	RAW 264.7	10 µg/cm <sup>2</sup>	6 h
		Secretion of IL-8	A549	50 µg/cm <sup>2</sup>	24 h
ZrO <sub>2</sub>	8.2	LDH release	A549	50µg/cm <sup>2</sup> (<10%)	48, 72 h
		Glutathion ↓	A549	1 µg/cm <sup>2</sup>	6 h
		HO-1 Expression ↑	RAW 264.7	10 µg/cm <sup>2</sup>	6 h
		COX-2 Expression ↑	RAW 264.7	0,1 µg/cm <sup>2</sup>	6 h
ZnO	9	metabolic activity ↓		25 µg/cm <sup>2</sup>	24, 48, 72 h
		LDH release		50µg/cm <sup>2</sup> (<10%)	24 h
			A549	25 µg/cm <sup>2</sup>	48, 72 h
		ROS		25 µg/cm <sup>2</sup>	1 h
		Glutathion ↓		1 µg/cm <sup>2</sup>	6 h
		Secretion of IL-8		5 µg/cm <sup>2</sup>	24, 48, 72 h

Material	No	Biological effects	Cell line	LOEL	time
BaSO <sub>4</sub>	10	metabolic activity ↓	A549	50 µg/cm <sup>2</sup>	24 h
		LDH release	A549	50µg/cm <sup>2</sup> (<10%)	24, 48, 72 h
		ROS	A549	25 µg/cm <sup>2</sup>	1 h
		Glutathion ↓	A549	5 µg/cm <sup>2</sup>	6 h
		HO-1 Expression ↑	RAW 264.7	1 µg/cm <sup>2</sup>	6 h
		Secretion of IL-8	A549	5 µg/cm <sup>2</sup>	24, 48, 72 h
SrCO <sub>3</sub> 1	11.1	metabolic activity ↓	A549	no effect	72 h
		LDH release		25 µg/cm <sup>2</sup>	
		Secretion of IL-8		25 µg/cm <sup>2</sup>	
SrCO <sub>3</sub> 2	11.2	metabolic activity ↓	A549	25 µg/cm <sup>2</sup>	72 h
		LDH release		no effect	
		Secretion of IL-8		0,5 µg/cm <sup>2</sup>	

### Key Results

**Viability:** A decreasing metabolic activity is an indicator for low cell viability. TiO<sub>2</sub> (1.2), Carbon Black (2), AlOOH (5.2), CeO<sub>2</sub>-D (3.4) and ZnO (9) showed effects (with WST-1 assay) at 25µg/cm<sup>2</sup> for 24h. No effect was seen with TiO<sub>2</sub>-40 (1.3), TiO<sub>2</sub>-70 (1.4) and SrCO<sub>3</sub>-2 (11.2).

**LDH release:** A release of lactate dehydrogenase (LDH), an indicator of plasma membrane integrity, was observed with Carbon Black (2), TiO<sub>2</sub>-40 (1.3) and TiO<sub>2</sub>-120 (1.5) after 24 hours at a conc. of 25 µg/cm<sup>2</sup>. No LDH was measured with SrCO<sub>3</sub>-2 (11.2).

**ROS:** The formation of intracellular ROS was measured by monitoring the increasing fluorescence of 2',7'-dichlorofluorescein (DCF). 0,5 µg/cm<sup>2</sup> of Carbon Black (2) and 1,5 µg/cm<sup>2</sup> of TiO<sub>2</sub> (1.2) caused ROS.

**Glutathion:** The cellular GSH and glutathione disulphide (GSSG) contents were measured after 6 hours, the strongest decrease was detected after ZnO and ZrO<sub>2</sub> incubation (1 µg/cm<sup>2</sup>, 8.2).

**IL-8 release** was measured in order to quantify the pro-inflammatory response of A549 cells to treatment with nanoparticles: the strongest effects were measured for ZnO (9) and BaSO<sub>4</sub> (10) at a concentration of 5 µg/cm<sup>2</sup> after 24 h; TiO<sub>2</sub> modifications (40 (1.3), 120 (1.5)) showed an effect after 24 hours only after incubation with ≥ 25 µg/cm<sup>2</sup>; 0,5 µg/cm<sup>2</sup> of SrCO<sub>3</sub>-2 (11.2) was sufficed to lead to an increased IL-8 release after 48h.

Expression of the anti-oxidative enzymes hemeoxygenase-1 (**HO-1**) and cyclooxygenase-2 (**Cox-2**) was investigated after exposure of the murine macrophage cell line RAW264.7 to nanoparticle dispersions. An increase of HO-1 and COX-2 expression was analysed after 6 hours of incubation. A concentration of 0,1 µg/cm<sup>2</sup> of CeO<sub>2</sub>-B (3.2) showed an increase of these indicators. TiO<sub>2</sub> (1.2), Carbon Black (2), CeO<sub>2</sub>-A (3.1), CeO<sub>2</sub> (3.5) and BaSO<sub>4</sub> (10) showed an effect at particle concentration of 1 µg/cm<sup>2</sup>. An increase of COX-2 was found after treatment with TiO<sub>2</sub> (1.2), Carbon Black (2), CeO<sub>2</sub>-B (3.2) and ZrO<sub>2</sub> (8.2) at 0,1 µg/cm<sup>2</sup> and for CeO<sub>2</sub>-A (3.1) and CeO<sub>2</sub> (3.5) at a concentration of 1 µg/cm<sup>2</sup>.

These results show that there are differences in biological effects of the investigated materials depending on their special character (Table 4.3) and that there are also differences in sensitivity of the investigated biological parameters.

### In vitro Testing of Engineered Nanoparticles Using a Set of Different Cell Lines

These experiments were designed to evaluate the cell type specific sensitivity to nanoparticle exposure. Up to eleven cell lines representing different routes and different lines of exposure (see Table 4.2) were exposed to 24 different nanoparticles (see Table 4.4). Cellular processes such as rapid oxidative stress response, metabolic activity and cell death were determined by standardised LDH release (cell death), DCF (ROS formation) and MTT (metabolic activity) assays. All tests were performed with nanoparticle concentrations of 0.01  $\mu\text{g}/\text{cm}^2$ , 0.1  $\mu\text{g}/\text{cm}^2$ , 1  $\mu\text{g}/\text{cm}^2$ , 5  $\mu\text{g}/\text{cm}^2$ , 10  $\mu\text{g}/\text{cm}^2$  and standardised according to newly developed SOPs. Cells were used at  $3 \times 10^5$  cells/well which corresponds at a concentration of 10  $\mu\text{g}/\text{cm}^2$  to 10.7 pg/cell or 10.7  $\mu\text{g}/10^6$  cells (well area 0.32  $\text{cm}^2$ ). Table 4.4 summarises the results from all cell lines and all nanoparticles tested.

**Table 4.4** Results of the in vitro tests for oxidative stress (ROS release), cell death (LDH release), and metabolic activity (MTT test). The reference material ( $\text{TiO}_2$ , 1.2), Carbon Black (2) and ZnO (9) were tested with all cell lines listed in Table 4.2 except for Mono-Mac-6. All other materials were tested with the cell lines listed in Table 4.2 except for human carcinoma cell line T84 and Mono-Mac-6. ZnO nanoparticles (9) were tested with all concentrations mentioned above in addition to nanoparticle concentrations of 7.5 and 2.5  $\mu\text{g}/\text{cm}^2$ .

Material	No	Biological effects	Cell line	LOEL	time
$\text{TiO}_2$	1.1a	metabolic activity (MTT)	all 10 cell lines	no effect	24 h
		LDH release	all 10 cell lines	no effect	24 h
		ROS formation	all 10 cell lines	no effect	1 h
$\text{TiO}_2$	1.1b	metabolic activity (MTT)	all 10 cell lines	no effect	24 h
		LDH release	all 10 cell lines	no effect	24 h
		ROS formation	all 10 cell lines	no effect	1 h
$\text{TiO}_2$ (reference material)	1.2	metabolic activity (MTT)	all 11 cell lines	no effect	24 h
		LDH release	all 11 cell lines	no effect	24 h
		ROS formation	A549	5 $\mu\text{g}/\text{cm}^2$	1 h
			CaCo2	5 $\mu\text{g}/\text{cm}^2$	
			HaCaT	5 $\mu\text{g}/\text{cm}^2$	
			MDCK	5 $\mu\text{g}/\text{cm}^2$	
			MDCK II	no effect	
			NIH3T3	5 $\mu\text{g}/\text{cm}^2$	
			NRK52E	5 $\mu\text{g}/\text{cm}^2$	
			RAW267.4	10 $\mu\text{g}/\text{cm}^2$	
	RLE-6TN	5 $\mu\text{g}/\text{cm}^2$			
	T84	10 $\mu\text{g}/\text{cm}^2$			
	CaLu3	10 $\mu\text{g}/\text{cm}^2$			
Carbon Black (reference material)	2	LDH release	all 11 cell lines	No effect	24 h
		ROS formation	all 11 cell lines	5 $\mu\text{g}/\text{cm}^2$	1 h

Material	No	Biological effects	Cell line	LOEL	time
CeO <sub>2</sub> -A	3.1	metabolic activity (MTT)	all 10 cell lines	no effect	24 h
		LDH release ROS formation	all 10 cell lines A549 CaCo2 HaCaT MDCK MDCK II NIH3T3 NRK52E RAW267.4 RLE-6TN CaLu3	no effect 10 µg/cm <sup>2</sup> 1 µg/cm <sup>2</sup> 10 µg/cm <sup>2</sup> 10 µg/cm <sup>2</sup> no effect 10 µg/cm <sup>2</sup> 10 µg/cm <sup>2</sup> 10 µg/cm <sup>2</sup> 10 µg/cm <sup>2</sup> no effect	24 h
CeO <sub>2</sub> -B	3.2	metabolic activity (MTT)	all 10 cell lines	no effect	24 h
		LDH release ROS formation	all 10 cell lines A549 CaCo2 HaCaT MDCK MDCK II NIH3T3 NRK52E RAW267.4 RLE-6TN CaLu3	no effect no effect no effect 10 µg/cm <sup>2</sup> 10 µg/cm <sup>2</sup> no effect 10 µg/cm <sup>2</sup> 10 µg/cm <sup>2</sup> 10 µg/cm <sup>2</sup> no effect no effect	24 h 1 h
CeO <sub>2</sub> -C	3.3	metabolic activity (MTT)	all 10 cell lines	no effect	24 h
		LDH release ROS formation	all 10 cell lines A549 CaCo2 HaCaT MDCK MDCK II NIH3T3 NRK52E RAW267.4 RLE-6TN CaLu3	no effect 10 µg/cm <sup>2</sup> 10 µg/cm <sup>2</sup> 10 µg/cm <sup>2</sup> 10 µg/cm <sup>2</sup> no effect 10 µg/cm <sup>2</sup> 10 µg/cm <sup>2</sup> 10 µg/cm <sup>2</sup> no effect no effect	24 h 1 h
CeO <sub>2</sub> -D	3.4	metabolic activity (MTT) LDH release ROS formation	all 10 cell lines all 10 cell lines all 10 cell lines	no effect no effect no effect	24 h 24 h 1 h
CeO <sub>2</sub>	3.5	metabolic activity (MTT) LDH release ROS formation	all 10 cell lines all 10 cell lines all 10 cell lines	no effect no effect no effect	24 h 24 h 1 h
AIOOH (Boehmite I)	5.1	metabolic activity (MTT) LDH release ROS formation	all 10 cell lines all 10 cell lines all 10 cell lines	no effect no effect no effect	24 h 24 h 1 h
AIOOH (Boehmite II)	5.2	metabolic activity (MTT) LDH release ROS formation	all 10 cell lines all 10 cell lines all 10 cell lines	no effect no effect no effect	24 h 24 h 1 h

Material	No	Biological effects	Cell line	LOEL	time
Ti-Zr Mixed Oxide 1	6.1	metabolic activity (MTT)	all 10 cell lines	no effect	24 h
		LDH release	all 10 cell lines	no effect	24 h
		ROS formation	all 10 cell lines	no effect	1 h
Ti-Zr Mixed Oxide 2	6.2	metabolic activity (MTT)	all 10 cell lines	no effect	24 h
		LDH release	all 10 cell lines	no effect	24 h
		ROS formation	all 10 cell lines	no effect	1 h
Ti-Zr Mixed Oxide 3	6.3	metabolic activity (MTT)	all 10 cell lines	no effect	24 h
		LDH release	all 10 cell lines	no effect	24 h
		ROS formation	A549	10 µg/cm <sup>2</sup>	1 h
			CaCo2	no effect	
			HaCaT	10 µg/cm <sup>2</sup>	
			MDCK	10 µg/cm <sup>2</sup>	
			MDCK II	no effect	
			NIH3T3	10 µg/cm <sup>2</sup>	
			NRK52E	10 µg/cm <sup>2</sup>	
			RAW267.4	10 µg/cm <sup>2</sup>	
	RLE-6TN	no effect			
	CaLu3	no effect			
Al-Ti-Zr Mixed Oxide 1	7.1	metabolic activity (MTT)	all 10 cell lines	no effect	24 h
		LDH release	all 10 cell lines	no effect	24 h
		ROS formation	all 10 cell lines	no effect	1 h
Al-Ti-Zr Mixed Oxide 2	7.2	metabolic activity (MTT)	all 10 cell lines	no effect	24 h
		LDH release	all 10 cell lines	no effect	24 h
		ROS formation	all 10 cell lines	no effect	1 h
Al-Ti-Zr Mixed Oxide 3	7.3.	metabolic activity (MTT)	all 10 cell lines	no effect	24 h
		LDH release	all 10 cell lines	no effect	24 h
		ROS formation	all 10 cell lines	no effect	1 h
ZrO <sub>2</sub>	8.1	metabolic activity (MTT)	all 10 cell lines	no effect	24 h
		LDH release	all 10 cell lines	no effect	24 h
		ROS formation	all 10 cell lines	no effect	1 h
ZrO <sub>2</sub>	8.2	metabolic activity (MTT)	all 10 cell lines	no effect	24 h
		LDH release	all 10 cell lines	no effect	24 h
		ROS formation	all 10 cell lines	no effect	1 h
ZrO <sub>2</sub>	8.3	metabolic activity (MTT)	all 10 cell lines	no effect	24 h
		LDH release	all 10 cell lines	no effect	24 h
		ROS formation	all 10 cell lines	no effect	1 h

Material	No	Biological effects	Cell line	LOEL	time
ZnO	9	metabolic activity (MTT)	A549	5 µg/cm <sup>2</sup>	24 h
			CaCo2	7.5 µg/cm <sup>2</sup>	
			HaCaT	5 µg/cm <sup>2</sup>	
			MDCK	5 µg/cm <sup>2</sup>	
			MDCK II	5 µg/cm <sup>2</sup>	
			NIH3T3	5 µg/cm <sup>2</sup>	
			NRK52E	2.5 µg/cm <sup>2</sup>	
			RAW267.4	5 µg/cm <sup>2</sup>	
			RLE-6TN	5 µg/cm <sup>2</sup>	
			CaLu3	7.5 µg/cm <sup>2</sup>	
			T84	7.5 µg/cm <sup>2</sup>	
	LDH release	A549	10 µg/cm <sup>2</sup>	24 h	
		CaCo2	7.5 µg/cm <sup>2</sup>		
		HaCaT	5 µg/cm <sup>2</sup>		
		MDCK	5 µg/cm <sup>2</sup>		
		MDCK II	5 µg/cm <sup>2</sup>		
		NIH3T3	5 µg/cm <sup>2</sup>		
		NRK52E	5 µg/cm <sup>2</sup>		
		RAW267.4	5 µg/cm <sup>2</sup>		
		RLE-6TN	5 µg/cm <sup>2</sup>		
		CaLu3	7.5 µg/cm <sup>2</sup>		
		T84	7.5 µg/cm <sup>2</sup>		
		ROS formation	all 11 cell lines	no effect	1 h
BaSO <sub>4</sub>	10	metabolic activity (MTT)	9 cell lines	no effect	24 h
			NIH-3T3	1 µg/cm <sup>2</sup>	
		LDH release	all 10 cell lines	no effect	24 h
		ROS formation	all 10 cell lines	no effect	1 h
SrCO <sub>3</sub> 1	11.1	metabolic activity (MTT)	all 10 cell lines	no effect	24 h
			all 10 cell lines	no effect	24 h
		LDH release	all 10 cell lines	no effect	1 h
		ROS formation	all 10 cell lines	no effect	1 h
SrCO <sub>3</sub> 2	11.2	metabolic activity (MTT)	all 10 cell lines	no effect	24 h
			all 10 cell lines	no effect	24 h
		LDH release	all 10 cell lines	no effect	1 h
		ROS formation	all 10 cell lines	no effect	1 h

## Key Results

Caspase-3 is a key regulator of apoptosis as its activation inevitably leads to programmed cell death. To investigate the influence of nanoparticle dispersions on apoptosis, eight cell lines were tested for the activation of Caspase-3 after exposure to five selected nanoparticles (Table 4.5). Furthermore, the integrity of cell-cell contacts in monolayers of MDCK II and NRK52E cells in the presence of five selected nanoparticles was studied. A certain type of cell-cell contacts, so-called tight junctions prevent the diffusion of ions across cell layers and thereby establish an electrical resistance across cell monolayers. This electrical resistance is referred to as TransEpithelial Electrical Resistance (TEER). While TiO<sub>2</sub> (1.2), Carbon Black (2), and a mixed oxide (6.3) provoked the formation of ROS (Table 4.4), they induced neither Caspase-3 activity nor a change in TEER. Zirconium dioxide (8.1) did not affect ROS formation, metabolic activity, and cell death as shown above (Table 4.4) and behaved equally inert regarding apoptosis and TEER (Table 4.5). On the other hand, ZnO nanoparticles (9) increased Caspase-3 activity in six of eight cell lines tested at a

concentration of 10  $\mu\text{g}/\text{cm}^2$  and dramatically decreased the transepithelial electrical resistance of MDCK II and NRK52E cells at a concentration of 7.5  $\mu\text{g}/\text{cm}^2$  (Table 4.5).

**Table 4.5** Results of the in vitro tests for apoptosis (Caspase-3) and transepithelial electrical resistance (TEER). Caspase-3 activity was tested with the cell lines A549, CaCo2, HaCaT, MDCK II, NIH-3T3, NRK52E, RAW264.7, RLE-6TN with particles concentrations of 0.1, 1, 10  $\mu\text{g}/\text{cm}^2$ . Transepithelial resistance was measure with MDCK II and NRK52E cell and particle concentrations of 10 and 7.5  $\mu\text{g}/\text{cm}^2$ .

Material	No	Biological effects	Cell line	Effect	time
TiO <sub>2</sub> (reference material)	1.2	Caspase-3 activity TEER	all 8 cell lines all 2 cell lines	no effect no effect	24 h 24 h
Carbon Black (reference material)	2	Caspase-3 activity TEER	all 8 cell lines all 2 cell lines	no effect no effect	24 h 24 h
Ti-Zr Mixed Oxide 3	6.3	Caspase-3 activity TEER	all 8 cell lines all 2 cell lines	no effect no effect	24 h 24 h
ZrO <sub>2</sub>	8.1	Caspase-3 activity TEER	all 8 cell lines all 2 cell lines	no effect no effect	24 h 24 h
ZnO	9	Caspase-3 activity  TEER	A549 CaCo2 HaCaT MDCK II NIH-3T3 NRK52E RAW264.7 RLE-6TN MDCK II NRK52E	no effect no effect 10 $\mu\text{g}/\text{cm}^2$ 10 $\mu\text{g}/\text{cm}^2$ 10 $\mu\text{g}/\text{cm}^2$ 10 $\mu\text{g}/\text{cm}^2$ 10 $\mu\text{g}/\text{cm}^2$ 10 $\mu\text{g}/\text{cm}^2$ 10 $\mu\text{g}/\text{cm}^2$ 7.5 $\mu\text{g}/\text{cm}^2$ 7.5 $\mu\text{g}/\text{cm}^2$	24 h  24 h

### Key results

Only a small fraction of the 24 types of nanoparticles examined showed a detectable biological activity when used in concentrations ranging from 0.1 to 10  $\mu\text{g}/\text{cm}^2$  in a broad panel of cell lines (see Table 4.4). Carbon Black (2) and the reference TiO<sub>2</sub> nanoparticles (1.2) induced oxidative stress in all cell lines studied while dispersions of two other TiO<sub>2</sub> nanoparticles (1.1a and 1.1b) did not evoke ROS formation. A mixed Ti-Zr oxide (6.3) only provoked an increase in oxidative stress in some cell lines. BaSO<sub>4</sub> nanoparticles (10) selectively increased cell death in mouse fibroblasts (NIH-3T3), while ZnO (9) nanoparticles lead to an increase in cell death and to a decrease in metabolic activity in all cell lines tested.

Zinc oxide nanoparticles (9) increased Caspase-3 activity, a marker of apoptosis, in most cell lines tested and dramatically reduced TEER in MDCK II and NRK52E cells. Carbon Black (2), TiO<sub>2</sub> (1.2), a mixed oxide (6.3), and ZrO<sub>2</sub> (8.1) did not influence these parameters.

Furthermore, biological effects varied significantly in different cell lines with the same nanoparticle at the same concentration. In addition to the conclusions drawn in the previous chapter, these results show that a set of different cell types and assays has to be used for a reliable and sensitive nanoparticle risk assessment.

### In vitro Testing of Proinflammatory Effects of Engineered Nanoparticles in Coculture Systems

In order to study possible proinflammatory effects of nanoparticles in vitro, a coculture model of A549 and the monocyte/macrophage-like cell line Mono-Mac-6 (MM6) was developed. This system provides a relatively simple model of the alveolar response to nanoparticle exposure. An existing inflammatory state can be simulated in the coculture model by LPS-activation of the monocytes/ macrophages. The optimum cell culture conditions, controls, stimulation conditions, cell numbers and ratios as well as the most useful inflammatory parameters to be measured were determined previously in a series of studies or selected according to literature, respectively. In the A549/Mono-Mac-6 coculture model, the proinflammatory potential of different nanoparticles at concentrations of  $1 \mu\text{g}/\text{cm}^2$  and  $10 \mu\text{g}/\text{cm}^2$  was determined by measuring the release of the inflammatory mediator IL-8 (Table 4.6).

**Table 4.6** Test results of IL-8 induction (IL-8-ELISA) in different coculture conditions with engineered nanoparticles (all tests were performed in triplicates in two separate assay series). Prestimulation was done with lipopolysaccharide. Symbols used: (+) weak increase; (++) significant increase; (+++) strong increase; (MM6) Mono-Mac-6; (\*) prestimulated with LPS (1 ng/ml for 16 h).

Material	No	Biological effects	Cell line	Effect	Time
TiO <sub>2</sub>	1.1a	Inflammatory marker secretion	all culture types	no effect	24 h
TiO <sub>2</sub>	1.1b	Inflammatory marker secretion	all culture types	no effect	24 h
TiO <sub>2</sub>	1.2	Inflammatory marker secretion	A549	+	24 h
			MM6	no effect	24 h
			MM6 (*)	no effect	24 h
			A549 + MM6	+	24 h
			A549 + MM6 (*)	++	24 h
Carbon Black	2.0	Inflammatory marker secretion	A549	+	24 h
			MM6	no effect	24 h
			MM6 (*)	no effect	24 h
			A549 + MM6	+	24 h
			A549 + MM6 (*)	++	24 h
CeO <sub>2</sub>	3.1	Inflammatory marker secretion	A549	no effect	24 h
			MM6	no effect	24 h
			MM6 (*)	no effect	24 h
			A549 + MM6	+	24 h
			A549 + MM6 (*)	+	24 h
CeO <sub>2</sub>	3.2	Inflammatory marker secretion	all culture types	no effect	24 h
CeO <sub>2</sub>	3.3	Inflammatory marker secretion	A549	no effect	24 h
			MM6	no effect	24 h
			MM6 (*)	no effect	24 h
			A549 + MM6	+	24 h
			A549 + MM6 (*)	no effect	24 h
CeO <sub>2</sub>	3.4	Inflammatory marker secretion	all culture types	no effect	24 h
CeO <sub>2</sub>	3.5	Inflammatory marker secretion	all culture types	no effect	24 h

Material	No	Biological effects	Cell line	Effect	Time
Ti-Zr Mixed Oxide	6.1	Inflammatory marker secretion	all culture types	no effect	24 h
Ti-Zr Mixed Oxide	6.2	Inflammatory marker secretion	all culture types	no effect	24 h
Ti-Zr Mixed Oxide	6.3	Inflammatory marker secretion	all culture types	no effect	24 h
Ti-Al-Zr Mixed Oxide	7.1	Inflammatory marker secretion	all culture types	no effect	24 h
Ti-Al-Zr Mixed Oxide	7.2	Inflammatory marker secretion	all culture types	no effect	24 h
Ti-Al-Zr Mixed Oxide	7.3	Inflammatory marker secretion	all culture types	no effect	24 h
ZrO <sub>2</sub>	8.1	Inflammatory marker secretion	all culture types	no effect	24 h
ZrO <sub>2</sub>	8.2	Inflammatory marker secretion	all culture types	no effect	24 h
ZrO <sub>2</sub>	8.3	Inflammatory marker secretion	all culture types	no effect	24 h
ZnO	9	Inflammatory marker secretion	A549	+	24 h
			MM6	+	24 h
			MM6 (*)	+	24 h
			A549 + MM6	++	24 h
			A549 + MM6 (*)	+++	24 h
BaSO <sub>4</sub>	10	Inflammatory marker secretion	all culture types	no effect	24 h

## Key Results

Of all 18 particles tested, only TiO<sub>2</sub> (1.2), Carbon Black (2), ZnO (9) and CeO<sub>2</sub> (3.1, 3.3) induced elevated IL-8 levels. All other materials tested including different TiO<sub>2</sub> (1.1, 1.1b) did not show any significant effects on IL-8 production in different cell culture types.

The strongest increase in IL-8 release was observed when LPS-prestimulated A549/MM6 cocultures were exposed to ZnO (9). Likewise, Carbon Black or TiO<sub>2</sub> induced a significant IL-8 increase in prestimulated A549/MM6 cocultures.

Coculturing different cell lines and variation in culture conditions increased the secretion of proinflammatory markers for some nanoparticles. These results indicate the potential benefit and increased sensitivity of coculture systems for in vitro toxicology studies.

Taken together, the nanoparticles mediated induction of proinflammatory markers heavily depends on culture conditions with strongest effects observed in LPS-prestimulated coculture systems.

### Investigations Using the Vector Model

Freshly isolated alveolar macrophages (AM) have been used for many years to study effects of respirable particles. The assay concept is based on the finding that macrophages lavaged from the lungs of healthy donor animals retain most of their native properties such as extensive phagocytosis of particles and generation of mediators such as reactive oxygen species (ROS) and/or tumour necrosis factor (TNF). Adaptations of alveolar macrophages to their micro-environment inside the lung alveolus, which might influence the reaction to particles, are most likely preserved making primary AM a unique cell model.

**Table 4.7** Low effect levels investigated with the Vector Model in a multi-dose approach (15, 30, 60 and 120  $\mu\text{g}/10^6$  cells). Quartz and corundum were used as positive and negative controls, respectively. Functional cell damage was derived from PMA-induced ROS production 16 hours after application of particles; Lactate dehydrogenase (LDH), glucuronidase (Gluc) and TNF- $\alpha$  were measured in the supernatant as described. Release of radical oxygen species (ROS) into the medium was measured as decay of scopoletin fluorescence over 2 hours in the presence of freshly added particles. n.e.: not evaluated due to interference of  $\text{CeO}_2$  with the assay system. n.d.: not done. Numbers in brackets show the maximum concentration tested.

		LOEL [ $\mu\text{g}/10^6$ Alveolar macrophages ]				
Material	No.	Functional damage	LDH	Gluc	TNF	ROS
Quartz DQ12	Control	<60	30	<30	30	60
Corundum	Control	>120	>120	120	120	>120
TiO <sub>2</sub>	1.1	60	15	15	n.d.	60
TiO <sub>2</sub>	1.2	30-60	30	60	60	60
CeO <sub>2</sub> -A	3.1	60-120	15-30	60	15	n.e.
CeO <sub>2</sub> -D	3.4	60-120	30	60	n.d.	n.e.
CeO <sub>2</sub> (doped)	4.4	30-60	15-30	30	15	n.e.
AlOOH	5.1	60-120	60-120	60-120	<15	None (120)
Ti-Zr Mixed oxide	6.1	60	30	30-60	60	
Ti-Zr Mixed oxide	6.3	60	30	30-60	60	
Al-Ti-Zr	7.1	30-60	30	30-60	60	None (60)
Al-Ti-Zr	7.3	30-60	30	30-60	15	None (60)
ZrO <sub>2</sub>	8.1	120	30	15	None (120)	None (60)
ZrO <sub>2</sub>	8.2	15	15	15	<30	60
ZrO <sub>2</sub>	8.3	15	15	15	<30	60
BaSO <sub>4</sub>	10	>120	>120	>120	<15	none
SrCO <sub>3</sub>	11.1	>120	60	120	None (120)	60
SrCO <sub>3</sub>	11.2	120	30	60	None (120)	None (120)

AM were lavaged from the lungs of healthy guinea pigs and pre-cultured in 96-wellplates in MEM medium before particle-containing medium was added. A multi-dose approach was used (for details see 4.3.1). Supernatant was retrieved after 16 hours after 10 min centrifugation such that no particulate matter can interfere with the assays. LDH and glucuronidase were measured colorimetrically. Release of glucuronidase is indicative of damage to phagolysosomes, and this parameter is mostly independent from LDH release. Production of TNF was determined with a bioassay by means of L-929 cells. Release of ROS into the medium was measured by the scopoletin assay. “Functional cell damage” was detected by measuring inducible ROS production subsequent to a 16 hour lasting exposure to particle. Further parameters which are routinely measured comprised cell vitality (uptake of fluoresceine diacetate), chromatin content (DAPI staining) and number of necrotic cells (propidium iodide staining).

A total of 20 NanoCare Materials was tested for effects on AM and the low effect levels for each parameter are listed in Table 4.7. In the majority of the cases there was a dose dependent increase in at least one of these parameters using a concentration range of 15-120  $\mu\text{g}/10^6$  AM (corresponding to 18-128  $\mu\text{g}/\text{cm}^2$ ). Also a “No Effect level” (NOEL) was found to be included in nearly all cases.

To control for effects of soluble constituents and/or non-sedimented nanoparticle fractions we conducted experiments with supernatants from particle suspensions which had been allowed to sediment for 24 h. However, these “24 hours supernatants” had no or very limited effects on AM (data not shown).

To obtain a more convenient measure of in vitro toxicity based on multiple parameters, we created a sum index. To this aim values for LDH, glucuronidase, TNF and functional cell damage were normalized to the maximum value found within the same set of experiments. Summation of these values gave the toxicity index “S-vitro” which ranged from 0-400 (see Figure 4.5.1).

## Key Results

According to this sum index we obtained the following rank order of in vitro toxicity of NanoCare materials:

$\text{BaSO}_4(10) < \text{AlOOH}(5.1) < \text{CeO}_2(3.1) \leq \text{Ti-Zr}(6.3) \leq \text{TiO}_2(1.2) \leq \text{CeO}_2(4.4) < \text{Al-Ti-Zr}(7.3)$

In conclusion, screening tests with the vector model could be used to analyse the biologic activity of NanoCare materials in vitro. Based on these results the type and doses of seven materials were selected for further in vivo experiments (see 4.4.1).

#### 4.4. In vivo Test Systems

J. Bruch, R. Landsiedel, L. Ma-Hock, J. Pauluhn, J. Ragot, M. Wiemann

Three different set of in vivo tests were conducted in the framework of NanoCare following two approaches: a) Intratracheal Instillation to challenge a lung by a single well defined dose with well defined material and b) short- and long-term inhalation studies mimicking the “real” exposure and uptake of airborne nanomaterials into the lung.

##### 4.4.1 Intratracheal Instillation Study

The intratracheal instillation (ITI) of particles is an appropriate method to test for adverse or toxic effects of respirable particles. In contrast to the weeks-lasting deposition of particulate matter necessary to achieve an appropriate lung burden during inhalation experiments, responses of the lung are challenged by a single bolus application of defined doses. It should be pointed out that as an indispensable precondition the ITI exposure must be given in the sub-overload domain, which is determined by the volumetric load of the present alveolar macrophages in the experimental animal. Though the ITI is often regarded as non-physiological because the applied particles are deposited in a more centralized manner, the technique appears advantageous if precise dosing and/or short observation times are required, e.g. in case of comparative in vitro studies. The ITI technique fairly well mimics known toxicity profiles of positive and negative standards such as quartz DQ12 and corundum. With respect to the comparison of in vitro and in vivo experiments, which was one major goal of the NanoCare project (see section 4.5), it appears furthermore advantageous to deliver aqueous suspension of particles to the lung parenchyma, because they were prepared in a similar way for in vitro studies with the vector model (see section 4.3.1).

In order to get a first insight into the relevance of the vitro results obtained with the vector model, seven materials BaSO<sub>4</sub> (10), SrCO<sub>3</sub> (11.1), SrCO<sub>3</sub> (11.2), AlOOH (5.1), CeO<sub>2</sub> (3.1), Ti-Zr (6.3), TiO<sub>2</sub> (1.2), doped CeO<sub>2</sub> (4.4), and Al-Ti-Zr (7.3) were intratracheally instilled into the lungs of female Wistar rats (200-250 g). Animals were kept at a 12 hr light-dark-cycle. Food and water were accessible ad libitum. Particles were suspended in the instillation fluid, vortexed and suspended by brief ultrasonication shortly before application. Negative controls received instillation fluid; quartz DQ12 (1.2 mg per rat lung), a strongly fibrogenic dust, was used as positive control. All studies were in accordance to the EU animal welfare regulations.

We conducted a first set of experiments with a low and a high dose of particles (0.6 and 4.8 mg per lung) using 10 animals per group and time point. AlOOH was tested at 1.2 instead of 0.6 mg/lung. After 3 days, 5 animals were sacrificed for BALF analysis (differential cell counts, protein, fibronectin and TNF $\alpha$  activity); the remaining animals were used for histological examination of the lung to determine lung fibrosis (Sirius Red staining), proliferation (Ki67 antigen), mutation rate (p-53 protein), and DNA adducts (8-oxo-Guanin).

Most materials induced a dose-dependent increase of inflammatory cells (PMN) of BALF protein, fibronectin and epithelial cell proliferation. Only small increments were found for the number of macrophages in case of BaSO<sub>4</sub> (10), SrCO<sub>3</sub> (11.1), TiO<sub>2</sub> (1.2) and Ti-Zr (6.3). In analogy to the in vitro experiments with alveolar macrophages (vector model) we formed a sum index “S-vivo” from 5 parameters (macrophages, PMN, protein, fibronectin, TNF $\alpha$ ); before each of the parameters was normalized to the maximum value of the experiment. Results of this 3-day in vivo study are also described in section 4.5.1, where they were correlated to the sum index “S-vitro”. As can be seen there, values from low dose (0.6 mg/lung) and high dose experiments (4.8 mg/lung) correlated with data of the in vitro testing of the vector model. In using the S-vivo data for the 4.8 mg/lung exposure we obtained the

following rank order of biologic activity:  $\text{BaSO}_4$  (10) <  $\text{CeO}_2$  (3.1) <  $\text{TiO}_2$  (1.2)  $\leq$  Ti-Zr (6.3)  $\leq$  AIOOH (5.1)  $\leq$  doped  $\text{CeO}_2$  (4.4)  $\leq$  Al-Ti-Zr (7.3). It is important to note that none of the seven nanomaterials exceeded the inflammatory potential of the positive control quartz DQ12 (1.2 mg/ lung), even when applied at 4-fold higher concentration.

According to the results obtained so far, three nanomaterials AIOOH (5.1), Al-Ti-Zr (7.3), and  $\text{CeO}_2$  (4.4) were selected for further testing with a multi-dose and multi-time approach using 0.6, 1.2, 2.4 and 4.8 mg per rat lung. In addition,  $\text{BaSO}_4$  (10) and  $\text{SrCO}_3$  (11.1) were tested to confirm their possible role as inert, non-reactive and biocompatible nanomaterial. Effects of these materials were tested after observation periods of 21 and 90 days; the results are summarised in Table 4.2.1. Particular emphasis was laid on the determination of the NOEL (no-effect-level) and LOEL (lowest-effect-level), the latter being defined as the first value significantly different from control. NOELs and LOELs were not attributed to levels of TNF $\alpha$  and to the percentage of Ki67 positive nuclei, both of which provided valuable information about the immunological state and repair processes of the lung epithelium.

**AIOOH (5.1)** exerted a NOEL in the range of 0.6 mg for all cell counts after 21 day. This value was increased to 1.2-2.4 mg after 90 days, most likely due to lung clearing mechanisms. Damage to the epithelium, as indicated by increased BALF protein after 90 days, started at >2.4 mg/lung. AIOOH was the only nanomaterial tested so far which resulted in a dose-dependent increase in TNF $\alpha$ . This effect is probably related to the pronounced effect of AIOOH to release of TNF $\alpha$  from alveolar macrophages in vitro (section 4.3.2). The effect may be associated to the moderately increased proliferation rate. Taken together, AIOOH (5.1) evoked adverse effects after 21 days at 1.2 mg/lung. This finding is in good agreement with the inhalation study described in section 4.4.3.

**Al-Ti-Zr (7.3)** also showed a NOEL of 0.6 mg with respect to PMN and macrophage occurrence after 21 days. Compared to AIOOH the NOEL increased to 0.6-1.2 mg after 90 days. Increased protein in BALF occurred at >1.2 mg/lung. Al-Ti-Z (7.3) also increased TNF $\alpha$ , and led to a mild proliferation. In contrast to AIOOH, Al-Ti-Zr (7.3) evoked a concentration-dependent increase of fibronectin after 21 but not after 90 days; proliferation was only slightly increased. Thus, Al-Ti-Zr evoked adverse effects after 21 days at 0.6-1.2 mg/lung.

**Doped  $\text{CeO}_2$  (4.4)** is known as a ROS scavenger, a fact interfering with some in vitro tests (see section 4.3.2). This  $\text{CeO}_2$  (4.4) elicited comparably strong effects after instillation even at a concentration of 0.6 mg and after 21 days. Interestingly, there was no dose-dependency at this time point. However, after 90 days dose-dependency was detected for nearly all parameters investigated (see Table 4.2.1). This allows us to extrapolate the NOEL to a range of 0.2-0.4 mg/lung. These findings exemplify that observation periods of 90 days are necessary to adequately describe adverse effects of particles in lung. Furthermore, the surface reactivity of a given nanoparticle may be involved into biological processes in a complex and unforeseeable manner and thus deserves particular attention.

**$\text{BaSO}_4$  (10)** and both types of  **$\text{SrCO}_3$  (11.1, 11.2)** elicited nearly no biological effect in concentrations up to 4.8 mg/lung. Excessive TNF $\alpha$  induction as seen in vitro did not occur. Both types of material may therefore be used as a nanostructured material with extremely low biological activity.

In conclusion, by means of the in vitro vector model, we are able to identify contrasts in toxicity of the test samples for this in vivo study. Moreover, the use of macrophages allowed us to select the appropriate dose range necessary to identify the threshold dose by means of animal experiments. Thus, based on in vitro data, predictions of the in vivo toxicity of

respirable nanostructured materials appear feasible for the future. When looking at the toxic potential of the nanomaterials after 21 and 90 days and in comparison to quartz DQ12 it is important to note, that none of the nanomaterials investigated in this part of the study showed a similarly high toxicity or fibrogenic potential.

**Table 4.8** Effects of 5 different nanomaterials on lung parameters 21 and 90 days after instillation. TCC: total cell count, MPH: macrophages, PMN: polymorph nuclear cells, Protein: total Protein (Lowry method), Fibronectin (ELISA) relative to DQ12 control, Ki67: Proliferating cells relative to DQ12 control **N**: No effect level, i.e. value not different from NaCl control; L: Low effect level; 0: no effect + ...+++++: response relative to NaCl and DQ12 controls.

NOEL (N) / LOEL (L) after 21 days									
	Material	Dose mg/lung	BALF parameter					Fibro-nectin	Histo Prolif. (Ki67)
			TCC	MPH	PMN	Protein	TNF		
	NaCl		+	+	0	+	+++	+	+
	DQ12	1.2	+++	+++	+++	+++	++	+++	+++
5.1	AlOOH	0.6	N	N	N	N	+	N	++
		1.2	L	L	L	N	++	L	++
		2.4	+	+	+	N	+++	++	++
		4.8	++	++	+	L	++++	++	++
7.3	Al-Ti-Zr	0.6	N	L	N	N	++++	L	++
		1.2	L	+	L	L	+++	+++	+++
		2.4	+	++	++	++	++	+++	++
		4.8	++	++	+++	+++	++++	++++	++
4.4	doped CeO <sub>2</sub>	0.6	+++	+++++	++	++++	+++	+++++	++
		1.2	+++	++++	++	++	++	++++	+++
		2.4	+++	+++	++	++	+++	++++	++
		4.8	+++	+++++	++	+++	+++++	++++	+
10	BaSO <sub>4</sub>	2.4	N	N	N	N	+	N	+
		4.8	N	N	N	N	+++	L	+
11.1	SrCO <sub>3</sub>	4.8	N	N	N	N	+++	N	++
11.2	SrCO <sub>3</sub>	4.8	N	N	N	N	+++	N	++

NOEL (N) / LOEL (L) after 90 days									
	Material	Dose mg/lung	BALF parameter					Fibro-nectin	Histo Prolif. (Ki67)
			TCC	MPH	PMN	Protein	TNF		
	NaCl		+	+	0	+	++	+	++
	DQ12	1.2	+++++	+++++	+++ ++	+++++	++	+++	+
5.1	AlOOH	0.6	N	N	N	N	++++	N	+
		1.2	N	N	N	N	+++	N	++++
		2.4	N	N	L	L	++	L	+
		4.8	L	L	+	+	++++	L	++++
7.3	Al-Ti-Zr	0.6	N	N	N	N	+++++	N	++
		1.2	L	L	N	N	++++	N	++
		2.4	+	++	L	L	++++	N	++
		4.8	++	++	+	+	+++++	N	++
4.4	doped CeO <sub>2</sub>	0.6	L	L	L	N	++++	N	++
		1.2	++	++	++	L	++++	N	++
		2.4	+++	++++	+++	++	+++	L	+++
		4.8	++++	+++++	+++ +	++	++++	L	+++
10	BaSO <sub>4</sub>	2.4	N	N	N	N	++++	N	+
		4.8	N	N	N	N	+++	N	+
11.1	SrCO <sub>3</sub>	4.8	N	N	N	N	++++	N	++
11.2	SrCO <sub>3</sub>	4.8	N	N	N	N	+++	N	++

#### 4.4.2 Standard Short-Term Inhalation Test for Nanomaterials

Inhalation is regarded as the most critical exposure route for aerosols from nanomaterials. Aerosols from nanomaterials are, however, complex systems and the inhalation of those aerosols as well as the deposition, uptake and effects of particles from those aerosols are intricate processes, which are not yet understood in detail. Thus it is not yet sufficient to predict toxic effects of inhaled nanomaterials only by in vitro methods. Data from inhalation studies in vivo are rather necessary to develop and validate in vitro studies. Therefore a valid inhalation study method was designed and used to measure the uptake of inhaled as well as its effects in the lung.

A short-term inhalation study was developed as the standard inhalation method to assess the toxicity of aerosols from nanomaterials. A short-term study is an adequate and sufficient method to determine the toxicity of inhaled particles based on the hypothesis, that the main effects in the lung are inflammation and / or cytotoxicity. And any observed effects would be related to these initial events; i.e. long-term effects (including fibrosis and cancer) would be the result of the progression of those initial inflammations or cytotoxic lesions. Hence it is possible to determine the toxicity of inhaled nanomaterials by measuring these early, primary effects. These effects would be influenced by the type and amount of particles disposed in the lung and the subsequent reaction of the lung. Understanding the deposition and primary effects of inhaled nanomaterials in the lung will enable the validation and application of appropriate in vitro methods.

The standard short-term inhalation method was used to study the deposition, fate and effects of various inhaled nanomaterials. Several parts of these inhalation methods needed to be optimised and adapted to fit this purpose:

1. Method to generate aerosols from nanomaterials for inhalation studies
2. Method to characterise aerosols from nanomaterials in inhalation studies
3. Method to expose rats to aerosols from nanomaterials
4. Method to measure the deposition of inhaled nanomaterials in the lung
5. Method to measure the effects in the lung short-term inhalation exposure

With the optimised standard short-term inhalation study, the effects of various nanomaterials were tested and compared to each other and to the results of the in vitro studies.

6. Compare the effects of various nanomaterials in the standard short-term inhalation test

#### Generation of Aerosols from Nanomaterials

Two methods of aerosol generation were used. Nano-Titanium dioxide (uncoated) was suspended in doubly distilled water and sprayed as liquid aerosol in a nebulisation system. For the other test substances (Table 2) a dry powder aerosol generator was used.

##### a) Generation of the Inhalation Atmospheres by Dry Dispersion

Dust aerosols were produced by dry dispersion of powder pellets with a brush dust generator (developed by the Technical University of Karlsruhe, Germany (Figure 4.14)). The aerosols were generated with compressed air in a mixing stage, mixed with conditioned dilution air and passed via a cyclone (to separate particles > 3 µm) into a head-nose inhalation system.

To reduce electrostatic charging, brushes made of stainless steel were used. The generator itself and all conducting tubes were grounded.

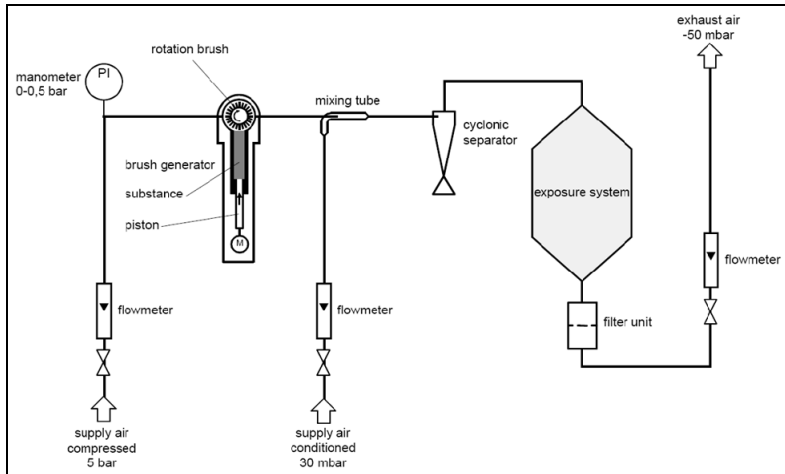


Figure 4.14 Brush feed aerosol generator.

#### b) Generation of the Inhalation Atmospheres by Nebulisation

Dust aerosols were produced by spraying suspensions of test materials in water with a two-component nebuliser (stainless steel, Schlick mod. 970, Figure 4.15) fed at a constant rate by means of a piston metering pump (Sarstedt DESAGA). The aerosols were generated with compressed air in a mixing stage, mixed with conditioned dilution air and passed via a cyclone into a head-nose inhalation system. The solvent evaporated very quickly resulting in dry dust aerosols in the test atmosphere. No additives were used, so that the liquid phase evaporated very quickly resulting in dry dust aerosols in the test atmosphere.

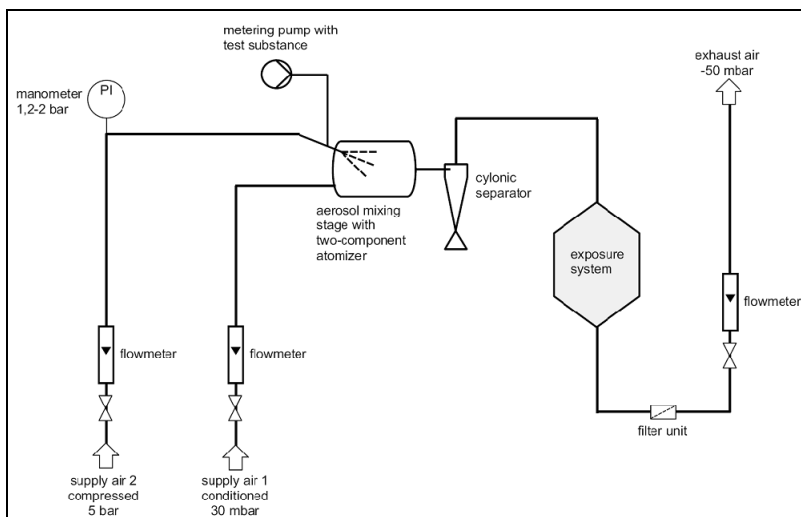


Figure 4.15 Nebulisation feed aerosol generator.

#### Characterisation of Aerosols from Nanomaterials

The mass concentration of the test substances in the inhalation atmosphere was determined gravimetrically after sampling of the particles in the exposure atmosphere onto a filter. The

particle size was determined gravimetrically, after separation in a cascade impactor, optically by an optical particle counter, and by their mobility using a scanning mobility particle sizer (SMPS).

#### a) Gravimetric Measurement of the Atmosphere Concentration

Gravimetric analysis was performed using a sampling device (Millipore) equipped with glass fibre filters (Macherey-Nagel, Dueren, Germany, type MN 85/90 BF, d = 4.7 cm) with organic binder for higher mechanical resistance. The sampling velocity was adjusted to 1.25 m/s and a sampling flow rate of 3 l/min. The sampling velocity of 1.25 m/s resembles the flow velocity of breathing and was recommended by DFG. The sample volume was ~ 90 litre. Sampling was performed adjacent to the place where the animals' noses were positioned in the exposure system. The filters were weighed before and after sampling using either a Sartorius M3P-000V001, a Mettler AE 240 or a Mettler AT 250 balance.

#### b) Particle Size Analysis by Cascade Impactor

Cascade impactor measurements were performed with an eight-stage Marple Personal Cascade Impactor (Sierra-Andersen). The effective aerodynamic cut-off diameters (EACD) were 21, 15, 10, 6.5, 3.5, 1, 0.7, or 0.4  $\mu\text{m}$  and the backup filter. A vacuum pump (Millipore) with a flow-limiting orifice calibrated to 3 l/min (Millipore) was used for sampling. The sampling probe had an internal diameter of 6.9 mm. The stages were weighed before and after sampling using a Sartorius M3P-000V001 or Mettler AT 250 balance. Samples were collected from the breathing zone of the animals at a sampling velocity of 1.25 m/s. Sample volumes were between 15 and 180 l.

#### c) Particle Sizes Analysis by Scanning Mobility Sizer Measurements

For each test atmosphere measurements with the Scanning Mobility Particle Sizer (SMPS) 3022A/3071A (TSI, USA) were performed by the Aerosol Technology Team of BASF SE. The SMPS system comprises a Model 3071A Electrostatic Classifier which separates the particles into known size fractions, and a model 3022A Condensation Particle Counter (CPC) which measures particle count concentrations. The instrument measures particles in the size range from 0.015  $\mu\text{m}$  to 0.805  $\mu\text{m}$  with 32 (or 64) size channels per decade. The SMPS sampled at 0.3 litres per minute (LPM) (sheath flow was 3 LPM). At this setting the single-stage, inertial impactor incorporated into the inlet of the SMPS to remove larger particles had a 50% cut size of 0.808  $\mu\text{m}$ .

#### d) Particle Size Analysis by OPC (Optical Particle Counter) Measurements

For each test atmosphere measurements with an optical particle counter (OPC) PCS 2000 (Palas, Karlsruhe) were performed to determine the size distribution of particles with diameters larger than 300 nm. The PCS 2000 uses a white-light source to illuminate a measurement volume through which particles have to move singly. The measuring range of the sensor was 0.3 to 23  $\mu\text{m}$  and the sampling flow rate 5 l/min.

Nano-TiO<sub>2</sub> was examined extensively. With the two component nebulizer, the influence of the vehicle, pump rate, concentration of the suspension on the particle size distribution in the test atmospheres were examined. The count-based size distributions are presented in Figure 4.16. In general, the higher the concentrations of the suspension to be nebulized the higher the median particle sizes mostly agglomerate were observed in the atmospheres regardless of the dust generation procedure.

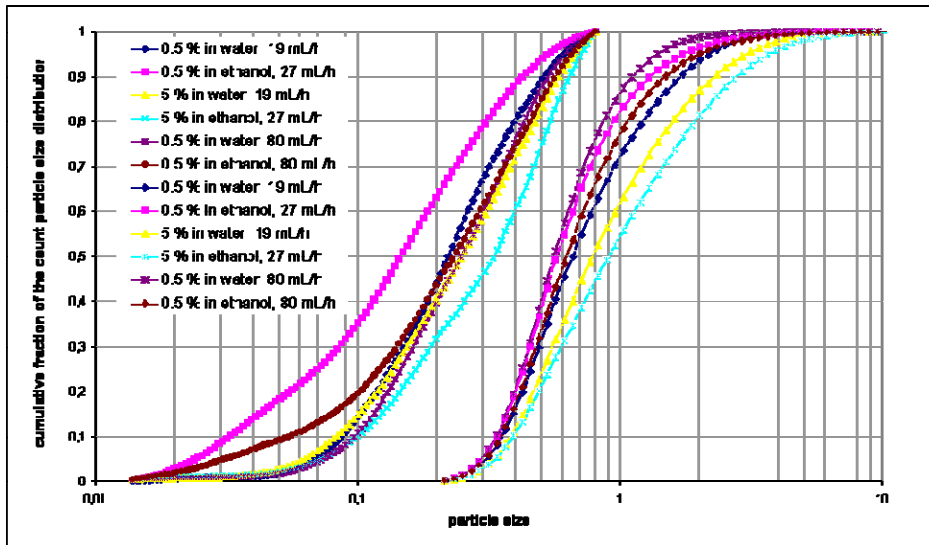


**Figure 4.16** Influence of vehicle, pump rate and the concentration of the suspension being nebulised on the particle size distribution, shown exemplarily by Nano-TiO<sub>2</sub> in water or ethanol.

Figure 4.17 shows the particle size distribution after nebulising and dry dispersion. In general, there were no substantial differences in the particle size distribution achieved with the nebulizing technique and the brush dust feeder.

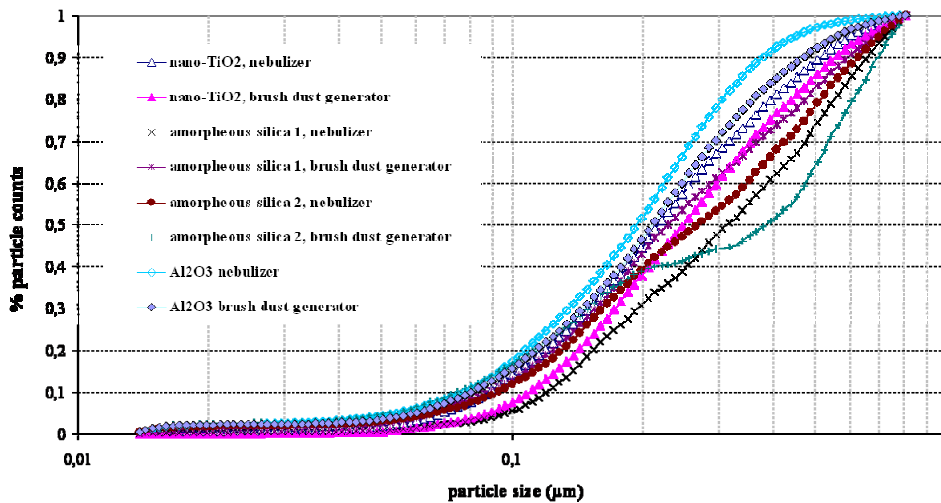


**Figure 4.17** Count based particle size distribution of nano-TiO<sub>2</sub>, Al<sub>2</sub>O<sub>3</sub>, and amorphous silica in the atmosphere generated by brush dust generator and by nebulisation, showing there were no substantial differences in the particle size distribution in the atmospheres generated by either of the generation techniques.

### Exposure of Rats to Aerosols from Nanomaterials: Design of the Standard Short-Term Inhalation Study

Male Wistar rats were exposed to the test materials for 6 hours per day on 5 consecutive days. Concurrent control groups were exposed to conditioned air. Animals were sacrificed either shortly after the last exposure or after a recovery period.

**Table 4.9** Study design and number of animals for the different examinations.

		Exposure days					Study days of recovery period									
		1	2	3	4	5	6	7	8	9 - 15	16	17	18	19	20	21
1	nano-TiO <sub>2</sub>		I			P O			L		I			P L		
	p-TiO <sub>2</sub>		I			P O			L		I			P L		
	quartz		I			P O			L		I			P L		
2	TiO <sub>2</sub>		I			P O			L		I			P O		L

- I = implantation of BrdU-minipumps for determination of cell proliferation (n = 6 rats per concentration and time point)
- P = electron microscopic examination examination (n = 3 rats per concentration and time point)
- L = broncho alveolar lavage (n = 5 rats per concentration and time point)
- O = organ burden (n = 3 rats per concentration and time point)

To establish the study design a first study was performed with high atmospheric concentrations nano-TiO<sub>2</sub> (1.2), pigmentary TiO<sub>2</sub> and quartz. The study design was further evaluated in a second study with nano-TiO<sub>2</sub> at 3 different concentrations. An overview of the study designs as well as the number of animals for the different examinations in these two studies is given in Table 4.9.

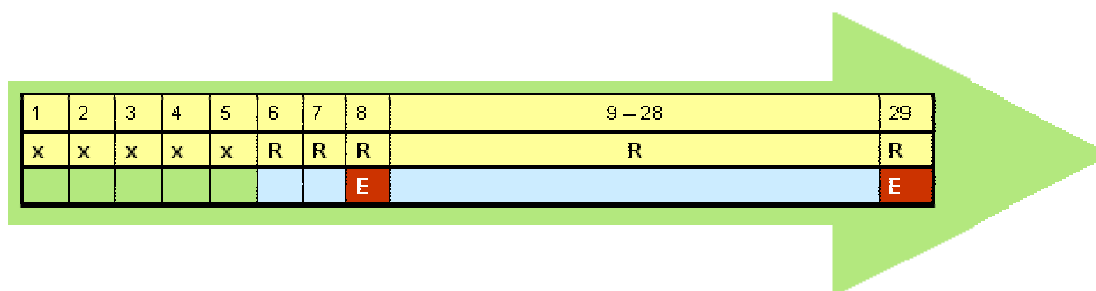


**Figure 4.18** Study design of 5-day inhalation study (study 3 and 5). X Head-nose exposure to aerosols for 6 hours per day on 5 consecutive days R Post-exposure time H Histology of selected organs E Examinations of blood and broncho-alveolar lavage fluid

Within the establishment of these 5-day inhalation studies we could not find significant differences in histological findings between immediately after the last exposure and those after 3-day recovery, whereas the most prominent changes in BALF parameters occurred on day 3 after the last exposure. So, within the last studies (Study 3, Study 4) analysis of BALF of the main test group as well as histological examinations were performed 3 days after the last exposure. The most appropriate time point for examining cell proliferations was considered to be on study day 5, directly after the last exposure. Cell proliferation and apoptosis were labor-intensive but not more sensitive than the parameters in BALF. Therefore, in the following studies this endpoint was not determined as a routine parameter. The study design for the following studies (Study 3 and Study 4) is presented in Figure 4.18.

The substances were tested at different concentrations as shown in Table 4.10.

Aim of the first study was to compare the toxicity of nano-TiO<sub>2</sub>, pigmentary TiO<sub>2</sub> and quartz. For nano-TiO<sub>2</sub>, the targeted atmospheric concentration was 100 mg/m<sup>3</sup>, which was 10 times as high as the concentration, which had caused increased incidence of benign squamous-cell tumor, adenocarcinoma and squamous-cell carcinoma in rats after 18 months inhalation exposure to a similar material (Heinrich et al., 1995). This high concentration was justified by the short exposure time of five days. Following this argument 250 mg/m<sup>3</sup> was chosen for pigmentary TiO<sub>2</sub> and 100 mg/m<sup>3</sup> for quartz based on two year carcinogenicity studies (Lee et al., 1985, Muhle et al., 1991).

In a following 5-day study (Study 2) we tried to establish the No Adverse Effect Concentration (NOAEC) for TiO<sub>2</sub>. Based on the information of the first study, considering the data of the previous 90 day inhalation study (Bermudez et al., 2004) in Study 2 nano-TiO<sub>2</sub> was tested at 2, 10 and 50 mg/m<sup>3</sup>. Concentrations for CeO<sub>2</sub> and BaSO<sub>4</sub> were based on data from in vitro studies.

**Table 4.10** Target concentrations of the test materials.

	Test Material	Target Concentrations [mg/m <sup>3</sup> ]
Study 1	nano-TiO <sub>2</sub>	100
	p-TiO <sub>2</sub>	250
	quartz	100
Study 2	TiO <sub>2</sub> (1.2)	2 / 10 / 50
Study 3	CeO <sub>2</sub> (3.5)	0.5 / 2.5 / 10
Study 4	BaSO <sub>4</sub> (10)	2 / 10 / 50
	CeO <sub>2</sub> (Al doped, 4.4)	0.5 / 2.5 / 10

## Deposition of Inhaled Nanomaterials in the Lung

Test materials were only detected in lungs and lung associated lymph nodes. In the liver, kidney, spleen and basal brain with olfactory bulb, no nanomaterial could be detected (detection limit for Ti 0.5 µg/tissue, detection limit for Ce 0.37 µg/tissue). Table 4.11 shows the mean values of organ burden analysed within 3 days after the last exposure.

**Table 4.11** Mean values of organ burden.

	Test Material	Target concentration (mg/m <sup>3</sup> )	Test material (µg)	
			Lung	Mediastinal lymph nodes
Study 1	nano-TiO <sub>2</sub>	100	2018.8	2.2
	p-TiO <sub>2</sub>	250	9151.4	8.2
Study 2	TiO <sub>2</sub>	2	118.5	< 0.5
		10	544.9	< 0.5
		50	1634.7	2.1
Study 3	CeO <sub>2</sub>	0.5	51.9	< 0.37
		2.5	165.6	< 0.37
		10	417.2	< 0.37

Further, electron microscopic examination demonstrated that nano-TiO<sub>2</sub> particles deposited in all lung lobes. Particles were found in all regions of all lung lobes (Table 4.12).

**Table 4.12** Semi quantitative analysis of the deposition pattern of TiO<sub>2</sub> in the lung using SEM/EDX analysis. The values given in the table refers to relative signal intensity of X-ray fluorescence signal of Ti to C (mean ± SD, n =20 to 55) of each lung lobe.

Test substance	pulmo sinister	Lobus cranialis dexter	Lobus medialis dexter	Lobus caudalis dexter	Lobus accessorius
nano-TiO <sub>2</sub>	0.42 ± 0.23	0.41 ± 0.24	0.67 ± 0.76	0.39 ± 0.10	0.38 ± 0.33
pigmentary TiO <sub>2</sub>	0.76 ± 0.63	1.72 ± 3.19	0.96 ± 0.53	1.97 ± 1.29	0.99 ± 0.81

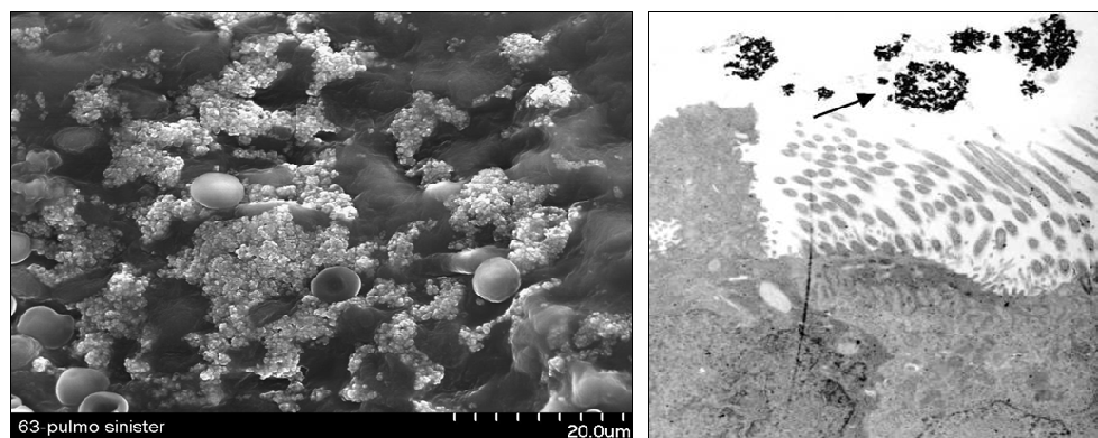


**Figure 4.19** TiO<sub>2</sub> (1.2) in the lung by 5-day inhalation study. TiO<sub>2</sub> on the lung surface, SEM (left), TiO<sub>2</sub> agglomerates of various sizes on the lung surface, TEM (right).

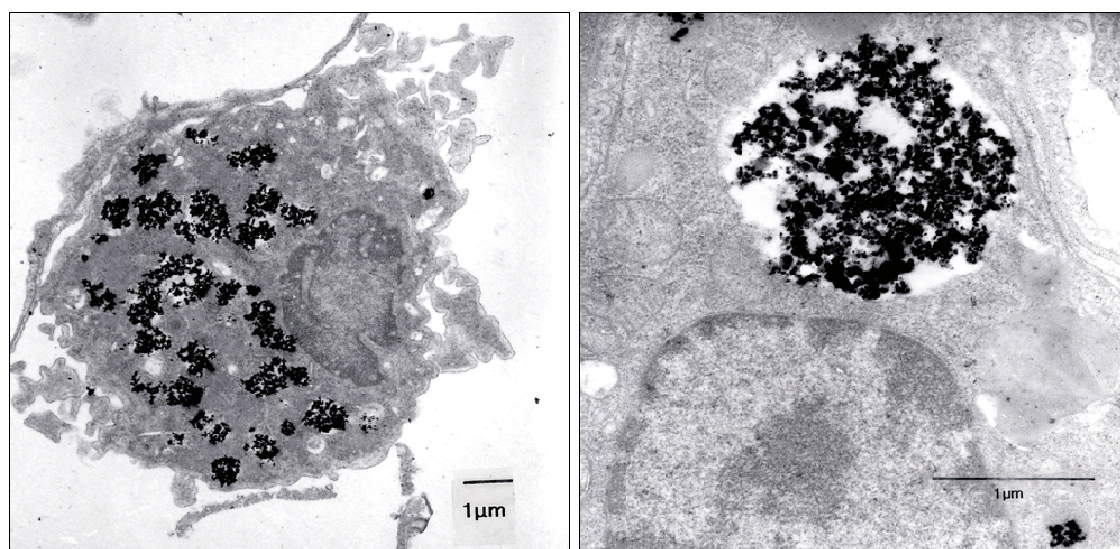


**Figure 4.20** TiO<sub>2</sub> (1.2) in the lung by 5-day inhalation study. TiO<sub>2</sub> agglomerates of various sizes in a macrophage in the lung, TEM (left), enlarges picture of an agglomerate of TiO<sub>2</sub> in a macrophage, TEM (right).

Further electron microscopic examination showed that particles were found either in the lumen of the alveoli or within macrophages, as agglomerates consisting many primary particles (Figure 4.19 and Figure 4.20).

### Identifying Relevant Biological Parameters for Nanomaterials in vitro Testing

#### Clinical Pathology Parameters in BALF

**Table 4.13** Biological parameters measured in the standard inhalation test for nanomaterials.

Histopathology	Cytokines <i>et al.</i>		
<b>Proliferation and Apoptosis</b>	1. Apolipoprotein A1	24. IL-1a	47. MDC
	2. $\beta$ -2 Microglobulin	25. IL-1 $\beta$	48. MIP-1a
	3. Calbindin	26. IL-2	49. MIP-1 $\beta$
	4. CD40	27. IL-3	50. MIP-1?
	5. CD40L	28. IL-4	51. MIP-2
	6. Clusterin	29. IL-5	52. MIP-3 $\beta$
	7. C-Reactive Protein	30. IL-6	53. MMP-9
	8. Cystatin	31. IL-7	54. Myoglobin
	9. EGF	32. IL-10	55. OSM
	10. Endothelin-1	33. IL-11	56. Osteopontin
	11. Eotaxin	34. IL-12p70	57. RANTES
	12. Factor VII	35. IL-17	58. SCF
	13. FGF-basic	36. Insulin	59. Serum Amyloid P
	14. FGF-9	37. IP-10	60. SGOT
	15. Fibrinogen	38. KC/GROa	61. TIMP-1
	16. GCP-2	39. Leptin	62. Tissue Factor
	17. GM-CSF	40. LIF	63. TNF-a
	18. Growth Hormone	41. Lipocalin-2	64. TPO
	19. GST-a	42. MCP-1	65. VCAM-1
	20. GST-1 Yb	43. MCP-2	66. VEGF
	21. Haptoglobin	44. MCP-3	67. von Willebrand Factor
	22. IFN- $\gamma$	45. MCP-5	
	23. IgA	46. M-CSF	
<b>Clinical chemistry</b>			
Protein			
lactate dehydrogenase (LDH)			
Alkaline phosphatase (ALP)			
$\gamma$ -Glutamyltransferase (GGT)			
N-acetyl- $\beta$ -Glucosaminidase (NAG)			
total cell count			
cell differential analysis			
-macrophage (MPH)			
-polymorph nuclear granulocytes (PMN)			
-lymphocyte (LYMPH)			
Troponin I			
<b>Parameters of oxidative stress</b>			
Carboxymethyllysin (CML)			
Malondialdehyd (MDA)			
$\delta$ -OHdG			

The inhalation exposure to the different test materials caused concentration related increases in total cell counts, total protein content and enzyme activities. The increase in total cell counts was due to increased numbers of polymorphonuclear neutrophils (PMN), whereas the effects on BALF eosinophil, lymphocyte and macrophage cell counts were not significant. Increases in BALF proteins are associated with enhanced permeability of vascular proteins into alveolar regions and many also reflect dead cells and secretions. LDH is a general marker of cell injury, whereas ALP is considered to be a marker of type II epithelial cell toxicity and GGT is a marker for damage to Clara and typ II cells. Increased NAG activity may represent activation of macrophages.

Within the course of method establishment, more than 70 parameters (Table 4.13) were examined in the respiratory tract, in bronchoalveolar lavage, in the blood serum, at different time point. The most relevant parameters were examined in Study 3 and 4 at two time points.

### Results of Inhalation Studies with Nanomaterials

Figure 4.21 shows the effect of BALF parameters for n-TiO<sub>2</sub>, pigmentary TiO<sub>2</sub> and quartz. For TiO<sub>2</sub> (Study 1 and Study 2) and CeO<sub>2</sub> (Study 3 and Study 4) we found concentration-related effects of the BALF parameters as shown in Figure 4.22 for TiO<sub>2</sub> and in Figure 4.23 for CeO<sub>2</sub>. All concentrations of BaSO<sub>4</sub> (Study 4) only caused slight effects which were comparable to the control level (Figure 4.24).

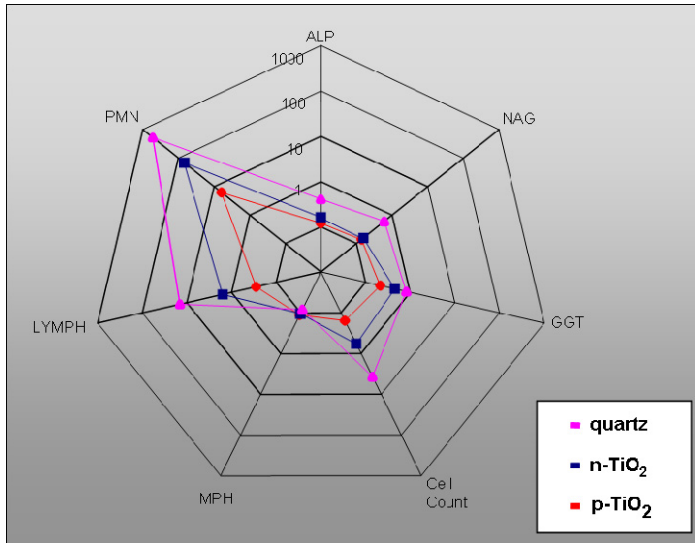


**Figure 4.21** Effects of quartz, nano-TiO<sub>2</sub> and pigmentary TiO<sub>2</sub> in the lavage fluid 3 days after exposure. ALP = Alkaline phosphatase, LYMPH = lymphocytes, NAG = N-Acetylaminglucosaminidase, GGT =  $\gamma$ -Glutamyltransferase, MPH = Macrophage, PMN = Polymorph nuclear neutrophilic granulocytes

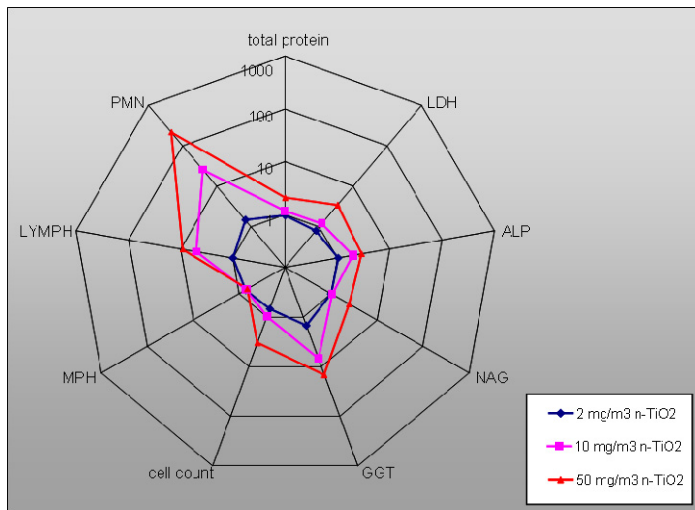


**Figure 4.22** Relative increase of the BALF parameters of animals exposed to 2, 10 and 50 mg/m<sup>3</sup> nano-TiO<sub>2</sub> immediately after exposure. LDH = Lactate dehydrogenase, ALP = Alkaline phosphatase, LYMPH = lymphocytes, NAG = N-Acetylaminglucosaminidase, GGT =  $\gamma$ -Glutamyltransferase, MPH = Macrophage, PMN = Polymorph nuclear neutrophilic granulocytes

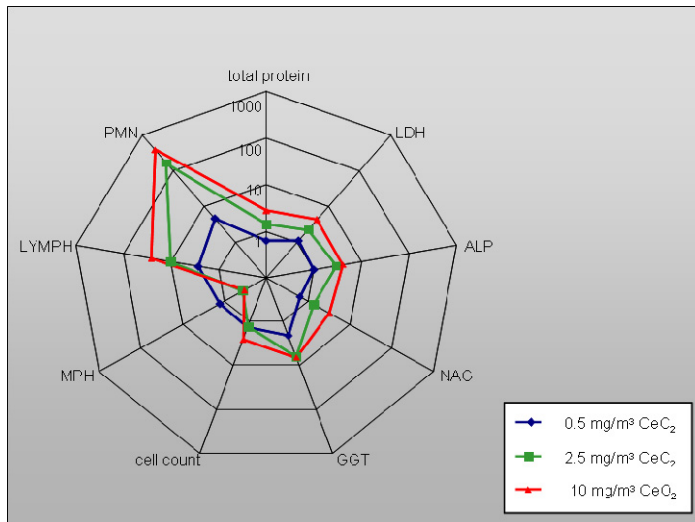


**Figure 4.23** Results of BALF parameters for 0.5, 2.5 and 10 mg/m<sup>3</sup> CeO<sub>2</sub> (3.5, Study 3). Inflammation markers were increased even at the lowest concentration. LDH = Lactate dehydrogenase, ALP = Alkaline phosphatase, LYMPH = lymphocytes, NAG = N-Acetylaminglucosaminidase, GGT =  $\gamma$ -Glutamyltransferase, MPH = Macrophage, PMN = Polymorph nuclear neutrophilic granulocytes

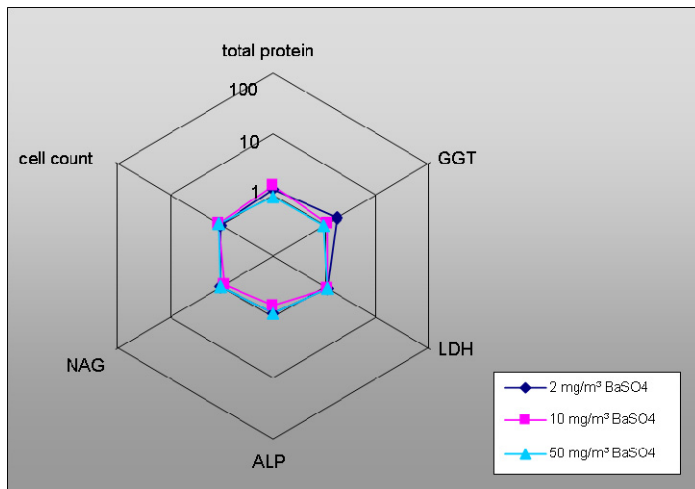


**Figure 4.24** Concentration-Effect Diagram of BaSO<sub>4</sub> (10). LDH = Lactate dehydrogenase, ALP = Alkaline phosphatase, GGT =  $\gamma$ -Glutamyltransferase, NAG = N-Acetylaminglucosaminidase

The most prominent changes in biochemical and cytological parameters occurred 3 days after the last exposure. After a recovery period of 16 days or longer, most of the parameters returned to the control level as shown in Figure 4.25 for TiO<sub>2</sub> (10 mg/m<sup>3</sup>; 1.2, Study 2).

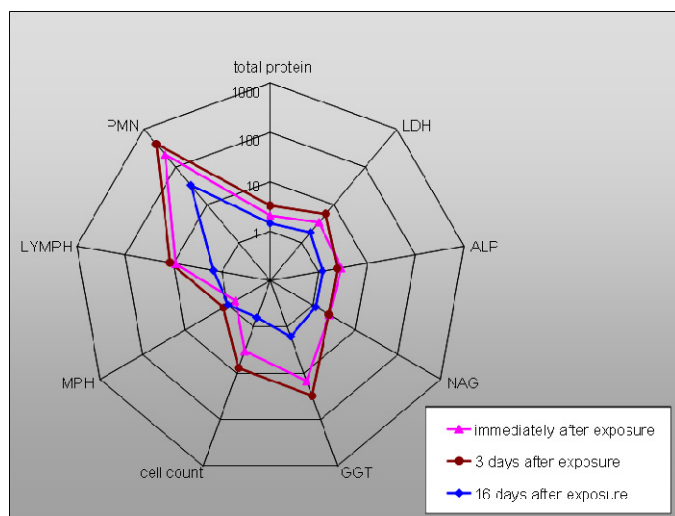


**Figure 4.25** Relative increase of the BALF parameters of animals exposed to 50 mg/m<sup>3</sup> Nano-TiO<sub>2</sub> at different time points showing that the most appropriate time point for examination of the lavage fluid is 3 days after the exposure (Study 2). LDH = Lactate dehydrogenase, ALP = Alkaline phosphatase, LYMPH = lymphocytes, NAG = N-Acetylaminglucosaminidase, GGT =  $\gamma$ -Glutamyltransferase, MPH = Macrophage, PMN = Polymorph nuclear neutrophilic granulocytes.

### Clinical Pathology Parameters in Blood

No significant changes in any of the hematological parameters measured were observed in all exposure groups of the different test materials at any time point.

### Histopathology

Figure 4.26 shows representative lung sections from control and rats exposed to 50 mg/m<sup>3</sup> TiO<sub>2</sub> (Study 2). In all treated animals histiocytes were observed, which contained a golden-brown pigment in their cytoplasm. The pigment could also be observed free and non-phagocytosed within the alveolar lumina. The bronchiole and bronchi of the animals exposed to 50 mg/m<sup>3</sup> showed a minimal to mild increase of epithelium thickness which was interpreted as hypertrophy/hyperplasia. Additionally pigment-loaded macrophages were observed in mediastinal lymph nodes in all animals exposed to 50 mg/m<sup>3</sup> TiO<sub>2</sub>.

After a recovery period of 16 days all treated animals still revealed pigment-loaded macrophages within the lungs.

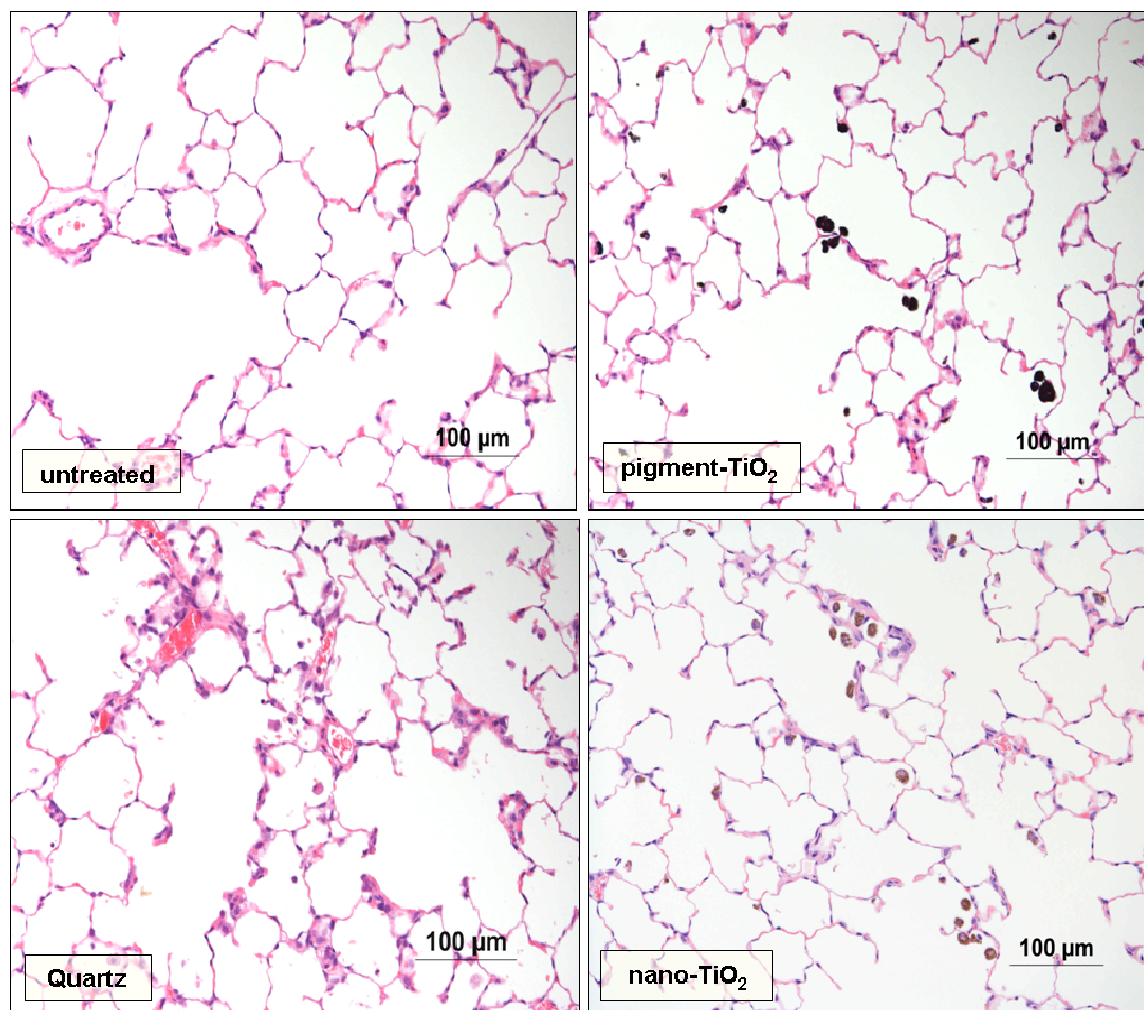


**Figure 4.26** Light microscopic image of lung sections of an untreated animal and animals after inhalation of aerosols from micron-scale TiO<sub>2</sub> (pigmentary TiO<sub>2</sub>), TiO<sub>2</sub> nanomaterial (nano-TiO<sub>2</sub>) and quartz. The pictures show various degrees of inflammations due to the particles in the lungs; the test material is also visible within the alveolar lumina and in the cytoplasm of alveolar macrophages.

#### 4.4.3 28-Day Inhalation Study

In addition to the short-term inhalation studies, a study with longer exposure period of 4 weeks and up to 3-month recovery period was performed.

The objective of this study was to assess lung toxicity of two aluminium oxyhydroxides (AlOOH, No 5.1, 5.2) bracketing a size-range of primary particles from  $\approx 10$  nm (Boehmite I, 5.1) to  $\approx 40$  nm (Boehmite II, 5.2) using a subacute 4-week inhalation rat-bioassay followed by a 3-month postexposure period. Poorly soluble particles have long elimination half-times in the pulmonary system, especially under over-loading conditions. The selection of exposure concentrations took into account results from a previous subchronic 13-week inhalation study with ultrafine TiO<sub>2</sub> (Bermudez et al., 2004). Exposure duration adjusted, the intermediate and high cumulative exposure doses used in this study were in the same range as used for TiO<sub>2</sub> (13-week exposure to 2 and 10 mg TiO<sub>2</sub>/m<sup>3</sup> is deemed to be dosimetrically equivalent to 6 and 30 mg AlOOH/m<sup>3</sup> after 4-week exposure). Following exposure to TiO<sub>2</sub>, pulmonary toxicity

was considered to be lung overload-related which was also reflected by increased translocation of particles from the lung to the lung-associated lymph nodes and changes in inflammatory endpoints in BAL (total protein, LDH, and neutrophils). The elimination half-time for alveolar clearance in the non-overloading state (rats) has been reported to be in the range of 50-65 days. Therefore, in the current study, a 3-months postexposure period was used to evaluate and compare retention-related differences in the toxicokinetics and toxicodynamics of inhaled Boehmite I and II (nano)particles, which was of low solubility.

The rationale for this approach was twofold, *viz.* to demonstrate that dispositional effects may affect biopersistence, localised dose and chronicity due to high retained doses. This means biological responses may not necessarily be related to specific particle properties. Hence, the driving force for effects to occur is the cumulative dose and not the particle property per se. In other words dosimetry over time appears to be most important for hazard characterisation and risk assessment. In compliance with the spirit and objective of NanoCare attempts were made to make intrapulmonary dosages comparable across species. For that purpose the particle dose per accessible alveolar cell by bronchoalveolar lavage was performed. Conceptually, this approach appears to be suitable to determine noninvasively this critical dose at the level of the target organ of humans. Findings can then not only dosimetrically be adjusted they also can then suitably be compared with data from rat inhalation studies or even *in vitro* studies focusing on the same target cell. In addition, this approach would allow simulating *in vitro* testing conditions that would resemble the non-overloading and overloading conditions in rats.

Nanoparticles may enter the blood stream, either directly via the lung (after disintegration of inhaled agglomerated particles) or perhaps also via the lymphatic system. However, the fate of nanoparticles within the lung and from the lung into the blood is imperfectly known and needs further study. Accordingly, the toxicodynamic endpoints measured in this study were complemented by pulmonary and extrapulmonary toxicokinetic data. Uptake of systemically available particles can occur by the reticulo-endothelial system and especially the liver sinusoids. Also excretion via the kidney cannot be ruled out. These organs, including the brain, have been addressed in this study. Further attempts were made to compare toxicodynamic findings with the internal dose-related "partico-kinetics" and to which extent the target-organ dose and effect parameters depend on the MMAD of agglomerated particles in inhalation chambers.

The size-range of primary particles of the alumina examined was similar to that of ultrafine anatase/rutile TiO<sub>2</sub> (average particle size ≈25 nm). The advantage of using AlOOH as a nanosized model structure is that different crystal structures with resultant differences in toxic potency due to dissimilarities in crystal properties (Warheit et al., 2007) are not expected to occur. A common finding in inhalation studies is that the MMAD of agglomerated airborne particles is relatively independent on the primary particle size. In studies reported by Bermudez et al. (2002, 2004) the TiO<sub>2</sub> primary particle size ranged from 25 nm (ultrafine) to 300 nm (pigment-grade). Yet, the MMADs of particles in inhalation chambers for the two TiO<sub>2</sub> particle-types were similar (MMAD ≈1.4 μm). Despite exposure to agglomerated particles of similar aerodynamic properties, the potency of the ultrafine TiO<sub>2</sub> to cause inflammation and cytotoxicity in subchronically exposed rats was approximately 5x greater compared to the pulmonary effects of the inhaled pigment-grade TiO<sub>2</sub> particles. The MMAD of agglomerated particle in inhalation chambers of several alumina in the primary particle size-range 25±15 nm was compared prior to this study (data not shown). This comparison revealed that under the inhalation testing conditions of this study, Boehmite I produced the smallest MMAD (≈0.6 μm) while Boehmite II produced dust atmospheres with the largest MMAD (≈1.7 μm). Therefore, these two nanosized materials were chosen to study the impact of differences in

the agglomerated particle size in inhalation chambers in the absence of potential confounding factors due to changes in crystal properties.

The analysis of particle-associated aluminum in BAL-cells after the 4-week exposure period in lavaged lungs and BAL-cells revealed quite similar relative percentages of particle burden in BAL-cells relative to the total pulmonary burden. The BAL-cell load *per se* was clearly dependent on the respective exposure concentration and respirability of the inhaled alumina. The high correlation between BAL-cell and lung tissue particle burdens appears to suggest equilibrium of particles between these two compartments. Alternatively, it can also be hypothesized that most of the particle lung burden ( $\approx 80\%$ ) is associated with particle-laden resident alveolar macrophages not retrieved by bronchoalveolar lavage.

In the rat inhalation studies with 3 months postexposure periods, a high correlation ( $r^2 = 0.94$ ) between BAL-cell and lung tissue particle burdens was found. This data suggest that most of the particle lung burden ( $\approx 80\%$ ) is associated with particle-laden resident alveolar macrophages not retrieved by bronchoalveolar lavage. Inflammatory responses occurred in rats with accumulated doses of approximately 2.2 and 1.5 mg aluminum per lung or 3.9 and 2.7 mg AIOOH-40 nm/MMAD-0.6  $\mu\text{m}$  (Boehmite I) or AIOOH-10 nm/MMAD-1.7  $\mu\text{m}$  per gram lung (Boehmite II). At these lung burdens the BAL-cell particle dose was  $69 \times 10^{-12}$  and  $92 \times 10^{12}$  g AIOOH/BAL-cell for AIOOH-40 nm/MMAD-0.6  $\mu\text{m}$  and AIOOH-10 nm/MMAD-1.7  $\mu\text{m}$ , respectively (Pauluhn, 2009a,b). The concentration-dependence and time-course changes of aluminum in the lung demonstrate a precipitous increase in elimination half-time at this cumulative dose (at 28  $\text{mg}/\text{m}^3$ ) which is consistent with lung-overload. The half-time of poorly soluble particles for alveolar clearance in rats under non-overloading conditions has been reported to be in the range of 50-60 days. Longer elimination half-times occur when the intracellular particle volume exceeds approximately 6% or 60  $\mu\text{m}^3$  of the phagocytic cell. The reduction in clearance has been attributed, at least in part, to the loss of macrophage mobility at high particle burdens and by volumetric increase of cells by phagocytized particles. Hence, it appears to be justified to conclude that the pool of particle-laden cells remaining in the lavaged lung equals that cellular pool not be accessible by lavage. The findings demonstrate also that absolute counts from BAL analyses depend on the degree of activation of BAL cells. Taking into account the interlaboratory variability of lavage procedures, a similar value ( $\approx 14\%$ ) was reported by Rehn et al. (1992). This also means that 'total lung particle burdens' may not be equalled with 'interstitialized particle burdens'. This data support the notion that lung burdens are mirroring the non-lavaged cellular compartment and not the parenchymal compartment. Suffice it to say, especially in rats, this sustained sequestration of overloaded/activated alveolar macrophages will eventually deteriorate the barrier function of the alveolar structures with associated long-term inflammatory response.

The determination of aluminum as tracer of exposure to AIOOH did not reveal any evidence of dose- or time-dependent increased Al in the brain, liver, and kidneys. Concentrations of aluminum in urine did also not demonstrate any conclusive time- or dose-dependent changes. These findings support the conclusion that extrapulmonary translocation of aluminum did not occur to any appreciable extent at any exposure level. Of note appears to be that the extent of translocation of Boehmite I to the LALNs at 28  $\text{mg}/\text{m}^3$  was approximately 2 % and 6 % after 2 and 4 weeks postexposure, respectively, while markedly lower concentrations in LALNs were observed following exposure to Boehmite II; despite somewhat similar inflammatory responses and organ weights.

The comparison of previous and current inhalation studies with fine and ultrafine (nano)particles demonstrate that determinations of target organ doses (lung) are most apt to integrate the particle mass deposited and retained in the lung. Hence, it is the most precise reflection of the cumulative inhaled dose and integrated multiple variables, such as the time-

weighted daily exposure concentration, the respiratory minute volume, the aerodynamic size-dependent deposition efficiency, solubility, and resultant fate of retained particles. The cumulative lung burdens at the end of the 4-week period demonstrate that the agglomerated particle size (MMAD) impacts the total lung burden to a greater extent than the size of primary particles. Thus, lung burdens appear to be more dependent on the MMAD of agglomerated airborne particles, which determine the site of initial deposition within the respiratory tract, than on the size of primary particles. Collectively, these results demonstrate that experimental approaches should address and differentiate deposition- and retention-related particular matter (PM)-induced effects. Suffice it to say, study protocols must allow for exposure and postexposure periods long enough to determine the time-course of particle loading and clearance, covering a cumulative range of lung burdens from non-overload to overload, to better understand whether pulmonary toxicity is clearly dependent on lung overload or is particle property-specific.

With regard to BAL-polymorphonuclear neutrophilic granulocytes (PMNs) the presentation of data relates either to “absolute” or “relative” counts which are used as such interchangeably in the published literature. Absolute counts take into account the total number of cells retrieved by BAL multiplied by the relative percentage obtained by cell cytodifferentiation. In this context, the terminology ‘absolute PMN counts’ appears to be somewhat inappropriate as the yield of cells harvested by BAL is much lower than the actual population of mobile cells types present in the alveoli and airways. In a previous study with AIOOH it was shown that approximately 20 % of the particle lung dose was found in BAL-cells while that the remaining 80 % of particle dose was likely in alveolar cells not accessible by the BAL procedures applied. The point of departure of endpoints in BAL suggestive of pulmonary inflammation matched the  $\approx 1$  mg PM/lung threshold at which lung overload starts to occur. Hence, the dispositional and toxicological findings are consistent with the common view held, namely that PM-related pulmonary toxicity is contingent upon the cumulative lung dose that exceeds overload conditions.

Optimally, the choice of dose metric and normalising factors should be based on the biological mechanisms mediating the toxic outcome. The analysis made in this study clearly demonstrates that the mass-based cumulative lung burden is a substantially better metric than surface area, suggesting toxicity is mediated via activated inflammatory cells rather than via particle properties. The mass-based (actual concentration  $\times$  cumulative exposure duration) exposure intensity appears to be also suitable; however, aerodynamic particle size related changes in pulmonary deposition have to be accounted for.

To conclude, this analysis provides strong evidence that the cumulative lung exposure dose corresponded well with the mass-based and agglomerated particle size-adjusted external exposure concentration and the associated pulmonary inflammatory response. The inhalation study with a MMAD in the range of  $\approx 0.5$   $\mu\text{m}$  yielded a higher pulmonary dose than MMADs in the 1–2  $\mu\text{m}$  range. In regard to the human significance of rat inhalation bioassays with poorly soluble particles, their outcome is highly contingent upon the total lung burden and especially whether overloading or non-overloading conditions had been attained. These conclusions are coherent with published evidence. Hence, a key premise for the dissymmetric adjustment across species is that comparable lung tissue doses should cause comparable effects. From that perspective, the determination of mass-based pulmonary lung burdens appears to be amongst the most important and critical nominator of dose. In regard to the toxicokinetics, the outcome is highly contingent upon the total lung burden and especially whether overloading and non-overloading conditions were attained. In order to reliably demonstrate retention-related differences in toxicity and fate of poorly soluble nanoparticles postexposure periods of at least 3 months appear to be indispensable.

#### 4.4.4 Conclusion to Chapter 4.4

Aerosols of nanomaterials are complex systems and the deposition and persistence of the inhaled particles in the lung as well as their interaction with the lung tissue are complex processes. Particles in the lung cause inflammations by recruiting and activating neutrophils and alveolar macrophages. This inflammation is critical for the lung toxicity of inhaled particles from nanomaterials. The fate of the inhaled particles and their interaction with neutrophils and macrophages govern the inflammation and hence the pulmonary toxicity of aerosols from nanomaterials.

A short-term inhalation study for nanomaterials was established to rapidly assess the toxicity of aerosols from nanomaterials. Six nanomaterials and three micron-scale materials have been compared in 5-day inhalation tests in rats. This short-term inhalation studies are flanked by two additional study types providing more specific information on retention kinetics and inflammation processes, respectively: A 28-day inhalation study with a follow-up period of 3 months was performed with AlOOH (No. 5) particles. And eleven different nanomaterials have been tested in rats using single intratracheal instillation (ITI) tests.

Most striking, the range of the toxic potencies found for all nanomaterials was strictly below that of crystalline silica (quartz DQ12). Whereas most nanomaterials formed agglomerates in the test systems, BaSO<sub>4</sub> (No. 10) formed nano-sized particles in suspension as well as in the air-borne state and elicited no effects in vivo, suggesting that there is no apparent toxic effect on lung tissue of nano-sized particles *per se*.

No measurable amount of any inhaled nanomaterial was detected in organs outside the lung (except in the draining lymph nodes). This may be due to a pronounced agglomeration of inhaled nanomaterials demonstrated for TiO<sub>2</sub> (1.2) and AlOOH (5) by electron microscopy. This finding is not at variance of earlier studies showing that a prerequisite of particle translocation is likely to be associated with an increased deterioration of the air-blood barrier system. The majority of both materials subsequent to inhalation were found within alveolar macrophages. A transport to lung associated lymph nodes was seen upon high particle concentration and increased lung burden.

Toxic or adverse effects observed so far peaked after 3 or 21 days, as seen for doped CeO<sub>2</sub> (4.4) in the instillation study. However, after a prolonged observation period (90 days) a dose-dependent delayed recovery of compromised lung function (namely due to dose-dependent inhibition of clearance) occurred also in these cases. Certainly, the appropriate study of lung clearance mechanism necessary to define the critical transition from non-overload to overload demands extended observation periods covering at least 1-2 clearance half-times (60 – 120 days). On the other hand, the short-term inhalation test established in the course of this project appeared well suited to describe e.g. the early inflammatory potential and adverse effects of inhaled nanomaterials. This type of study may, therefore, become a tool enabling toxicologists to screen and compare inflammatory effects of nanomaterials; whereas other parameters, such as biopersistence, can only be judged by studies with longer observation periods.

A direct comparison between different methods showed that e.g. BaSO<sub>4</sub> (10) proved non-toxic in both instillation and short-term inhalation approaches. In contrast, CeO<sub>2</sub> elicited comparatively high inflammatory responses in low aerosol concentration and was also highly bioactive after instillation. Inhalation and instillation of AlOOH (5.1) revealed very similar threshold values in the range of 1.2 mg per rat lung, further demonstrating that intratracheal instillation is a valuable tool for nanotoxicology, especially as it forms a bridge between in

vivo and in vitro experiments as long as dose- and effective particle-size-equivalence is considered. More complex nanomaterials, which behave differently in air and the liquid media used for instillation, may exert different toxic potencies and findings because of differences in agglomeration and surface activities. These points will be further discussed in section 4.5.4.

Collectively, all the industrially produced nanomaterials investigated in the NanoCare Project elicited no, moderate, or reversible toxic effects in rat lungs, depending on the particle properties and the deposited/retained pulmonary dose. It should, however, be emphasised that these nanomaterials had not been subjected to special surface modifications affecting the binding of proteins in the lung lining fluid and altering the agglomeration state of the nanoparticles in the lung.

A common response to particle retention is the recruitment and activation of neutrophils and alveolar macrophages. Both are ROS generating cells. The ROS burst from these cells may be orders of magnitudes higher than that generated by the particle *per se*. The dynamics of these factors and circumstances should be taken into account when in vivo results of the NanoCare investigation are compared to other studies. As a matter of fact, such comparisons require common denominators of dose and involved mechanisms.

## 4.5. Comparison of in vitro and in vivo Findings

M. Wiemann and J. Bruch

### 4.5.1 Objectives

The prediction of health effects possibly arising from ambient or manufactured nanoparticles is an important issue and was one major challenge of the NanoCare project. At present only a few studies focus on a direct comparison of in vitro and in vivo results obtained with the same material (Sayes et al., 2007, Donaldson et al., 2008). The production of ROS and associated over-expression of ROS related genes has been recognized as one major consequence of nanoparticle treatment (Nel et al., 2006, Xia et al., 2009) and first studies tried to estimate the toxic potential of nanomaterials from in vitro studies of ROS production (Park and Park, 2009). Thanks to the possibility to investigate the same type of thoroughly characterised nanomaterials by different groups, the NanoCare project was able to compare results from parallel in vitro and in vivo studies. These investigations comprised studies on many different cell lines (see 4.3.2) as well as alveolar macrophages (AM), in which the cellular particles dose could roughly be adapted to the situation inside lung (see 4.3.1). The aim of these different approaches is to find a reliable method enabling us to predict biological effects of nanomaterials at least in part from in vitro studies. This chapter will oppose the results from in vivo studies outlined above to results from different in vitro approaches. The comparison will be made for each material investigated with at least one in vivo approach. A first successful correlation of in vitro and in vivo results will be shown for seven different materials applied to alveolar macrophages under serum-free conditions. Furthermore, we will briefly discuss the use of apparently more sensitive approaches based on established cell lines.

### 4.5.2 Data Overview

The analyses of in vivo studies were confined to effects on lung tissue, as no particulate matter was found to be transmitted from the lung into other organs (see 4.4.2 and 4.4.3). Three different in vivo testing protocols were used: 28-day inhalation, 5-day inhalation and intratracheal instillation. For the in vitro analyses we focussed on those cells which are of some relevance for the lung: freshly isolated alveolar macrophages (AM) and related macrophages from mice (RAW264.7), as well as lung epithelial cells A549, RLE-6TN and CaLu3. The combination of protocols, particles, observation periods after application, and relevant in vitro data is shown in table 4.5.1.

**Table 4.15** Data used for the comparison of in vitro and in vivo effects. An “X” indicates informative experiments. Alveolar macrophages (AM) were exposed to 15-120  $\mu\text{g}/10^6$  cells. Cell lines were treated with 0.1-50  $\mu\text{g}/\text{cm}^2$  as indicated in section 4.3.2.

		Considered in vivo Studies - Rat Lung -									Considered in vitro Results - Lung relevant Cells -					
		28-d Inhalation				5-d Inhalation			Instillation		AM	RAW 264.7	A549	RLE- 6TN	CaLu3	
	Section	4.4.3				4.4.2			4.4.1		4.3.2					
No.	Observation Period [d]	1	12	31	91	0	3	14	3	21	90	1	1-3	1-3	1-3	1-3
1.2	TiO <sub>2</sub>					X	X	X	X			X	X	X	X	X
3.1	CeO <sub>2</sub>					X	X	X	X			X	X	X	X	X
4.4	doped CeO <sub>2</sub>					X	X	X	X	X	X	X	X	X	X	X
5.1	AlOOH	X	X	X	X				X	X	X	X	X	X	X	X
5.2	AlOOH	X	X	X	X							X	X	X	X	X
6.3	Ti-Zr								X			X	X	X	X	X
7.3	Al-Ti-Zr								X	X	X	X	X	X	X	X
8.1	ZrO <sub>2</sub>								X			X	X	X	X	X
8.2	ZrO <sub>2</sub>								X			X	X	X	X	X
10	BaSO <sub>4</sub>					X	X	X	X	X	X	X	X	X	X	X
11.1	SrCO <sub>3</sub>								X	X	X		X	X	X	X
11.2	SrCO <sub>3</sub>								X	X	X		X	X	X	X

#### 4.5.3 Comparative Analysis of Selected Nanomaterials

The following paragraph will mainly focus on the effects of AlOOH (5.1, 5.2), BaSO<sub>4</sub> (10), TiO<sub>2</sub> (1.2), CeO<sub>2</sub> (3.1, 4.4) and Al-Ti-Zr (7.3), all of which have been tested with at least one in vivo approach.

Inhaled **AlOOH** (5.1 and 5.2) caused signs of inflammation upon a cumulative burden of >1mg/rat lung. Under these conditions BALF parameters such as PMN count, LDH, and protein remained significantly elevated even after 91 days post exposure, although there was a clear trend towards recovery. Results from the instillation study (AlOOH (5.1)), which were conducted with 0.6, 1.2, 2.4 and 4.8 mg per lung, were in good accordance, as significant effects remained obvious upon  $\geq 1.2$  mg per lung after 21 days. Effects of AlOOH on PMN counts, macrophage counts and protein in BALF decreased and reached control levels after 90 days, if the dose was below 2.4 mg which may be close to overload (compare section 4.4.3). These very moderate effects of AlOOH were furthermore reflected by the in vitro test on macrophages (vector model): Acute effect of AlOOH on release of LDH, and glucuronidase started to occur at a nominal loading of 60-120 pg/cell. Functional cell damage (impairment of PMA-stimulated ROS generation) was observed upon >60 pg/cell while spontaneous extracellular ROS production (decomposition of fluorescence indicator scopoletin) did not occur. The nominal loading of AM matched the range observed in macrophages in vivo, as outlined in section 4.3.1. As vitality and mobility of AM were not impaired, it may be concluded that these AlOOH (5.1) loads did not markedly compromise AM thus allowing them to further participate in lung clearance. It may be speculated that the consistency of in vivo and in vitro findings may at least partly be due to the absence of serum components and/or to the fact that particles were similarly coated with lung surfactant or PC.

However, there were also some inconsistent findings: AlOOH (5.1) elicited production of TNF $\alpha$  in vitro, an effect not seen in vivo. In the presence of serum A549 cells showed a reduction of the glutathione level (AlOOH (5.1)  $\leq 5$   $\mu\text{g}/\text{cm}^2$ ) and an increased expression of HO-1 at very low doses (AlOOH (5.2), 10  $\mu\text{g}/\text{cm}^2$ ). Since AlOOH particles were hardly detected in epithelial cells in the course of our EM study on lung tissue (4.4.2) and because

the content of AIOOH within A549 cells is not known, the relevance of these findings remains obscure. However, those mechanisms may account for some cell damage in case that AIOOH particles penetrate the epithelial lung barrier, which has not been observed in healthy animals so far. The synopsis from these results is that loading of alveolar macrophages with ALOOH in vivo largely equals the nominal load used in vitro. Under both conditions AIOOH (5.1) caused significant increases suggestive of cell membrane deterioration and ROS generation at doses  $\geq 60$  pg/AM.

Inhaled **BaSO<sub>4</sub>** (10) elicited no noticeable effects in the rat lung (see section 4.4.2). The same was true for instilled BaSO<sub>4</sub> (up to 4.8 mg) and SrCO<sub>3</sub> (11.1 and 11.2) analysed after 3, 21 and 90 days (4.4.1). Assays of the vector model and most other cell tests also failed to reveal any adverse effects, except for a constant induction of TNF $\alpha$  in AM in the range of 15-120 pg/cell. TNF $\alpha$  was, however, not increased in BALF 3 days after instillation. So far, BaSO<sub>4</sub> was rated as the least toxic nanomaterial of the study. However, A549 cells and RAW264.7 macrophages exhibited induction of IL-8, decay of glutathione and increased HO-1, all pointing to some oxidative stress upon  $\geq 1$ -5  $\mu\text{g BaSO}_4/\text{cm}^2$ . However, these effects on ROS formation seen in RAW.264.7 macrophages and A549 cells have no obvious counterpart in vivo. Interestingly, BaSO<sub>4</sub> tended to persist as a nanoparticle also in serum-free medium. Furthermore it may be of relevance, that the affinity of BaSO<sub>4</sub> for serum protein components was very low (see section 4.3.1) such that a direct interaction of BaSO<sub>4</sub> nanoparticles or small aggregates with cell surface receptors may play a role. Considerable contribution of soluble additives leaking from BaSO<sub>4</sub> nanocrystals was found to be involved in the induction of TNF $\alpha$ . BaSO<sub>4</sub> is regarded a nanomaterial whose non-toxic properties in vivo were largely reflected by the vector model procedure and most other cell culture models.

Inhaled **TiO<sub>2</sub>** (1.2) distributed quite equally in the rat lung and was found nearly exclusively within alveolar macrophages (see 4.4.2). A burden of 0.54 mg/rat lung increased PMN counts and activity of glutamyl transferase in BALF after 3 days. At 1.6 mg per rat lung the number of PMN as well as protein concentration and enzyme activities were further increased; changes were partially reverted after 14 days. Also in the instillation study a dose of 0.6 mg elevated the number of PMN to 10% of the total cell count after 3 days. This mild granulocytosis was the most prominent sign of a low lung burden with TiO<sub>2</sub> and is in line with current literature. In analogy to what was measured for the disposition of AIOOH in the lung, the mean uptake of TiO<sub>2</sub> (1.2) into alveolar macrophages may be calculated as follows: a mass of 0.54 mg TiO<sub>2</sub> (1.2) (close to the low effect level) would be distributed to  $1.3 \times 10^7$  macrophages which is the whole population of macrophages inside a rat lung (Rehn et al., 1991). This would result in a mean dose of  $\leq 41.5$  pg/cell. Interestingly, in the vector model TiO<sub>2</sub> (1.2) elicited adverse effects (elevated LDH, glucuronidase, functional cell damage) at about 30 pg/cell, while TNF induction was increased at 60 pg/cell. In any case TiO<sub>2</sub> (1.2) was clearly more bioactive than AIOOH. It should also be noted that supernatants from sedimented suspensions (0.025mg PC/ml, serum free medium) slightly enhanced the release of LDH (<10%) and glucuronidase from macrophages, indicating that smaller particles were present and may have exerted biological effects. In this context it is also noteworthy that TiO<sub>2</sub> (1.2) strongly binds to BSA and/or surfactant protein A (see 4.3.2) and will thus be coated with serum proteins when interacting with cells. This might be of particular relevance for macrophages such as RAW264.7 whose scavenger receptors are highly influenced by denaturated BSA (Dutta et al., 2007). TiO<sub>2</sub> (1.2) also enhanced the inflammatory enzyme cox-2 at extremely low concentration (0.1  $\mu\text{g}/\text{cm}^2$ ) as well as HO-1, an indicator of ROS production. ROS induction occurred at 1  $\mu\text{g}/\text{cm}^2$  in A549 cells which was close to the lowermost value found for carbon black (see 4.3.2). In conclusion, TiO<sub>2</sub> showed only moderate lung toxicity although ROS generation and cox-2 were enhanced in vitro.

**CeO<sub>2</sub>** (3.5 and 4.4) were used in 5-day inhalation studies, in which lung doses of approximately 0.05 mg, 0.17 mg and 0.42 mg were found for CeO<sub>2</sub> (3.5). Signs of inflammation such as increased PMN counts occurred after 3 days at the lowest concentration, pointing to a higher biologic activity than TiO<sub>2</sub> (3.5). First results showed that effects of doped CeO<sub>2</sub> (4.4) on differential cell counts were even more pronounced. In the instillation study the Al-doped modification of CeO<sub>2</sub> (4.4) was used due to better dispersion characteristics. This type of CeO<sub>2</sub> showed a comparatively high toxicity since its NOEL was below the lowermost concentration of 0.6 mg instilled per lung. Even 0.6 mg CeO<sub>2</sub> (4.4) elicited severe focal epithelial damage indicated also by enhanced protein release and, after 21 days, increased levels of protein and fibronectin in BALF which exceeded those of the time-matched quartz DQ12 value (1.2 mg per lung were used as positive control). After 90 days and at concentrations larger than 0.6 mg all inflammation markers were still elevated. Histological analysis (Sirius Red staining) showed progressive fibrosis diffusely scattered throughout the lung parenchyma. In the vector model most variants of CeO<sub>2</sub> and in particular CeO<sub>2</sub> (4.4) showed a steep increase in cytotoxic potential at concentrations  $\geq 60$  pg/cell. Levels of glucuronidase, indicating pronounced damage of phagolysosomes, were at very high levels. Most striking, CeO<sub>2</sub> (3.5 and 4.4) induced high amounts of TNF $\alpha$  in a dose-dependent manner. Levels for cox-2 and HO-1 expression in RAW264.7 showed a large disparity depending on the type of CeO<sub>2</sub>. CeO<sub>2</sub> (4.4) showed a comparatively high inflammatory potential. Nevertheless, after 90 days its inflammatory and fibrogenic potential was 4-times less than quartz DQ12.

One of the mixed oxides **Al-Ti-Zr** (7.3) was used in the instillation study because it exhibited a somewhat increased in vitro toxicity in vector model studies (section 4.3.2). Similar to AlOOH but with a higher efficacy instilled Al-Ti-Zr (7.3) led to a dose dependent recruitment of PMN seen after 3 and 21 days. After 90 days high TNF- $\alpha$  levels were found in the BALF. Also in the vector model Al-Ti-Zr induced comparatively high levels of TNF $\alpha$ , while cytotoxic effect started at 30 pg/cell. Damage of phagolysosomes was observed at 60 pg/cell. There were no effects on other cell lines up to a concentration of 10  $\mu\text{g}/\text{cm}^2$ . Based on these results Al-Ti-Zr (7.3) has a pronounced in vivo and in vitro toxicity.

#### 4.5.4 Correlation of Data from Vector Model Investigations and Intratracheal Instillation

According to manifold similarities of results from intratracheal instillation study and data obtained with the vector model using alveolar macrophages we correlated both approaches in a quantitative manner. To this aim we used the sum indices described in section 4.3.2 and 4.4.1 as overall measures of in vitro and in vivo toxicity, respectively. In case that low particle concentrations were used in vivo (0.6 mg per rat lung) and in vitro (15 pg/cell) we found a linear correlation of seven nanoscaled materials (Fig. 4.5.1A). At high exposure levels (4.8 mg in vivo, 120 pg/cell in vitro) we obtained a similar value ( $R^2=0.787$ , Fig. 4.5.1B). TNF values, usually measured as part of the in vitro model, were not incorporated due to high inter-individual differences seen after 3 days in vivo. The same in vitro results could be correlated to in vivo results obtained after an observation period of 90 days (Wiemann et al., 2009b). It should be stressed that all materials exhibit a comparatively low in vivo toxicity in comparison to quartz DQ12, which was used at a 4-fold lower dose. These results show for the first time, that in vitro effects of different poorly soluble nanomaterials can be quantitatively correlated to in vivo results.

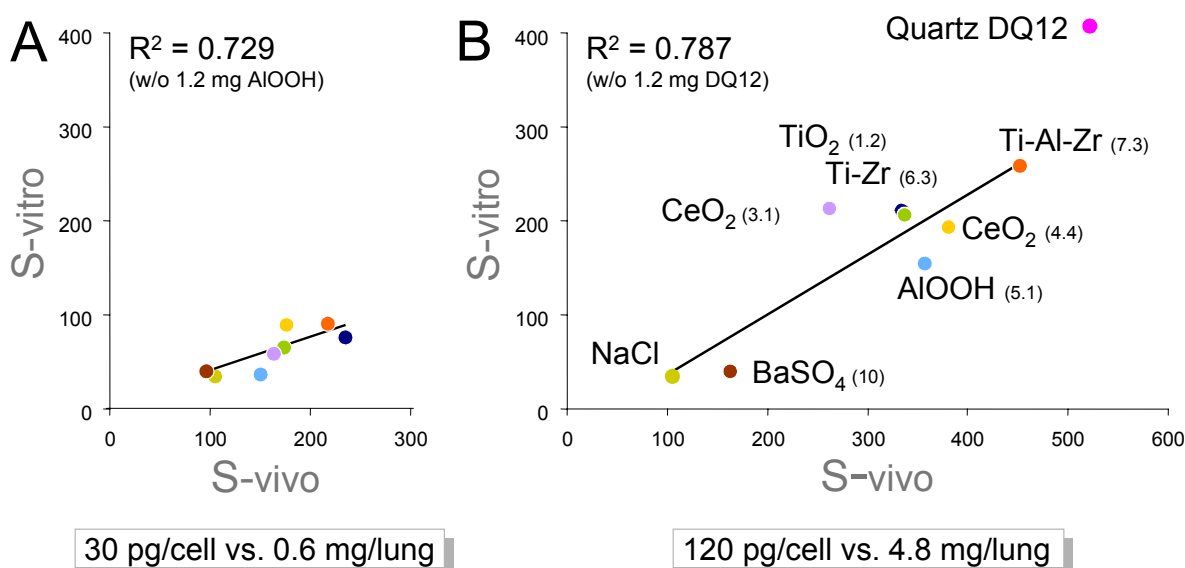


**Figure 4.27** Correlation of in vitro and in vivo results from seven NanoCare samples. Sum indices were calculated from in vitro studies of isolated alveolar macrophages (S-vitro) and from BALF analyses of rats instilled with the same particles (S-vivo); see section 4.3.2 and 4.4.1 for further explanation. (A) and (B) are low and high concentration approaches, respectively. Nominal doses are indicated underneath. Colour-coding in (A) is identical to (B). Values from 1.2 mg AlOOH in (A) and 1.2 mg quartz DQ12 in (B) were not used for calculation.

#### 4.5.5 Predictive Value of Cell Culture Experiments on Cell Lines

In contrast to the vector model data, the determination of inflammatory markers (cox-2) and ROS-defence strategies (HO-1) of A549 cells or RAW264.7 cells appeared to be far more sensitive. This offers the chance to detect effects originating from low concentrations of nanoparticles, which will be especially helpful to model particle exposure of the lung epithelium or other tissues, where the number of particles is supposed to be low. A concentration of  $0.1 \mu\text{g TiO}_2/\text{cm}^2$  which increased cox-2 in RAW264.7 macrophages, is equivalent to approximately 80 fg/cell under confluent cell culture conditions. Assuming all particles as to be spherical and 50 nm-sized, and provided that the material is completely bound to or taken up, a cell responding with an increase in cox-2 might contain only 300 nanoparticles. In practice however, particle size, surface properties and aggregation state determined for the air-borne state may change in a concentration-dependent manner. Also the calcium concentration of the extracellular fluid or cell culture medium will influence agglomeration state. Thus, as long as nanosized and fine particles of the same material are not compared site-by-site size-dependent effects cannot be unequivocally distinguished in vitro.

Nevertheless, these sensitive tests also distinguished between different materials with different biological activity in vivo. Thus the threshold values for HO-1 expression were equally low ( $1 \mu\text{g}/\text{cm}^2$ ) for  $\text{BaSO}_4$  (10),  $\text{CeO}_2$  (3.1) and  $\text{TiO}_2$  (1.2). Reduction of glutathione was, however, 5-fold lower for  $\text{BaSO}_4$  than for  $\text{CeO}_2$  or  $\text{TiO}_2$ , which was somewhat surprising as  $\text{BaSO}_4$  obviously lacked any biological activity inside the lung (the effect may be due to leaking substances, see above).

Enhanced expression of cox-2 was obtained with 0.1-10  $\mu\text{g}/\text{cm}^2$  in the order:

Carbon Black (2) =  $\text{TiO}_2$  (1.2) =  $\text{CeO}_2$  (3.2) =  $\text{ZrO}_2$  (8.1) <  $\text{CeO}_2$  (3.1) =  $\text{CeO}_2$  (3.5) <  $\text{CeO}_2$  (3.3)

In line with this, the ROS production was elicited by  $\text{TiO}_2$  and Carbon Black at very low concentrations. The possibility to compare these results to those of inhalation and instillation studies is limited by the lack of corresponding in vivo data. However, if one considers the results on ROS production, glutathione decrease, HO-1 and cox-2 expression as one common feature, a preliminary rank order of cytotoxicity may be established:  $\text{BaSO}_4 < \text{AlOOH} < \text{CeO}_2 < \text{TiO}_2$ . In line with this, experiments with MM6/A549 co-cultures also showed positive result for IL-8 production upon  $\text{TiO}_2$  (1.2) and  $\text{CeO}_2$  (3.1) at low concentrations, while all other materials had no effect. Taken together, in vitro experiments with cell lines appear to be more sensitive especially when macrophage derived cell lines were used. Results obtained so far qualitatively reflect the biologic activity of nanomaterials in vivo.

#### 4.5.6 Conclusions

The common evaluation of all tests carried out in the NanoCare project has shown that in vitro tests are, to a certain extent, able to reflect some of the in vivo results as long as they are directly particle-derived. As to whether in vitro conditions can be translated to the real-life situation was beyond the scope of this study which was to comparatively rank toxic properties of particles without considering durability, associated biopersistence, and/or the organism's long-term response to injury. In any case a combined evaluation of different endpoints appeared necessary. Both, inhalation and intratracheal instillation were suitable methods to administer nanomaterials to the lung. Results from intratracheal instillation of seven nanostructured particles and tests on acutely isolated alveolar macrophages under serum-free conditions yielded very similar results, enabling an in vitro – in vivo correlation for the first time. Significant differences of the toxicities of the tested nanomaterials underline the necessity to check for the toxic potential of newly developed nanomaterials. Further measurements of particle load of macrophages from BALF and cell culture are necessary to obtain equal cellular particle doses in vivo and in vitro. However, it is important to note that in both test systems, the in vitro tests on one side and the in vivo tests on the other, no-effect-levels could be determined. Conceptually, the method devised attempts to simulate the most critical dose range in vivo, namely the transition from non-overload to overload. We think that testing at this cross-road provides a means not only to define the most meaningful dose used in in vitro systems but also to make a relative ranking of particle properties. As long as the most critical metrics of dose is incompletely defined, extrapolation to the real-life situations has to await further study.

In the presence of serum in the culture medium complementary findings were seen using cultured macrophages and lung epithelial cells. These cells responded to very low concentrations of nanostructured particles. They may therefore serve as model systems to study effects of nanoparticles in the depth of the lung tissue where concentrations of particles appear to be very low. Reaching deeper areas of the lung, particles are ultimately coated with biomolecules such as peptides or proteins. Further studies to comprehensively estimate the toxicity of particles in vitro should therefore combine serum-dependent and serum-free methods.

## 5. Exposure to Nanoparticles: Measurement, Modelling and Agglomerate Stability

C. Asbach, D. Dahmann, H. Kaminski, K.H. Kampmann, T.A.J. Kuhlbusch,  
C. Monz, U. Rating, B. Stahlmecke, M. Voetz, S. Wagener

### 5.1 Objectives

Exposure to nanoparticles is currently discussed within the framework of risk assessment. A potential risk may only arise if an exposure to particles of concern exists. Besides investigations of the toxicity of nanoparticles in work packages 3 and 4, the study and eventually the prevention of possible exposure to nanoparticles is thus a major step towards sustainable development of nanotechnology.

To understand the exposure scenarios, nanoparticles in workplace air can either be measured using appropriate measurement technology, or modelled by using computational fluid dynamics simulations. Both approaches were followed in work package 5 and are briefly described here.

The measurement of engineered nanoparticles in workplaces is challenging because they have to be distinguished from the ever-present background particles. Strategies were developed to differentiate those particles that were potentially emitted, e.g., from a NP production process from ubiquitous particles.

It may be erroneous to assume that airborne particle concentration and properties in the breathing zone of exposed persons are identical to those of the particles that are present in, e.g., the synthesis reactor during production or in a commercial powder, because these particles may undergo physical and/or chemical changes while being released (Seipenbusch et al., 2008). Therefore, an important work package within NanoCare was the investigation of the propensity of the nanostructured materials to release airborne nanoparticles into the breathing zone of workers.

In this context it needs to be stressed that an important parameter for merging toxicity with exposure data is particle size (e.g. Oberdörster, 2000). Nanoparticles usually appear in the shape of larger agglomerates, which however may break up during transmission and release into smaller aggregates or even primary particles if exposed to sufficiently high energy (Froeschke et al., 2003; Jensen et al., 2009; Tsai et al., 2009). The stability of agglomerates was, therefore, also systematically studied under different conditions.

### 5.2 Measurement Technology

Current legislative limits for ambient or workplace airborne particle concentrations are based on the integral particle mass concentration of all particles below a certain size. Internationally used size limits are 10  $\mu\text{m}$  ( $\text{PM}_{10}$ ) or 2.5  $\mu\text{m}$  ( $\text{PM}_{2.5}$ ) for ambient air (EN12341; EN14907), and e.g. 4  $\mu\text{m}$  (“ $\text{PM}_4$ ”) for workplaces. However, NPs have only very small masses and therefore generally contribute negligibly to these integral mass concentrations. More NP-sensitive techniques are therefore required to detect those particles in air. Unlike the particle mass, which is weighted with the particle diameter to the third power, the particle number is

unweighted and therefore the most sensitive measure for NP concentrations (Kuhlbusch et al., 2008). The most widely spread method to determine airborne (nano-) particle number concentrations as a function of particle size, i.e. particle number size distributions, is based on electrical mobility analysis of the particles (Fissan et al., 1983). In electrical mobility analysis, particles are initially electrically charged to a known charge distribution, which is a function of particle size (Fuchs, 1963). Particles are then classified in an electric field according to their charge to size ratio, i.e. their electrical mobility (Pui and Liu, 1974). The mobility classified particles are detected by either their induced electrical current or by direct counting. With the known size-dependent charge distribution, the measured data is deconvoluted into a number size distribution.

Exposure measurements may face aerosols that can be everything from quickly-changing to stable over longer time depending on processes and activities in the vicinity of the measurement location. Time resolution may therefore play a crucial role when choosing an appropriate mobility particle sizer, besides its accuracy and size resolution. Within this work package, different mobility particle sizers were used by the different partners in order to measure number size distributions, e.g. in workplaces. These instruments have been subject to a detailed intercomparison study, which involved a Fast Mobility Particle Sizer (Tammet et al., 1998; FMPS, TSI model 3091, time resolution 1 s, size range 5.6 – 560 nm), a Sequential Mobility Particle Sizer (Heim et al., 2004; SMPS-G, Grimm Aerosol Technik SMPS+C) with either a long DMA (size range: 11.1 – 1083.3 nm, time resolution 406 s) or a short DMA (size range: 5.5 – 350.4 nm, time resolution 230 s) and two Scanning Mobility Particle Sizers (Wang and Flagan, 1990; SMPS-T1 and SMPS-T2, TSI model 3936 equipped with long DMA, size range: 13.8 – 749.9 nm, time resolution 240 s). The two TSI SMPSs were substantially identical, except for the condensation particle counters (CPCs); SMPS-T1 used a water based (TSI model 3786), and SMPS-T2 a butanol based (TSI model 3010) CPC. The instruments simultaneously sampled either compact sodium chloride particles or with typical diesel soot agglomerates. The aerosols were generated and fed through a wind tunnel which expands into a 20 m<sup>3</sup> chamber, which ensured homogenous mixing of the particles with dilution air, resulting in equal sampling conditions for all instruments. SMPS-T1 was always operated with default settings, whereas the other SMPSs were either used with their default settings (comparable with SMPS-T1) or modified settings concerning flow rates (SMPS-T2) or installed DMA (SMPS-G1). The FMPS doesn't allow for any changes and was therefore always operated with its default settings. In order to be able to compare the results from the different instruments, measured number size distributions were mathematically fitted. Figure 5.1 shows the fitted size distributions for sodium chloride aerosol. The left graph shows measurements with basic settings, whereas the right graph shows the variations. The left graph shows that SMPS-T1, SMPS-T2 and FMPS showed very comparable results when operated with their basic settings. An increase of the flow rates of SMPS-T2, however, delivered a noticeably higher concentration, despite the fact that the software should correct for the effect of the changed flow rates. Concentrations from SMPS-G1 were consistently higher than those from TSI instruments. A change of the DMA in SMPS-G1 did not substantially influence the measured results. Concerning the sizing, all instruments delivered fairly similar results.

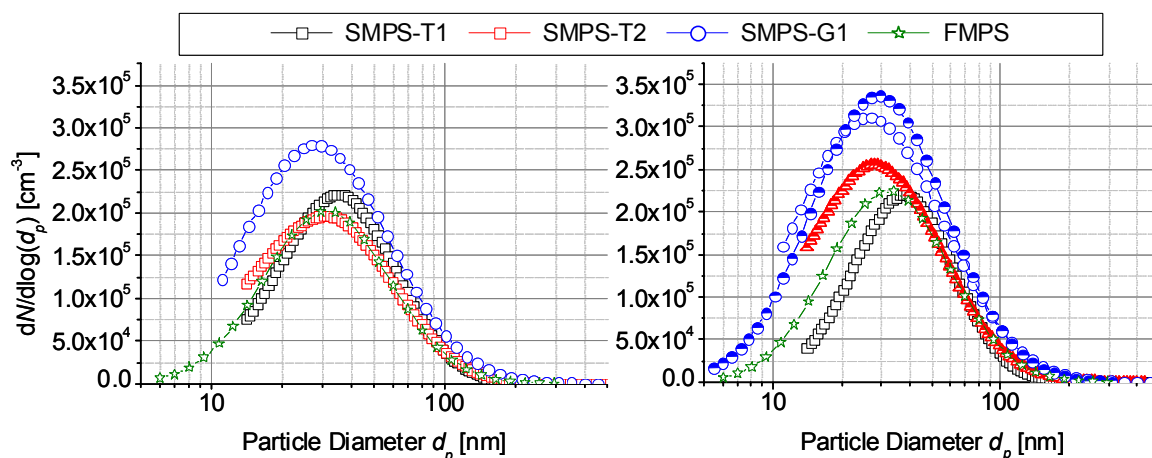


**Figure 5.1** Measured number size distribution of sodium chloride aerosol; left: all instruments in basic setting, right: variations illustrated as half closed symbols: SMPS-G1 – DMA changed from long to short DMA, SMPS-T2 flow rates switched from 0.3/3 l/min to 0.6/6 l/min (Asbach et al., 2009a).

Figure 5.2 shows the fitted size distributions for the diesel soot measurements, which generally confirmed the findings with NaCl aerosol. Again, the concentration in SMPS-T2 was increased with increased flow rates and a change of the DMA in SMPS-G1 didn't noticeably affect the result. The FMPS however seemed to react more differently to the different aerosols than the other instruments. While concentrations measured by FMPS in case of NaCl aerosol were comparable with those from SMPS-T1 and the width of the distribution was broader, FMPS concentrations were significantly higher in case of diesel soot than in case of NaCl and the distributions noticeably narrower. It should be noted that no number concentration standard exists, so the "true" number concentration could not be determined.

A detailed analysis of the investigations has been submitted to Journal of Nanoparticle Research (Asbach et al., 2009a).

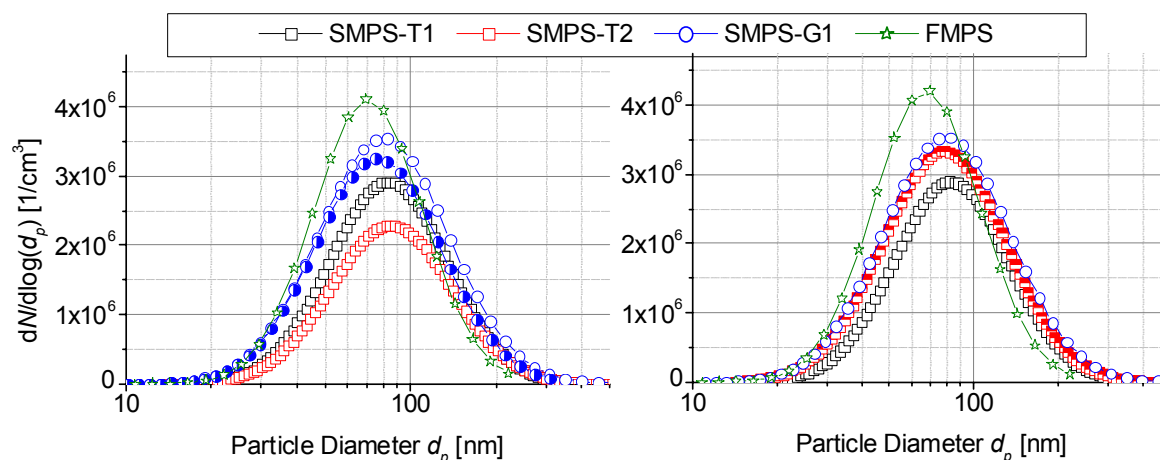


**Figure 5.2** Measured number size distribution of diesel soot aerosol; left: all instruments in basic setting, right: variations illustrated as half closed symbols: SMPS-G1 – DMA changed from long to short DMA, SMPS-T2 flow rates switched from 0.3/3 l/min to 0.6/6 l/min (Asbach et al., 2009a).

### 5.3 Measurement Strategy for Nanoparticles in Workplaces and Validation

In order to improve the necessary knowledge to assess the possible implications of nanoparticles, it is necessary to be able to detect and quantify nanoparticles in the workplace environment. Different measurement and sampling techniques are necessary as well as task specific strategies to identify and quantitatively determine nanoparticles.

For the detection of the possible release of nanoparticles into workplaces a measurement strategy was developed using a combination of measurement and sampling systems. Particle counters (CPC), surface area measuring devices (NSAM, TSI model 3550; Fissan et al., 2007; Asbach et al., 2009b) and mobility spectrometers (SMPS, FMPS) are used for the determination of particle concentrations and size distribution. Electrostatic Precipitators (NAS, TSI model 3089 or ESP, Grimm model #5.561; Dixkens and Fissan, 1999) are used to deposit particles onto substrates for consecutive single-particle or bulk analyses of physical and chemical properties. Different standard operation procedures (SOP) were developed for the execution of such workplace measurements. These SOPs present the

- general procedure to measure nano- and ultrafine particles in workplaces,
- data analysis for the determination of particle release,
- reporting of measurements and data analysis, and
- general handling and maintenance of the different measuring devices.

The possible release of engineered nanoparticles was investigated at several work places within four different plants to allow for an assessment of the exposure of workers and validate the newly developed strategies. These plants were facilities for the production of nanoparticles or their further processing. For the determination of the number concentration/ presence of nanoparticles in workplace environments two sets of measurement devices (SMPS/FMPS, NSAM, NAS/ESP) with concurrent measurements in the work area and a comparison site were used (see Figure 5.3). Particle mass concentrations of particles <1 µm were measured gravimetrically alongside in order to compare measured results with regulatory workplace exposure limits.

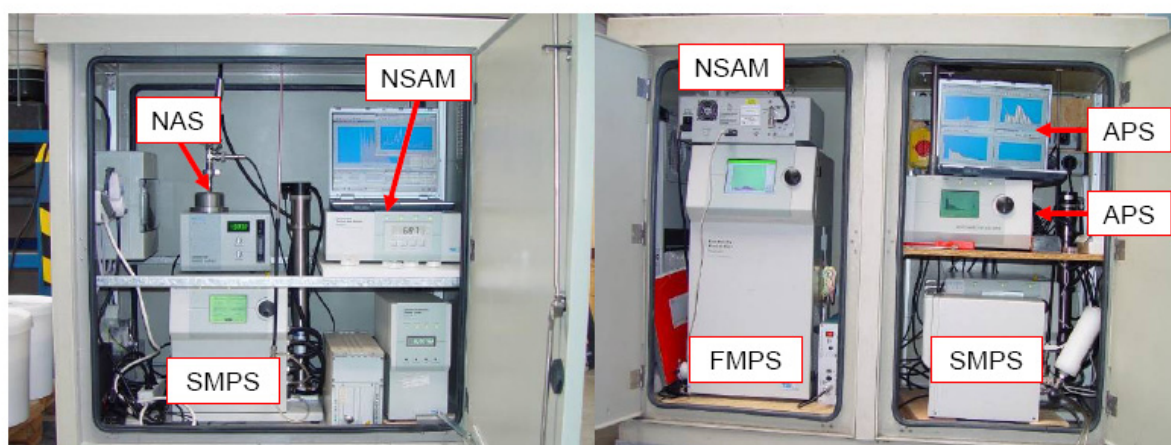


**Figure 5.3** Measurement devices for the comparison site (left) and the workplace (right).

Initially, simultaneous measurements in work area without work activities (inside area) and the comparison site (outside area) were carried out to determine the fraction of particles that infiltrate into the work environment from outside. Later the actual measurements were carried out simultaneously in the work area with work activities (inside area) and the comparison site

(outside area) as illustrated in Figure 5.4. The resulting data were compared to identify events in number concentrations and number size distributions (Kuhlbusch et al., 2009). The potential release of particles from the process was then calculated by subtracting the concentration infiltrating from outside from the measured concentrations. Data interpretation is based on the assumption that measurements at the comparison site mirror the surroundings of the workplace to be investigated. This includes that particle concentrations (size distributions) at the workplaces during no work activity can be calculated from those at the comparison site. The comparison site therefore has to be representative of the surroundings. To estimate the measurement uncertainty, the deviation of the devices used in the inside and outside area was determined experimentally as a function of particle size prior to the workplace measurements. Furthermore it was assumed that the infiltration factor may vary by a factor of two. An increase of the inside particle concentration was thus assumed to be significantly linked to the indoor work process only when the increase exceeded the measurement uncertainty.

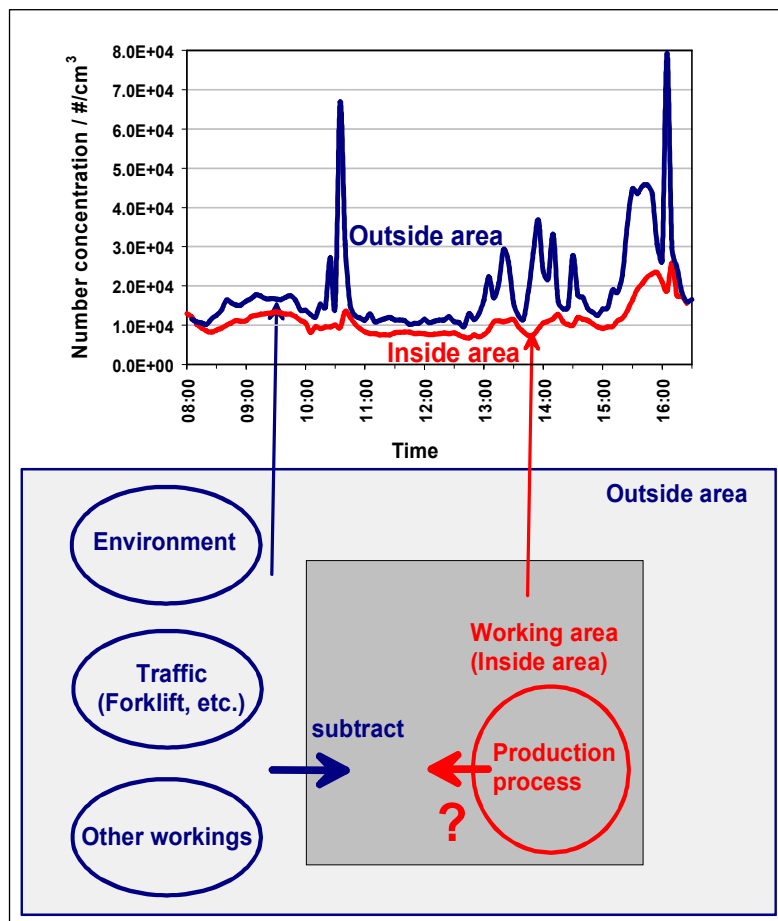


**Figure 5.4** Influence of ambient particles on workplace measurements is shown by the nearly parallel concentration changes in ambient and workplace particle concentrations (Kuhlbusch et al., 2009).

The introduced data analysis method delivers size resolved information about the exposure of workers. The results show that for all investigated locations no significant increase in concentration of particles  $\leq 100$  nm in diameter linked to the production process were determined, however in two cases significant increase in concentration of coarser particles  $> 450$  nm diameter was observed stressing that no relevant amounts of particles  $< 100$  nm diameter were released. The results are summarised in table 5.1.

**Table 5.1** Summary of particle releases at different workplaces (yellow cells indicate NPs and their agglomerates)

<u>Release of particles</u>	<u>≤100 nm</u>	<u>100-450 nm</u>	<u>≥ 450 nm</u>	<u>Instrument used</u>
Workplaces of Plant 1				
Reactor and filling area of cerium oxide	not significant	not significant	not significant	SMPS-T1, SMPS* FMPS
Reactor and filling area of mixed titanium silicon oxide	not significant	not significant	not significant	SMPS-T1, SMPS* FMPS
Workplaces of Plant 2				
Dryer area of barium sulphate	not significant	not significant	not significant	SMPS-T1, SMPS* FMPS
Filling area of barium sulphate	not significant	not significant	significant	SMPS-T1, SMPS* FMPS
Workplaces of Plant 3				
Autoclave and receiver tank area of titanium dioxide	not significant	not significant	significant	SMPS-T1, SMPS* FMPS
Milling area of titanium dioxide	not significant	not significant	not significant	SMPS-T1, SMPS* FMPS
Workplaces of Plant 4				
Manual mixing area with AIOOH	not significant	not significant	not significant	SMPS-G1, CPC
Automatic mixing area with AIOOH	not significant	not significant	not significant	SMPS-G1, CPC
Compounding area AIOOH	not significant	not significant	not significant	SMPS-G1, CPC
Granulating area with AIOOH	not significant	not significant	not significant	SMPS-G1, CPC
Injection moulding area with AIOOH	not significant	not significant	not significant	SMPS-G1, CPC

SMPS\* identical with SMPS-T1, but was not subject to intercomparison study (chapter 2).

## 5.4 Modelling of Spatial Variability of Exposure Levels Following Accidental NP Release

As of now, exposure has mainly been measured with stationary measurement equipment, such as mobility particle sizers, particle counters or surface area monitors. Some papers have recently been published that describe mapping of submicron and nanoscale particles using mobile equipment in order to obtain higher spatial resolution of the measurements. Only a few personal sampling devices that determine personal exposure specifically to nanoparticles exist. However, all the aforementioned methods have in common that they can only deliver results with limited or no temporal and/or spatial resolution. Modelling of particle

dispersion in a workplace, however, can provide information on temporal and spatial variations of aerosol or particle properties. Furthermore modelling can enable the study of the effects of single particle dynamic processes, such as coagulation or Brownian diffusion on the variation of aerosol and particle parameters. Another advantage of modelling is that boundary conditions, such as wall temperatures or ventilation scenarios can be varied in order to study their effect on particle dispersion and consequently possible exposure to particles in a workplace.

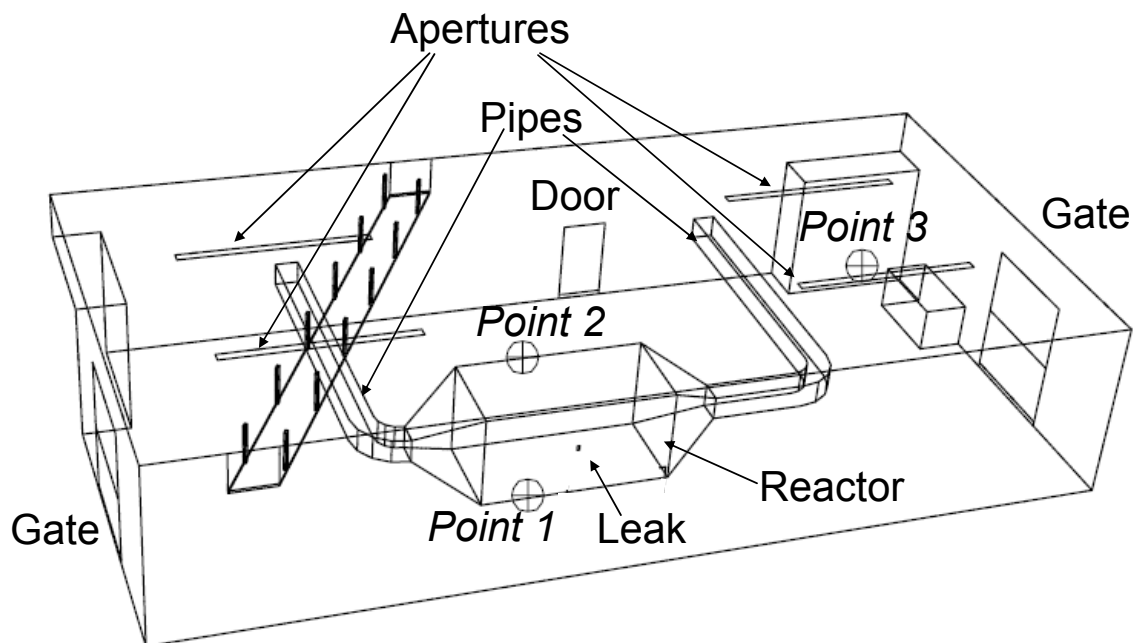


**Figure 5.5** Modelled geometry, including a reactor with pipes; a leak is assumed to emit particles from the reactor.

A simulation grid for a realistic, virtual workplace, including a reactor, transport pipes, furniture, gates and a door was developed. A leak is assumed in the reactor and particle dispersion is studied with the CFD software FLUENT along with the Fine Particle Model. The model allows for a detailed analysis of the parameters affecting particle dispersion and aerosol dynamic processes. The simulation domain is illustrated in Figure 5.5.

**Table 5.2** Variations of simulated parameters from the basic case.

Pos.	Variation	Values
1	Flow	Right gate (see Fig. 5.5) fully open
2	Emitted number concentration	$10^{14}$ #/m <sup>3</sup>
3	Emitted particle diameter	20 nm or 90 nm
4	Temperature of leak flow	350 K or 450 K
5	Wall temperature of reactor	350 K
6	Floor temperature	290 K
7	Background aerosol	200 nm, $5 \cdot 10^9$ #/m <sup>3</sup> , $\sigma_g = 2,0$ 200 nm, $2 \cdot 10^{10}$ #/m <sup>3</sup> , $\sigma_g = 2,0$
8	Flow velocity through door and gate apertures	2 cm/s

In a basic case, all temperatures in the room were assumed to be 300 K, gates and doors were left open 10 cm at the bottom. The size distribution emitted through the leak was assumed to be lognormal with a median diameter of 50 nm and a concentration of  $10^{16}$  m<sup>-3</sup>. Parameters affecting particle size distribution and dispersion, including emitted size distributions, ventilation scenarios, background aerosol, and temperatures of floor, reactor wall and leak flow were systematically varied. A number of variations, listed in Table 5.2 were simulated in order to study the effect of different processes on particle dispersion and size distribution.

An exemplary case, where the surface temperature of the reactor walls was increased from 300 K (basic case) to 350 K is shown in Figure 5.6. The graph shows the size distributions in the three points, defined in Figure 5.5. It can be seen that an increase of the reactor wall temperature only has a negligible effect in point 1, where the size distribution still mainly represents the diluted emitted size distribution. The effect on size distributions is much more pronounced in points 2 and 3, because particles have travelled over a longer distance and time before they reach these locations, and therefore processes leading to slower changes, such as coagulation and thermophoresis are more effective. The effect on particle concentration is obviously higher in point 2 compared with point 3. This is caused by the temperature gradient between the warmer reactor wall (350 K) compared with the surrounding air (300 K), which leads to a thermophoretic repulsion of particles away from the reactor.

Similar analyses were conducted for all variations listed in Table 5.2. It was shown that especially temperature changes have significant impact on the particle dispersion and deposition in the modelled workplace, because of thermophoresis and buoyancy effects. The results show that modelling can be a very efficient tool for studying dispersion and changes of particles during airborne transport in workplaces. It is intended to publish the results soon in an international industrial hygiene journal.

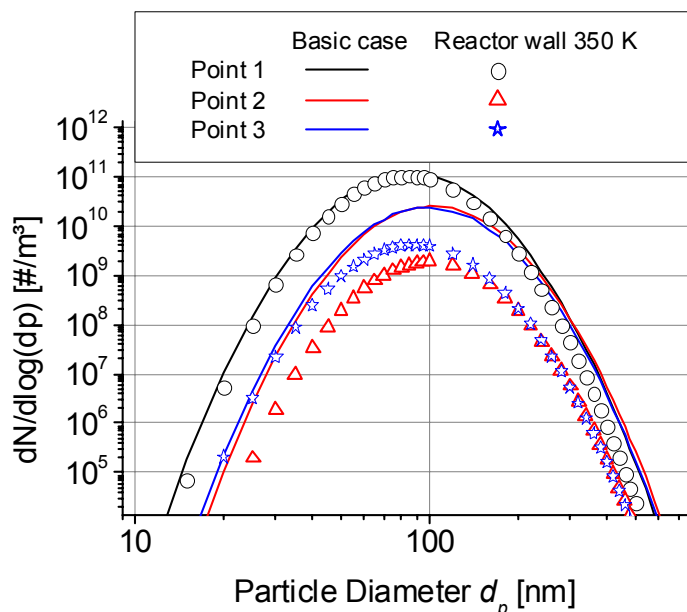


**Figure 5.6** Change of particle size distribution at three points (see Fig. 5.5) when the reactor wall temperature was increased from 300 K (basic case) to 350 K.

## 5.5 Agglomerate Stability and Material Properties

### 5.5.1 Release of Nanoparticles during Manual Handling of the Nanostructured Materials (“Stability under Weak Shear Forces”)

The propensity of nanoscaled materials to produce airborne particles during their handling in the range below approximately 100 nm is of interest for risk assessment in the respective workplaces (Jensen et al., 2009). Extensive measurements of the respirable and inhalable dust mass released by a dropping process of powders have yielded a wealth of dustiness data which are an important factor to judge a possible risk for workers’ health in advance of a real exposure situation. These measurements are performed according to a European Standard (EN 15051). In order to transfer this approach to the field of nanoparticles, NanoCare did include a work item for the quantification of this material property for the products included in the project. Starting point was the abovementioned European Standard. This standard describes two different experimental setups to investigate the dustiness of powders while being normally handled, with respect to so-called respirable, thoracic and inhalable dust (EN 481, EN 15051). One of these setups was modified in order to measure, under standardised conditions, the evolution of airborne nanoparticles from nanoscaled powders which are mechanically treated (dropped).

For this purpose the apparatus (“continuous drop method”) was reconstructed according to EN 15051. Several modifications were necessary, but in general all requirements of EN 15051 are also met by the modified continuous drop apparatus used in NanoCare. Therefore it could also be used for the determination of respirable and inhalable dust fractions (Dustiness according to EN 15051).

For example, in order to exclude the urban background aerosol of ultrafine particles, a high performance filter (“ULPA”) was installed in the back flow air stream. To minimise electrostatic effects the apparatus was completely made of stainless steel. The device is depicted in Figure 5.7.

The nanoscaled material is placed into the respective dispenser (1) and dropped via a vibrating chute (2) into the drop tube (3). The dropped material freely falls within the stainless steel tube (7) against an air flow of ULPA (9)-filtered back flow air into a collecting vessel (8). The back flow air stream is generated by a pump (6). Above the exit opening of the material flow a condensation particle counter (CPC) (4) as well as SMPS-T2 (5) continuously monitor the number concentration and its size distribution of ultrafine particles.

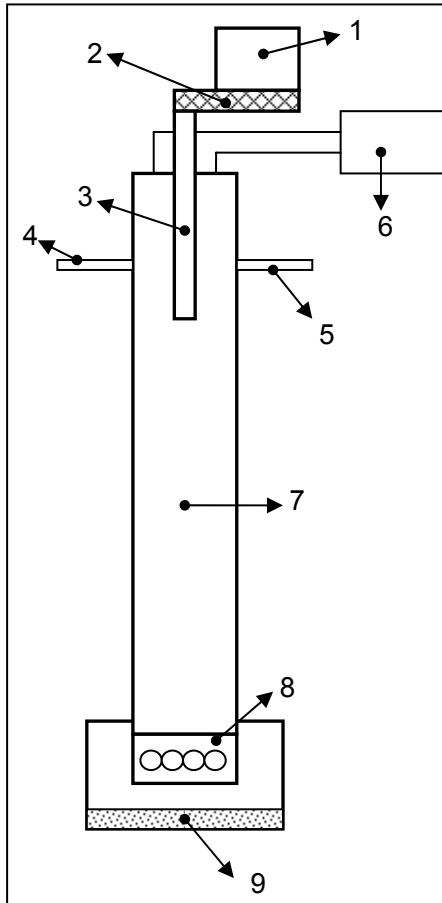


**Figure 5.7** Schematic picture of the apparatus

We use the term dustiness analogous but not identical to the EN 15051, as it does not take respirable or inhalable dust into account.

The measurements were performed according to a specifically developed standard operation procedure (SOP), which involves the measurement of the background concentration of ultrafine particles before the proper drop experiment, the repeated measurement of particle number size distribution with SMPS-T2 and subsequent averaging of their results, and the parallel use of a CPC device. Typical size distributions are shown in Figure 5.8. The mass flow of the dropped material is recorded as well as a reference for the intensity of the dispensing procedure. The processes are reproducible, and if a noteworthy release of nanoparticles is observed, this release is directly correlated to the intensity of the dispensing process (i.e. chute frequency).

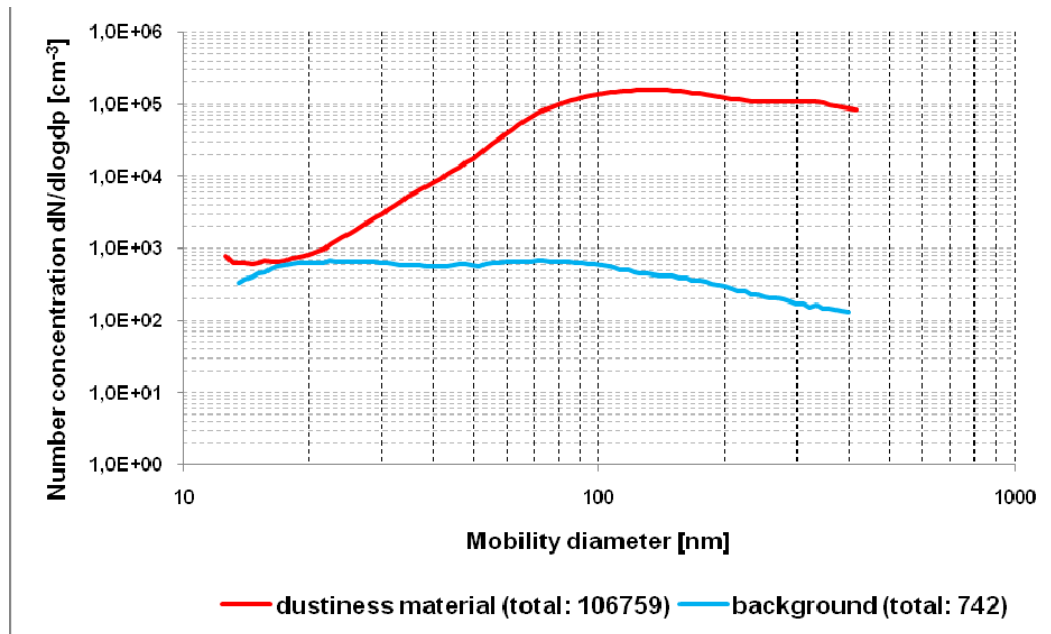


Figure 5.8 Size distribution for the product (ZrO<sub>2</sub>, 8.1) showing significant particle release during drop (red line) compared to the background (blank) concentration (blue line).

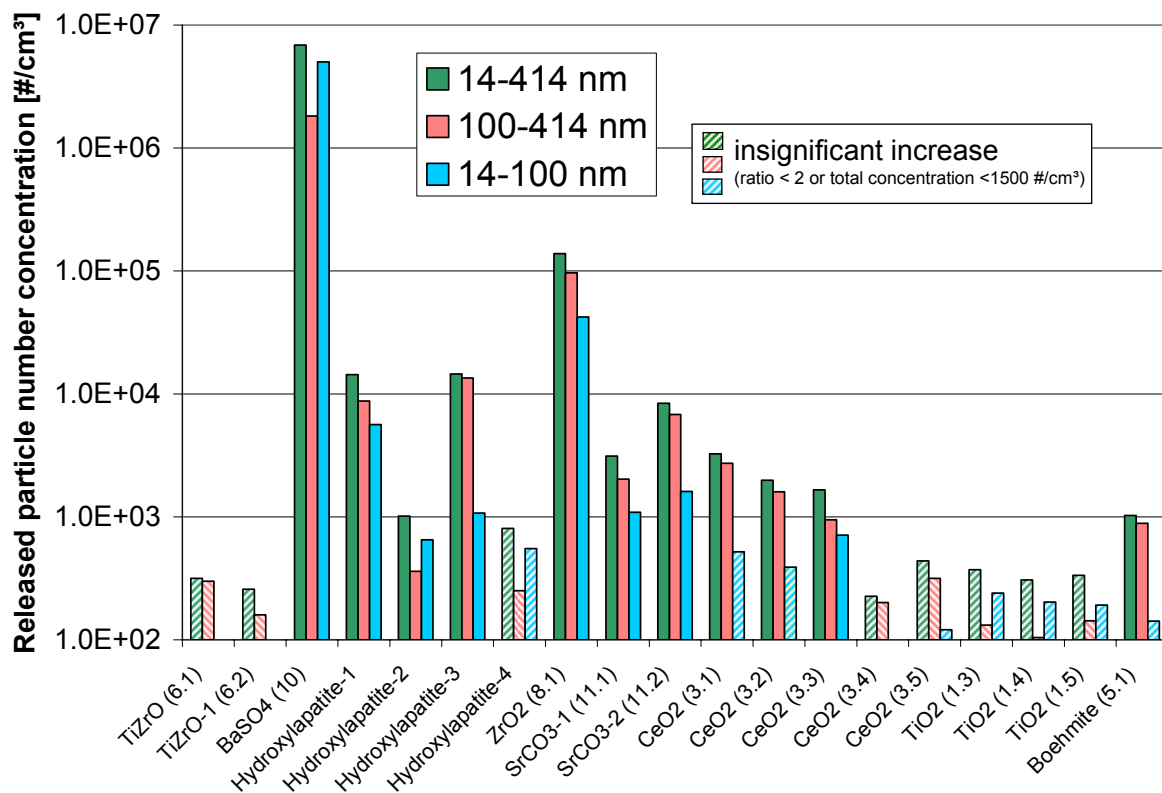


Figure 5.9 Released particle number concentration (background deducted) during drop experiments in size range 14-414 nm, 14-100 nm and 100-414 nm; numbers in parentheses refer to Table 3.1; four different hydroxylapatites not listed in the table; a release is only considered to be significant if the concentration increases twofold compared with background concentration in drop tube and if the total concentration is >1500 #/cm<sup>3</sup>.

A total of 19 different nanoscaled powders have been investigated in NanoCare. Size distributions were recorded with SMPS-T2 in a size range of 14-414 nm. Total number concentrations were calculated for the entire size range as well as for particles <100 nm (i.e. nanoscaled particles) and >100 nm. If the resulting total concentrations during the drop experiments were below 1500 #/cm<sup>3</sup>, the material was assumed to show no significant particle release because of a) the low concentration and b) the high uncertainty of the SMPS in the lower concentration range. A significant release was only assumed if the total concentrations exceeded this threshold and if the increase was at least twofold compared with the respective background concentrations in the drop tube. The results are summarized in Figure 5.9 It can be seen from the bar graph that for almost all tested materials, the increase was higher for the fraction of larger particles than for smaller particles. A significant increase of the concentration of larger particles was observed for eleven out the 19 tested materials, whereas only eight of them also showed a significant increase in the concentration of the smaller particles. These increases showed a large variety over several orders of magnitude. Concentrations of the larger particles (100-414 nm) were increased by 360 #/cm<sup>3</sup> (Hydroxylapatite-2) – 1.8x10<sup>6</sup> #/cm<sup>3</sup> (BaSO<sub>4</sub> – No 10 in table 1); the increase of sub-100 nm particles was between 650 #/cm<sup>3</sup> (Hydroxylapatite-2) and 5x10<sup>6</sup> #/cm<sup>3</sup> (BaSO<sub>4</sub> - 10).

### 5.5.2 Stability under Strong Shear Forces

During production and handling of nanopowders different levels of shear stress might occur. The abovementioned method of continuously dropping a nanopowder simulates weak shear forces which are applied to the agglomerates. To further investigate the deagglomeration of nanoparticle agglomerates as a function of different shear forces, a novel experimental setup was developed (Stahlmecke et al., 2009).

The nanopowder under investigation was magnetically stirred in a pressurised beaker under a constant particle free carrier gas flow (dry nitrogen) in order to aerosolise the particles. Large agglomerates were then removed by two consecutive cyclones, and the resulting aerosol passed through an orifice with an aperture of 508 µm diameter (with sharp edges) into a compensation tank. Bigger agglomerates may break up into smaller fragments due to shear forces induced by the highly turbulent flow inside the orifice. The magnitude of the shear forces is determined by the applied pressure difference across the orifice. The orifice can, e.g., be considered as an experimental substitute for a leak in a pressurised vessel.

The effect of shear forces on agglomerate size was studied for nine materials in 22 variations by applying overpressures ranging from 10 kPa to 140 kPa upstream of the orifice. To investigate the effect of the different shear forces, a measurement of the “as prepared” aerosol (without passing the orifice) was also conducted as reference. The resulting number size distribution in the compensation tank was measured using SMPS-T1. Prior to particle generation the compensation tank was flushed with particle free nitrogen to assure a negligible background particle concentration. Concentrations during actual measurements were at least one to three orders of magnitude higher than the background concentration. The resulting number size distribution was measured five times for each pressure step to obtain a reliable data base for the calculation of an average number size distribution.

Due to differences in the total concentration for each substance and each pressure step, the obtained number size distributions were normalised to enable a direct comparison for the different nanopowders. The relative number size distribution was therefore calculated by dividing each size class by the total number concentration of all measured size classes.

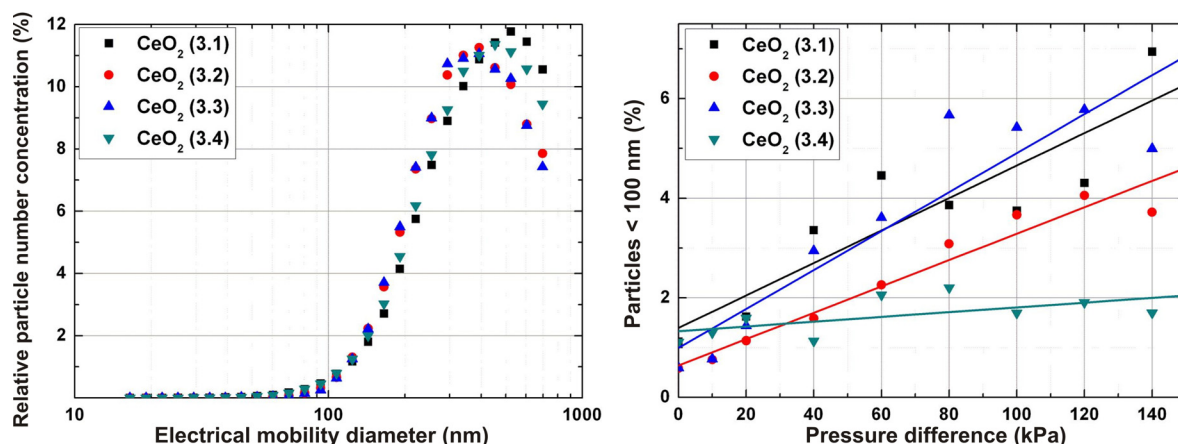


**Figure 5.10** Normalised number size distribution of four different CeO<sub>2</sub>-nanopowders (materials 3.1-3.4) as a function of electrical mobility diameter (left). Numbers in parentheses refer to Table 3.1. Influence of pressure differences across the orifice on the fraction of particles below 100 nm with respect to the measured total particle concentration (right).

Figure 5.10 and 5.11 show exemplarily the results for three CeO<sub>2</sub> (materials 3.1-3.4, Table 3.1) and three Ti-Zr (6.1-6.3) modifications, respectively. The relative particle number concentrations are shown in the left graphs of the figures. The right graphs of the Figures 5.10 and 5.11 show the fraction of particles up to 100 nm diameter with respect to the total concentration measured by the SMPS as a function of increasing pressure difference. Depending on the nanopowder under investigation these fractions increased for the case of the different CeO<sub>2</sub> modifications from a value around 1 % up to about 7 % for a differential pressure of 140 kPa. In case of two of the Ti-Zr modifications (6.1 and 6.2) and TiO<sub>2</sub> (1.2) the fraction increased from around 2 % up to about 5 %. While all these materials show a clear but moderate increase with increasing differential pressure, material 6.1 (Ti-Zr) shows a much more distinct dependence of sub-100 nm particle fraction on the pressure. It increases from about 5% with no differential pressure to approximately 30% at 120 kPa. It becomes apparent, that especially material 6.1 (Ti-Zr mixed oxide), which did not show a significant particle release during drop experiments (see Fig. 5.9), can generally be fragmented, but only if high shear forces are applied.

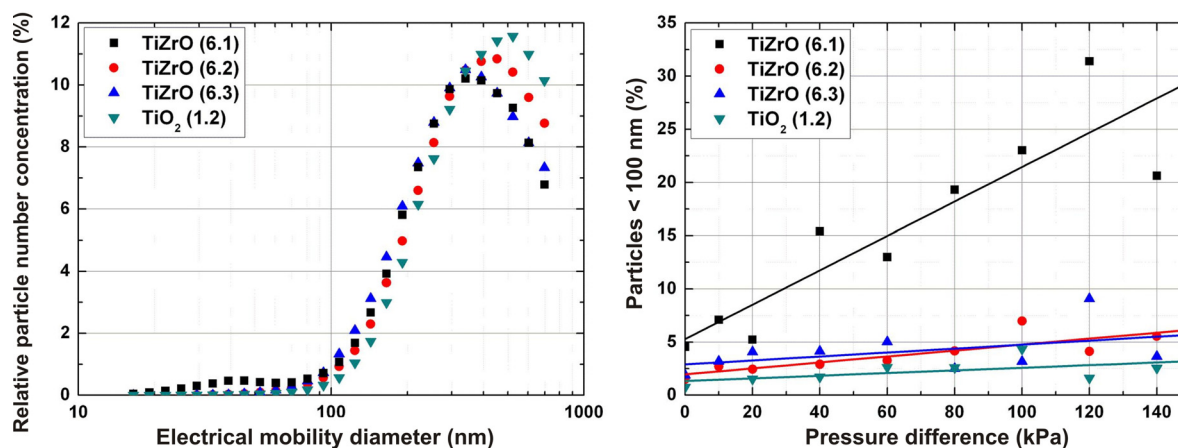


**Figure 5.11** Normalised number size distribution of three different Ti-Zr modifications (materials 6.1-6.3) and TiO<sub>2</sub> nanopowder (upstream of orifice) as a function of electrical mobility diameter (left). Numbers in parentheses refer to Table 3.1. Influence of pressure difference on the fraction of particles below 100 nm with respect to the measured total particle concentration (right).

The Figures 5.10 and 5.11 also show that the pressure dependence of the fraction of sub-100 nm particles can be linearly fitted. The slope of the linear fit is then an indicator for the deagglomeration of the materials under different pressure conditions. The increase of the sub-100 nm fraction per unit differential pressure, i.e. the abovementioned slope, is shown in Figure 5.12. Among the investigated 22 material variations  $\text{TiO}_2$  (1.5) showed the lowest and Ti-Zr (6.1) the highest propensity to release particles below 100 nm. The range was from 0.0028 %/kPa to 0.2125 %/kPa, i.e. within a factor of 75, whereas during the drop experiments the released sub-100 nm particle concentrations varied by a factor of 6700. It is noteworthy that the material, which showed the highest release under stress conditions, did not show a significant concentration increase in the drop tube. The same is true for  $\text{CeO}_2$  (3.5), which showed the second highest increase with increasing pressure. On the other hand,  $\text{BaSO}_4$  (10) that released the highest concentration in the drop tube only showed an average increase in the orifice experiments. These investigations revealed that a general propensity of a material and its variation to release particles smaller than 100 nm cannot be given, but each material has to be investigated case by case, because the increase of concentrations in the sub-100 nm range are strongly dependent on the handling of the material.

This increase in the fraction of particles below 100 nm clearly indicates that deagglomeration may occur during the passage through an orifice and that this increase is pressure- and material-dependent. Furthermore the results show that the deagglomeration is not only dependent on the material under investigation but also on the modification of the particles. A detailed analysis of this behaviour has been submitted to Journal of Nanoparticle research (Stahlmecke et al., 2009).

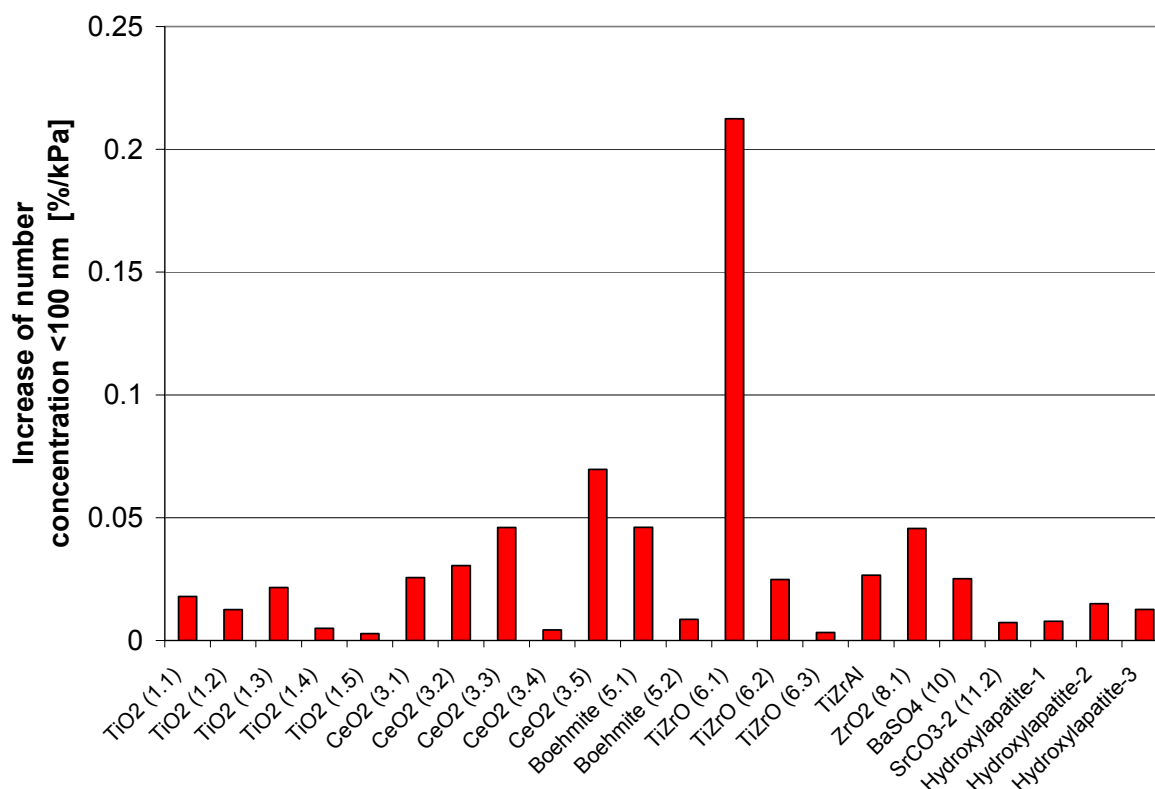


**Figure 5.12** Relative increase of particle number concentration below 100 nm per unit pressure difference across the orifice. Numbers in parentheses refer to Table 3.1.

### 5.5.3 Conclusions

Various aspects affecting worker exposure to nanoparticles in workplaces were studied. During measurements of exposure concentrations in altogether eleven workplaces, no significantly increased concentrations of sub-100 nm particles were detected. Also the fractions of particles up to 400 nm showed no significant increase. Only in two workplaces, a significant release of particle >400 nm was measured. To support the measured workplace exposure, nanoparticle dispersion from an accidental leak was also numerically modelled under various conditions. Modelling proved to be a powerful tool for predicting exposure to NPs with high spatial resolution. It can furthermore help to identify hot spots, e.g. areas with insufficient ventilation, where particles may accumulate over time.

The study of agglomerate stability under various shear forces showed that deagglomeration of NP agglomerates depends on many factors, including the NP material and its modification. In experiments with weak forces, e.g. simulating powder handling processes, almost all materials showed a higher release of particles >100 nm than of particles <100 nm. Only eight out of 19 tested materials showed a significant release of sub-100 nm particles, whereas eleven showed a significant release of particles larger than 100 nm. Experiments with strong shear forces in an orifice also showed a material dependence of the deagglomeration for all tested materials. The results showed a clear increase of the fraction of sub-100 nm particles with increasing pressure difference across the orifice. The extent of deagglomeration for equal pressure settings, however, showed a large variety. With 140 kPa pressure difference across the orifice, the increase of nanoscale particles was between 2% and 30%.

The results show that exposure assessment for NPs remains challenging. Measuring devices for measurement campaigns need to be carefully chosen. Furthermore the particle transport upon particle release may need to be taken into account, because particles may change physically and/or chemically during transmission. The elaborate standard operation procedure for workplace measurement allows, for the first time, to differentiate NPs in workplaces from background particles.

# 6. Conclusions

H.F. Krug, T.A.J. Kuhlbusch and the NanoCare-Consortium

The NanoCare consortium has been founded in 2005 as one of the largest project consortia within the so-called NanoCare-Cluster consisting out of three projects dealing with the possible health risks of nanomaterials. Within this group NanoCare was set up by the biggest group of different partners coming from the industry, academic institutes and independent organisations. The goals of this project were to define new and standardised methods for the investigation of nanomaterials, to collect new data for exposure and hazard and to communicate the results to stakeholders and also to the public in various open meetings or conferences. All of these issues have been successfully tackled despite but also especially due to the diversity of the partners. NanoCare was the first project in Germany and beyond with such a holistic approach in this research area:

- Generation of new data concerning material characterisation, in vitro and in vivo toxicology as well as exposure measurement at work places
- Processing of the new data and knowledge within the consortium (internal database) and describe well defined working procedures (SOPs)
- Distribution of the knowledge outside of the consortium, not only by scientific publications but also by stakeholder and public meetings

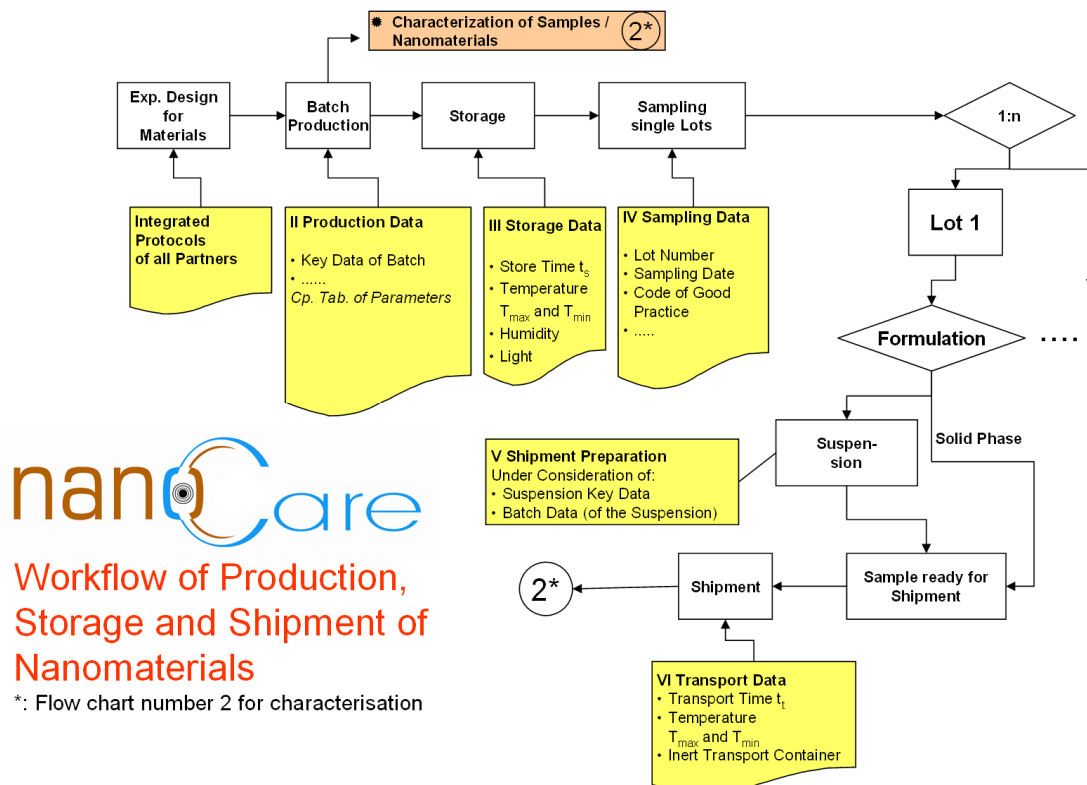


**Figure 6.1** Example for Work Flow Definitions and Standardisation within the Project.

The basic idea of NanoCare is to combine the work on hazard identification with the analysis of exposure scenarios and physico-chemical well characterised nanomaterials.

That nanomaterials used in different research areas related to risk assessment should be well characterised was also stressed by the “Nanokommission der deutschen Bundesregierung” in the Nanodialog-Bericht (2008). They stressed that a minimum of these information should be reported in all publications. Thus, only manuscripts regarding well-characterised nanomaterials should be published internationally as also demanded by others (Warheit, 2008). Nanomaterial characterisation in NanoCare included besides others particle size and size-distribution, aggregation and agglomeration status, especially in suspensions containing various organic molecules, specific surface area, zeta-potential and TEM characterisation.

The well described and interlinked approach chosen in NanoCare was than used to combine results from the different research areas and subsequently to put this information and interpretation into a knowledge base on the web to communicate about the outcome of the project. The strength of this project was also the use of well defined procedures throughout the project to achieve comparability beyond a single experiment and one nanomaterial. Therefore the NanoCare consortium defined several charts for procedures.

The chart for the production of the nanomaterials, the starting point, is given as an example in Fig. 6.1. It shows that the production by the industry, partners which was carried out directly comparable to the industrial processes, includes several steps for tailoring the materials and to keep them sterile for the biological experiments (Fig. 6.1). Moreover, two reference materials were defined, Carbon Black and titanium dioxide, which were produced in amounts sufficient for the project period and longer to allow comparability even beyond the time of the project.

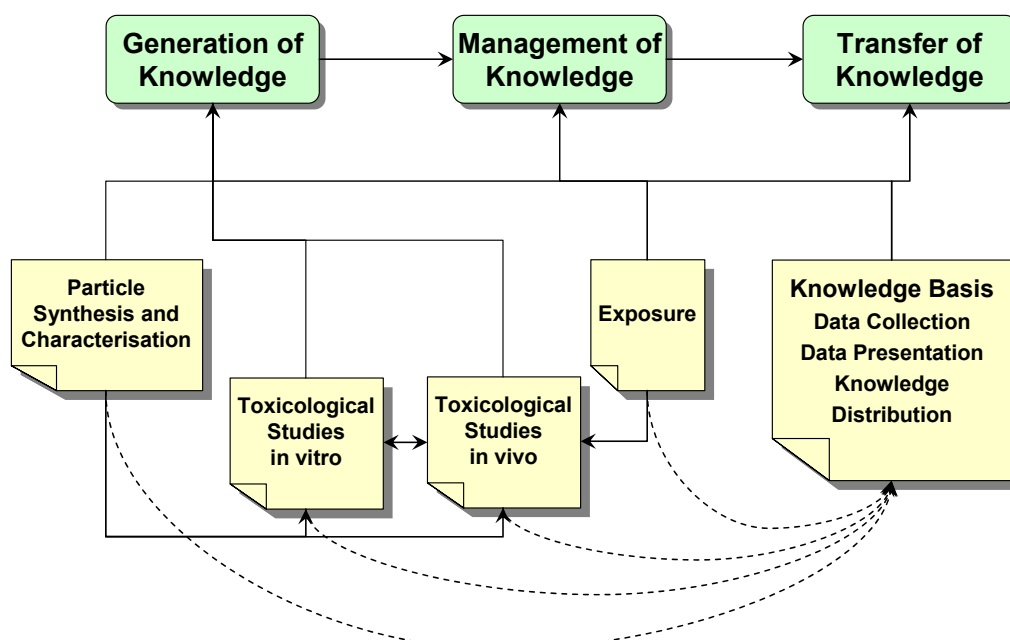


**Figure 6.2** Interaction (Output and Input) between the main Tasks of NanoCare.

Figure 1.1 within the chapter ‘Introduction’ demonstrates nicely the correlation between exposure and hazard within the procedure of risk assessment. Hence, NanoCare includes both aspects within the work packages, the evaluation of exposure scenarios at the workplace (WP5) and the determination of biological effects within the WP3 and 4 (Fig. 6.2).

Based on the delivery of well-characterised nanomaterials (WP1 and 2), all generated results were fed into the database and knowledgebase (WP6) and were used to inform the public and stakeholders (WP7).

Besides the innovative approaches to develop a new exposure system for cell cultures with aerosols made from particulate matter and the measurement of pulling forces by single cells, analysed with AFM-aided nanoparticle binding systems, a huge number of in vitro experiments has been carried out within the last three years by five different partners with many different cell types, nanomaterials and analysis of several biological endpoints. The results stimulate our partners from IBE, BASF and Bayer to observe specific parameters during their in vivo instillation and inhalation studies.

Overall, the project delivered new insights into the biological effects of nanomaterials, established several new methods for their characterisation and work place measurements and took over a leading role in the community of nanotoxicological oriented projects in Europe. The standard operation procedures (SOPs) have been applied into the process of the OECD Working Party on Nanotechnology and Germany took over the OECD-sponsorship for TiO<sub>2</sub> based on the results which NanoCare has delivered. Working groups take the results from NanoCare to make decisions for future projects or programs like the Nanokommission der Bundesregierung (Germany), the working plans and processes are the basis for the ongoing funding strategy in Germany (NanoNature and NanoCare) and NanoCare will publish more SOPs and peer reviewed journal papers during the next months although the project will be finished officially on the 31st of July 2009.

With the start of NanoCare we raised several questions we wanted to answer (compare Chapter 1) regarding the exposure related research as well as to the toxicology of nanomaterials and we have worked through and answered most of them. Without repeating these questions again, some answers reflecting the highlights of the project are presented here:

We found during the exposure related research that

- eight of the tested materials showed a tendency for releasing smaller particles from agglomerates after weak shear forces, but 11 showed no high dustiness,
- stronger shear forces, as they may appear during a leak, increase the number of small particles, but this effect depends strongly on the nanomaterial tested,
- modelling of particle dispersion in a workplace is a very good tool to assess the behaviour and distribution of nanoparticles and the possible exposure at the workplace,
- none of the measurements at real work places result in the detection of nanoparticles or nanoobjects from the production process,
- standardisation of measurement is needed and NanoCare delivered SOPs for the execution of workplace measurements,
- innovative approaches such as the “Karlsruher Exposure System” will enable the direct measurement of biological effects at the work place.

Toxicological studies as performed in vivo on rats exposed by inhalation and via intratracheal instillation (ITI) or in vitro on cell lines and on ex vivo alveolar macrophages show:

- Nearly all of the inhaled particles were taken up by alveolar macrophages and remain in the lung such as respirable particles. Lung clearance mechanisms via the conducting airways and, to a smaller extent, via the transport into the lung-associated lymph nodes are efficient. Thus, the qualitative aspects of deposition and clearance conform to the known defence mechanisms of the lung for respirable particles,.

- No systemic penetration into other body compartments could be detected in the frame of the applied analytical procedures on NanoCare materials. However, this result may be non-applicable to other types of nanomaterials since functionalized surfaces lead to very distinct effects inter alia on agglomeration.
- The tested samples exert different toxicities ranking some samples into the area of very low biological activity, others showed moderate or more elevated biological activities.
- All evaluated samples produced no effect levels (NEL) or lowest observed effect level (LOEL) in the multi dose approach as performed in the inhalation studies or in the ITI animal studies (acute toxicity for 3 days). Thus, a possible risk assessment would be feasible.
- The in vitro experiments on ex vivo alveolar macrophages with the standardized vector model (VM) delivered a varied pattern of toxicities in the dose range of the typical loading with respirable particles 15 – 120 pg/cell. NELs could be detected for all samples.
- The in vitro data on alveolar macrophages showed a good correlation with results of the animal experiments.
- Within the in vitro experiments on cell lines no concentrations could be applied similar to the workplace scenario to result in any measurable effect; NanoCare experiments revealed for all investigated materials only slightly effects or no effects.
- Agglomerates of nanoparticles show the tendency of deagglomeration in the presence of proteins in body fluids, subsequently the nanoparticles will be masked by the protein corona.
- NanoCare has delivered several SOPs for analytical methods to standardise the protocols for toxicological testing.

Two very important outcomes should be mentioned here in more detail. Firstly, none of the investigated nanomaterials exhibited a severe effect in the sense that cells or animals show signs of acute toxicity or a biological effect could be demonstrated by treatment with low concentrations. Secondly, the comparison of the in vitro and in vivo results showed a very good correlation, thus, in a first approximation the in vitro studies reflect relatively good the in vivo situation.

Of course we have to make the constriction that our results are limited to the investigated materials but they comprised already 11 different materials in more than 30 modifications. We have addressed very difficult scientific problems such as “how stable are agglomerates of nanoparticles during normal handling” and “how reliable are the measurements under real conditions”. We formulated an answer to the question if in vitro tests can to some extent replace in vivo studies when the correct indicators and valid correlations have been applied which shall be verified in the future. NanoCare has substantially contributed to the sustainability of nanotechnology even if we could not solve all problems and could not answer all questions. E.g., the work on biological effects of nanomaterials is yet not finished despite the fact that we have done a huge number of different experiments in vitro and in vivo as well as physico-chemical measurements.

Based on the work done during the last three and a half years the next projects can focus on more specific issues regarding nanomaterial toxicity, exposure and risk or can focus on important new materials for which no data are available. Our project and its results significantly helped to put the research on nanotoxicology on a firm footing.

## References

- Asbach, C., H. Kaminski, H. Fissan, C. Monz, D. Dahmann, S. Mülhopt, H.R. Paur, H.J. Kiesling, F. Herrmann, M. Voetz, T.A.J. Kuhlbusch (2009a). Comparison of four mobility particle sizers with different time resolution for stationary exposure measurements. *J. Nanoparticle Res.* in press.
- Asbach, C., H. Fissan, B. Stahlmecke, T.A.J. Kuhlbusch, D.Y.H. Pui (2009b). Conceptual limitations and extensions of lung-deposited Nanoparticle Surface Area Monitor (NSAM). *J. Nanoparticle Res.* 11, 101-109
- Bermudez, E., Mangum, J.B., Asgharian, B., Wong, B.A., Revery, E.E., Janszen, D.B., Hext, P.M., Warheit, D.B., and Everitt, J.I. (2002). Long-term pulmonary responses of three laboratory rodent species to subchronic inhalation of pigment-grade titanium dioxide particles. *Toxicological Sciences* 70, 86-97
- Bermudez, E., Mangum, J.B., Wong, B.A., Asgharian, B., Hext, P.M., Warheit, D.B., and Everitt, J.I. (2004). Pulmonary responses of mice, rats, and hamsters to subchronic inhalation of ultrafine titanium dioxide particles. *Toxicological Sciences* 77, 347-357
- Bihari, P. et al. (2008). Optimized dispersion of nanomaterials for biological in vitro and in vivo studies: *Particle and Fibre Toxicology*, v. 5, 14
- Bissinger, R. L., and Carlson, C. A. (2006). Surfactant. *Newborn and Infant Nursing Reviews* 6, 87-93
- Brouwer, D., J.J. Gijssbers, M.M. Lirvink (2004). Personal Exposure to Ultrafine Particles in the Workplace: Exploring Sampling Techniques and Strategies, *Ann. occup. Hyg.*, Vol. 48, No. 5, 439-453
- Cedervall, T., I. Lynch, M. Foy, T. Berggard, S. C. Donnelly, G. Cagney, S. Linse, and K. A. Dawson, (2007a). Detailed identification of plasma proteins adsorbed on copolymer nanomaterials: *Angewandte Chemie-International Edition*, v. 46, no. 30, 5754-5756
- Cedervall, T., Lynch, I., Lindman, S., Berggard, T., Thulin, E., Nilsson, H., Dawson, K. A., and Linse, S. (2007b). Understanding the nanoparticle-protein corona using methods to quantify exchange rates and affinities of proteins for nanoparticles. *Proceedings of the National Academy of Sciences of the United States of America* 104, 2050-2055
- DE-OS 10 2007 013 938 (25.9.2008) WO-OS 2008/116540 (2.10.2008)
- DIN EN 481 (1993). Workplace atmospheres; size fraction definitions for measurement of airborne particles
- DIN EN 12341 (1999). Air quality – Determination of the PM10 fraction of suspended particulate matter – reference method and field test procedure to demonstrate reference equivalence of measurement methods
- DIN EN 14907 (2005). Ambient air quality – standard gravimetric measurement method for the determination of the PM2.5 mass fraction of suspended particulate matter
- DIN EN 15051 (2006). Workplace atmospheres – measurement of the dustiness of bulk materials – requirements and reference test methods
- Dixkens, J., H. Fissan (1999). Development of an electrostatic precipitator for off-line particle analysis. *Aerosol Sci. Technol.* 30, 438-453
- Donaldson, K., P.J. Borm, G. Oberdorster, K.E. Pinkerton, V. Stone, C.L. Tran (2008). Concordance between in vitro and in vivo dosimetry in the proinflammatory effects of low-toxicity. Low-solubility particles: the key role of the proximal alveolar region. *Inhal. Toxicol.*, 20, 53-62
- Drexler E. (1987). *Engines of Creation: The Coming Era of Nanotechnology*, Anchor Press Norwell, MA, USA, ISBN: 0385199732, p.320
- Dutta, D, et al. (2007). Adsorbed proteins influence the biological activity and molecular targeting of nanomaterials. *Toxicol. Sci.*, 10, 303-315
- Fissan, H., C. Helsper, H.J. Thielen (1983). Determination of particle size distributions by means of an electrostatic classifier. *J. Aerosol Sci.* 14: 354-357
- Fissan, H., S. Neumann, A. Trampe, D.Y.H. Pui, W.G. Shin (2007). Rationale and principle of an instrument measuring lung deposited nanoparticle surface area. *J. Nanoparticle Res.* 9, 53-59

- Forbes, B. (2000). Human airway epithelial cell lines for in vitro drug transport and metabolism studies. *Pharmaceutical Science & Technology Today* 3, 18-27
- Forbes, B., and Ehrhardt, C. (2005). Human respiratory epithelial cell culture for drug delivery applications. *Eur. J. Pharm. Biopharm.* 60, 193-205
- Foresight Guidelines for Responsible Nanotechnology Development, <http://www foresight.org/guidelines/current.html>, cited in <http://www foresight.org/nano/history.html>
- Froeschke, S., S. Kohler, A.P. Weber, G. Kasper (2003). Impact fragmentation of nanoparticle agglomerates. *J. Aerosol Sci.* 34, 275-287
- Fuchs, N. A. (1963). On the stationary charge distribution on aerosol particles in bipolar ionic atmosphere. *Geofis. Pura Appl.* 56, 185-193
- Geys, J., Coenegrachts, L., Vercammen, J., Engelborghs, Y., Nemmar, A., Nemery, B., and Hoet, P. H. (2006). In vitro study of the pulmonary translocation of nanoparticles: a preliminary study. *Toxicol Lett* 160, 218-226
- Hartshorn, K. L., Crouch, E., White, M. R., Colamussi, M. L., Kakkanatt, A., Tauber, B., Shepherd, V., and Sastry, K. N. (1998). Pulmonary surfactant proteins A and D enhance neutrophil uptake of bacteria. *Amer. J. Physiology* 274, L958-969
- Heim, M., G. Kasper, G.P. Reischl, C. Gerhart (2004). Performance of a new commercial electrical mobility spectrometer. *Aerosol Sci. Technol.* 38, 3-14
- Heiss, A.; Jahnen-Dechent, W; Endo, H.; Schwahn, D. (2007). Structural Dynamics of a Colloidal Protein-Mineral Complex Bestowing on Calcium Phosphate a High Solubility in Biological Fluids; *Biointerfaces*, 2(1), 16-20
- Hickling, T. P., Clark, H., Malhotra, R., and Sim, R. B. (2004). Collectins and their role in lung immunity. *Journal of leukocyte biology* 75, 27-33
- <http://characterizationmatters.org>, (2008). Minimum Information for Nanomaterial Characterization Initiative
- Jensen, K.A., I.K. Koponen, P.A. Clausen, T. Schneider (2009). Dustiness behaviour of loose and compacted Bentonite and organoclay powders: What is the difference in exposure risk?, *J. Nanoparticle Res.* 11, 133-146
- King, S.M., P.C. Griffiths, Using SANS to Study Adsorbed Layers in Colloidal Dispersions; in *Applications of Neutron Scattering to Soft Condensed Matter*; Ed. B. J. Gabrys; Gordon and Breach Science Publishers, New York, 2000; Pp. xii and 362
- Kishore, U., A.L. Bernal, M.F. Kamran, S. Saxena, M. Singh, P.U. Sarma, T. Madan, T. Chakraborty (2005). Surfactant proteins SP-A and SP-D in human health and disease. *Archivum immunologiae et therapiae experimentalis* 53, 399-417
- Kroll, A., Pillukat, M. H., Hahn, D., Schneidenburger, J. (2008). Current in vitro methods in nanoparticle risk assessment: Limitations and challenges. *Eur J Pharm Biopharm*
- Kuhlbusch, T.A.J., H. Fissan, S. Neumann (2004). Number size distribution, mass concentration, and particle composition of PM 1, PM 2.5 and PM 10 in bag filling areas of carbon black production, ICBA-Study, *J. Occup. Env. Hygiene* 1: 660 – 674
- Kuhlbusch, T.A.J., H. Fissan, C. Asbach (2008). Measurement and detection of nanoparticles within the environment. Ed. H. Krug, In: *Nanotechnology – Volume 2: Environmental Aspects*, Wiley-VCH Weinheim, 229-266
- Kuhlbusch, T.A.J., H. Fissan, C. Asbach (2009). Nanotechnologies and environmental risks. Eds.: I. Linkov, J. Steevens, In: *Nanomaterials: Risks and Benefits*, Springer Science + Business Media B.V., 233-243
- Landsiedel, R., K. Wiench, and W. Wohlleben (2008). Geeignete Methoden zur Prüfung der Sicherheit von Nanomaterialien: *Chemie Ingenieur Technik*, v. 80, 1641-1651
- Lehr, C. M., Bur, M., and Schaefer, U. F. (2006). Cell culture models of the air-blood barrier for the evaluation of aerosol medicines. *Altex* 23 Suppl, 259-264
- Lewinski, N., Colvin, V., Drezek, R. (2008). Cytotoxicity of nanoparticles. *Small* 4, 26-49
- Limbach, L. K., Li, Y., Grass, R. N., Brunner, T. J., Hintermann, M. A., Muller, M., Gunther, D., and Stark, W. J. (2005). Oxide nanoparticle uptake in human lung fibroblasts: effects of particle size, agglomeration, and diffusion at low concentrations. *Environ Sci Technol* 39, 9370-9376

- Lundqvist, M., J. Stigler, G. Elia, I. Lynch, T. Cedervall, and K. A. Dawson (2008). Nanomaterial size and surface properties determine the protein corona with possible implications for biological impacts: *Proc. Natl. Acad. Sci. USA*, v. 105, no. 38, 14265-14270
- Lynch, I., K. A. Dawson, and S. Linse (2006). Detecting cryptic epitopes created by nanomaterials: *Sci Stke*, v. 2006, no. 327, e14
- Ma-Hock, L, Gamer, A, Landsiedel, R, Leibold, E, Frechen, T, Sens, B, Huber, G, van Ravenzwaay, B. (2007). Generation and Characterization of Test Atmospheres with Nanomaterials. *Inhal. Toxicol.* 19, 833-848
- Ma-Hock, L., S. Burkhard, V. Strauss, A. O. Gamer, K. Wiench, B. van Ravenzwaay, and R. Landsiedel, (2008). Development of a short-term inhalation test in the rat using nano-titanium dioxide as a model substance: *Inhalation Toxicology*, v. in press
- Maier, M, Hannebauer, B; Holldorff, H.; Albers, P. (2006). Does Lung Surfactant Promote Disaggregation of Nanostructured Titanium Dioxide? *J. Occ. Env. Med.*, 48(12), 1314-1320
- Mathias, N.R., Yamashita, F., and Lee, V. H. L. (1996). Respiratory epithelial cell culture models for evaluation of ion and drug transport. *Advanced Drug Delivery Reviews* 22, 215-249
- Mülhopt, S.; Paur, H.R.; Wäscher, T. Vorrichtung zur Messung von Feinstpartikelmassen DE-OS 10 2007 013 938 (2008.09.25)
- Murdock, R.C., L. Braydich-Stolle, A.M. Schrand, J.J. Schlager, S.M. Hussain (2008). Characterization of Nanomaterial Dispersion in Solution Prior to In vitro Exposure Using Dynamic Light Scattering Technique: *Toxicol.Sci.*, v. 101, 239-253
- Nanokommission der deutschen Bundesregierung (2008). Verantwortlicher Umgang mit Nanotechnologien. Bericht und Empfehlungen der Nanokommission der deutschen Bundesregierung. Catenhusen, W.-M., Grobe, A., und Bendisch, B. (Eds.), Bonn, Berlin.
- Nel, A., T. Xia, L. Madler, N. Li (2006). Toxic potential of materials at the nanolevel. *Science*, 311, 622–627
- Nepal, D., and K. E. Geckeler (2007). Proteins and Carbon Nanotubes: Close Encounter in Water: *Small*, v. 3, 1259-1265
- Oberdörster, Günther, Ferin, J., Gelein, R., Soderholm, S.C., Finkel (1992)., Role of the alveolar macrophage in lung injury: studies with ultrafine particles, *Environ. Health Perspect.* 97, 193-199
- Oberdörster, G. (2000). Toxicology of ultrafine particles: in vivo studies. *Philosoph. Transactions Royal Society, London* 358, 2719-2740
- Oberdörster, G., Oberdörster, E., Oberdörster, J. (2005a). Nanotoxicology: an emerging discipline evolving from studies of ultrafine particles. *Environ. Health Perspect.* 113, 823–839
- Oberdörster, G., Maynard, A., Donaldson, K., Castranova, V., Fitzpatrick, J., Ausman, K., Carter, J., Karn, B., Kreyling, W., Lai, D., Olin, S., Monteiro-Riviere, N., Warheit, D., Yang, H.; ILSI Research Foundation/Risk Science Institute Nanomaterial Toxicity Screening Working Group (2005b). Principles for characterizing the potential human health effects from exposure to nanomaterials: elements of a screening strategy. *Part. Fibre Toxicol.* 6, 2-8
- Park, E. J., K.Park, (2009). Oxidative stress and pro-inflammatory responses induced by silica nanoparticles in vivo and in vitro. *Toxicol. Lett.* 2009, 184, 18-25
- Pauluhn, J. (2009). Pulmonary Toxicity and Fate of Agglomerated 10 nm and 40 nm Aluminum Oxyhydroxides (AlOOH) following 4-week Inhalation Exposure of Rats: Toxic Effects are determined by agglomerated, not primary Particle Size. *Toxicological Sciences* 109: 152-167
- Pauluhn, J. (2009). Retrospective Analysis of 4-week Inhalation Studies in Rats with Focus on Fate and Pulmonary Toxicity of Two Nanosized Aluminum Oxyhydroxides (Boehmite) and Pigment-grade Iron Oxide (Magnetite): The key metric of dose is particle mass and not Particle surface area. *Toxicology* 259: 140-148
- Pauluhn, J. (2009). Comparative Pulmonary Response to Inhaled Nanostructures: Considerations on Test Design and End Points. *Inhalation Toxicology* (in press)
- Paur, H.R.; Mülhopt, S.; Weiss, C.; Diabate, S (2008). In vitro exposure systems and bioassays for the assessment of toxicity of nanoparticles to the human lung. *Journal für Verbraucherschutz und Lebensmittelsicherheit* 3, 319-29 DOI:10.1007/s00003-008-0356-2

- Perkins, S. J.; X-ray and Neutron Solution Scattering; in *Modern Physical Methods in Biochemistry*, Part B; Elsevier; 1988
- Powers, K. W., M. Palazuelos, B. M. Moudgil, S. M. Roberts (2007). Characterization of the size, shape, and state of dispersion of nanomaterials for toxicological studies: *Nanotoxicology*, v. 1, 42-51
- Pui, D., B. Liu (1974). A submicron aerosol standard and the primary absolute calibration of the condensation nuclei counter. *J. Colloid Interface Sci.* 47, 155-171
- Rehn, B., Bruch, J., Zou, T., and Hobusch, G. (1992). Recovery of rat alveolar macrophages by bronchoalveolar lavage under normal and activated conditions. *Environ. Health Perspect.* 97: 11-16
- Richter, V., Potthoff, A., Pompe, W., Gelinsky, M., Ikonomidou, H., Bastian, S., Schirmer, K., Scholz, S., Hofinger, J. BMBF project INOS - evaluation of nanomaterials - a contribution to sustainable development of nanotechnology. *Proceedings EuroNanoForum.* 145-147. 2007.
- Salvador-Morales, C., Flahaut, E., Sim, E., Sloan, J., Green, M. L., and Sim, R. B. (2006). Complement activation and protein adsorption by carbon nanotubes. *Molecular immunology* 43, 193-201
- Salvador-Morales, C., Townsend, P., Flahaut, E., Venien-Bryan, C., Vlandas, A., Green, M. L. H., and Sim, R. B. (2007). Binding of pulmonary surfactant proteins to carbon nanotubes; potential for damage to lung immune defense mechanisms. *Carbon* 45, 607-617
- Sayes, C. M., K.L Reed, D.B. Warheit (2007). Assessing toxicity of fine and nanoparticles: comparing in vitro measurements to in vivo pulmonary toxicity profiles. *Toxicol. Sci.*, 97, 163-180
- Schulze, C., A. Kroll, C.M. Lehr, U.F. Schaefer, K. Becker, J. Schnekenburger, C. Schulze Isfort, R. Landsiedel, W. Wohlleben (2008). Not ready to use - Overcoming pitfalls when dispersing nanoparticles in physiological media. *Nanotoxicology* 2, 51-61
- Schulze et al. (1) (2009). Transport of Metal oxide nanoparticles across an air-blood barrier model; manuscript in preparation
- Schulze et al. (2) (2009), Adsorption of Sp-A onto metal oxide nanoparticles; manuscript in preparation
- Seiler, F., B. Rehn, J. Bruch (2004). Different toxic, fibrogenic and mutagenic effects of four commercial quartz flours in the rat lung. *Int J. Hyg Environ. Health* 207, 115-124
- Seipenbusch, M., A. Binder, G. Kasper (2008). Temporal evolution of nanoparticle aerosols in workplace exposure. *Annals of Occupational Hygiene* 52, 707-716
- Stahlmecke, B., S. Wagener, C. Asbach, H. Kaminski, H. Fissan, T.A.J. Kuhlbusch (2009). Investigation of nanopowder agglomerate stability in an orifice under various differential pressure conditions. *J. Nanoparticle Res.* (accepted)
- Tammet, H., A. Mirme, E. Tamm (1998). Electrical aerosol spectrometer of Tartu University. *J. Aerosol Sci.* 29S1, S427-S428
- Taniguchi Norio, "On the Basic Concept of 'NanoTechnology'" 1974 Proc. ICPE
- Tiede, K., A. B. A. Boxall, S. P. Tear, J. Lewis, H. David, M. Hasselov (2008). Detection and characterization of engineered nanomaterials in food and the environment: *Food Additives and Contaminants*, v. 25, no. 7, 795-821
- Tsai, C. J., C.H. Wu, M.L. Leu, S.C. Chen, C.Y. Huang, P.J. Tsai, F.H. Ko (2009). Dustiness test of nanopowders using a standard rotating drum with a modified sampling train, *J. Nanoparticle Res.* 11, 121-131
- Valsami-Jones, E., D. Berhanu, A. Dybowska, S. Misra, A. R. Boccaccini, T. D. Tetley, S. N. Luoma, J. A. Plant (2008). Nanomaterial synthesis and characterization for toxicological studies: TiO<sub>2</sub> case study: *Mineralogical Magazine*, v. 72, no. 1, 515-519
- Wallace, W. E., M. J. Keane, D. K. Murray, W. P. Chisholm, A. D. Maynard, and T. M. Ong (2007). Phospholipid lung surfactant and nanomaterial surface toxicity: Lessons from diesel soots and silicate dusts: *Journal of Nanomaterial Research*, v. 9, no. 1, 23-38
- Wang, S. C., R. Flagan (1990). Scanning electrical mobility spectrometer. *Aerosol Sci. Technol.* 13, 230-240
- Warheit, D. B. (2008). How meaningful are the results of nanotoxicity studies in the absence of adequate material characterization?: *Toxicological Sciences*, v. 101, 183-185
- Wiemann, W., J. Bruch (2009). Coating of nanoparticles with phosphatidylcholine in aqueous suspension: a quantitative approach. In preparation for *J. Nanoparticle Res.*

- Wiemann, M., J. Bruch (2009b). A combined in vitro and in vivo study of poorly soluble nanostructured materials. Toxicol. Sci. (in preparation)
- Xia, T., N. Li, A.E. Nel (2009). Potential health impact of Nanoparticles. Annu. Rev. Public Health, 30, 137-150
- Yokel, R.A., R. Florence, M. Tseng, U. Graham, R. Sultana, D.A. Butterfield, P. Wu, E. Grulke (2008). Biodistribution and toxicity of systemically-introduced nanoscale ceria. Proceedings of Nanotox 2008 Zürich , 87

## Glossary

<b>AFM</b>	Atomic Force Microscopy
<b>AIOOH</b>	Boehmite
<b>ALP</b>	Alkaline phosphatase
<b>AM</b>	Alveolar Macrophage
<b>ATCC</b>	American Tissue and Culture Collection
<b>AUC</b>	Analytical Ultracentrifuge
<b>BAL</b>	Bronchoalveolar lavage
<b>BALF</b>	Bronchoalveolar lavage fluid
<b>BaSO<sub>4</sub></b>	Barium sulphate
<b>BCA</b>	Bicinchoninic acid
<b>BET</b>	Surface Area Analysis Developed by Brunauer, Emmett & Teller
<b>BSA</b>	Bovine Serum Albumin
<b><i>C. familiaris</i></b>	<i>Canis familiaris</i>
<b>c50, c100, c200</b>	Carboxylated Polystyrene Nanoparticles with a Diameter of 50, 100 or 200 nm
<b>CeO<sub>2</sub></b>	Cerium dioxide
<b>Cox-2</b>	Cyclooxygenase-2
<b>CLS</b>	Cell Lines Service, Eppelheim, Germany
<b>CPC</b>	Condensation particle counter; measures particle number concentration
<b>DAPI</b>	4',6-Diamidino-2-Phenylindole (double stranded DNA staining)
<b>DCF</b>	fluorescein
<b>DLS/PCS</b>	Dynamic/Static Light Scattering, Quasi-elastic Light Scattering, Photon Correlation Spectroscopy
<b>DMA</b>	Differential mobility analyser; selects particles according to their electrical mobility
<b>DMEM</b>	Dulbecco's Modified Eagles's Medium
<b>ECACC</b>	European Collection of Cell Cultures, Salisbury, UK
<b>EDXS</b>	Energy Dispersive X-ray Spectroscopy
<b>EELS</b>	Electron Energy Loss Spectroscopy
<b>ESCA</b>	Electron Spectroscopy for Chemical Analysis
<b>ESI</b>	Electron Spectroscopic Imaging

<b>ESP</b>	Electrostatic Precipitator (Grimm model #5.561)
<b>FCS</b>	Foetal Calf Serum
<b>FCS</b>	Fluorescence-Correlation-Spectroscopy
<b>FITC-BSA</b>	Fluoresceinisothiocyanate-labelled Bovine Serum Albumin
<b>FMPS</b>	Fast mobility particle sizer, TSI model 3091; determines number size distribution of particles between 5.6 and 560 nm with 1 s time resolution
<b>GGT</b>	$\gamma$ -Glutamyltransferase
<b>Glucuronidase</b>	Enzyme in Phagolysosomes
<b>h</b>	Hour
<b>HDF</b>	Hydrodynamic Fractionation
<b>H. sapiens</b>	<i>Homo sapiens</i>
<b>HO-1</b>	Hemoxygenase-1
<b>ICP-MS</b>	Inductively-Coupled-Plasma Mass-Spectrometry
<b>IL-8</b>	Interleukin-8
<b>KRB</b>	Krebs-Ringer-Buffer
<b>LALN</b>	Lung-Associated Lymph Node
<b>LDH</b>	Lactate dehydrogenase
<b>LOEL</b>	Lowest Observable Effect Level
<b>LPS</b>	Lipopolysaccharide
<b><math>\mu</math>g</b>	microgram
<b><math>\mu</math>m</b>	micrometer
<b>MMAD</b>	Mass Median Aerodynamic Diameter
<b>m. musculus</b>	<i>Mus musculus</i>
<b>MEM</b>	Minimal Essential Medium Eagle
<b>min</b>	minute
<b>ml</b>	mililiter
<b>mM</b>	milimolar
<b>MTT</b>	3-(4,5-Dimethylthiazol-2-yl)-2,5-diphenyltetrazoliumbromid
<b>NaCl</b>	Sodium chloride
<b>NAG</b>	N-Acetylaminoglucoseaminidase
<b>NAS</b>	Nanometer Aerosol Sampler (TSI model 3089); collects charged particles electrostatically
<b>nm</b>	Nanometer

<b>NOEL</b>	No Observable / Observed Effect Level
<b>NP</b>	Nanoparticle
<b>NSAM</b>	Nanoparticle surface area monitor (TSI model 3550)
<b>p50, p100</b>	plain (unmodified) Polystyrene Nanoparticles with a Diameter of 50 or 100 nm
<b>PB</b>	Phosphate Buffer
<b>pBALF</b>	porcine Bronchoalveolar Lavage Fluid
<b>PC</b>	Phosphatidylcholine
<b>pg</b>	picogram
<b>PM</b>	Particulate matter
<b>PM<sub>2.5</sub></b>	Mass concentration of particles <2.5 µm.
<b>PM<sub>10</sub></b>	Mass concentration of particles <10 µm
<b>PMA</b>	Phorbol 12-myristate 13-acetate
<b>PMN</b>	Polymorphonuclear Neutrophils
<b>R. norvegicus</b>	<i>Rattus norvegicus</i>
<b>ROS</b>	Radical Oxygen Species
<b>RPMI</b>	Cell culture medium, developed at the Roswell Park Memorial Institute
<b><math>\sigma_g</math></b>	Geometric standard deviation of lognormal size distribution
<b>Scopoletin</b>	Fluorescent substance, decomposed by ROS
<b>SDS-PAGE</b>	Sodium-Dodecylsulfate-Polyacrylamide-Gelelectrophoresis
<b>SEM</b>	Scanning Electron Microscopy
<b>Sirius Red</b>	Stain detecting collagen in histological sections
<b>SMPS</b>	Scanning Mobility Particle Sizer (TSI) or Sequential Mobility Particle Sizer (Grimm)
<b>SMPS-G1</b>	Grimm SMPS (model SMPS+C); determines number size distribution of particles between 11 and 1080 nm with 406 s time resolution with long DMA and between 5.5 and 350 nm with 230 s time resolution with short DMA
<b>SMPS-T1</b>	TSI SMPS (model 3936) equipped with water based CPC (TSI model 3786); determines number size distribution of particles between 14 and 750 nm (with standard settings) with 240 s time resolution
<b>SMPS-T2</b>	TSI SMPS (model 3936) equipped with butanol based CPC (TSI model 3010); determines number size distribution of particles between 14 and 750 nm (with standard settings) with 240 s time resolution
<b>SMPS*</b>	TSI SMPS (model 3936); identical to SMPS-T1
<b>SOP</b>	Standard operation procedure
<b>Sp-A, B, C, D</b>	Lung surfactant protein A, B, C, D

<b>SrCO<sub>3</sub></b>	Strontium carbonate
<b>TEER</b>	Transepithelial electrical resistance
<b>TEM</b>	Transmission Electron Microscopy
<b>TiO<sub>2</sub></b>	Titanium dioxide
<b>TiZrO</b>	Titanium zircon oxide
<b>TNF</b>	Tumor Necrosis Factor
<b>TOF-SIMS</b>	Time of Flight - Secondary Ion Mass Spectrometry
<b>ZnO</b>	Zinc oxide
<b>ZrO<sub>2</sub></b>	Zircon dioxide
<b>ULPA</b>	Ultra low penetration air filter; capture efficiency >99.9995%
<b>w</b>	weight
<b>WDXS</b>	Wavelength Dispersive X-ray Spectroscopy
<b>XPS</b>	X-ray Photoelectron Spectroscopy

## NanoCare Partners

---

BASF SE, Ludwigshafen (R. Landsiedel, W. Wohlleben)

Bayer MaterialScience AG, Leverkusen (J. Ragot, Bayer MaterialScience AG; J. Pauluhn, Bayer Shering Pharma AG; M. Voetz, Bayer Technology Services GmbH)

DECHEMA Gesellschaft für Chemische Technik und Biotechnologie e.V., Frankfurt a.M. (A. Förster, C. Steinbach)

Evonik Degussa GmbH, Hanau-Wolfgang (N. Krüger, M. Kroell, C. Schulze-Isfort)

Forschungszentrum Karlsruhe GmbH, Eggenstein-Leopoldshafen  
Institut für Toxikologie und Genetik (K. Nau, H.F. Krug)  
Institut für Angewandte Informatik (O. Kusche, M. Dickerhof)  
Institut für Technikfolgenabschätzung und Systemanalyse (C. Quendt, T. Fleischer)  
Institut für Technische Chemie - Bereich Thermische Abfallbehandlung (S. Mülhopt, H.-R. Paur)

IBE R&D Institute for Lung Health gGmbH, Marl (J. Bruch, M. Wiemann)

Institute of Energy and Environmental Technology (IUTA) e.V., Air Quality & Sustainable Nanotechnology Unit, Duisburg (T. A. J. Kuhlbusch, C. Asbach, B. Stahlmecke, S. Wagener, H. Kaminski, H. Fissan)

Institut für Gefahrstoffforschung (IGF) der Bergbau Berufsgenossenschaft, Bochum (D. Dahmann, C. Monz)

ItN Nanovation AG, Saarbrücken (C. Goebbert)

Kompetenznetz Nanomaterialen, Forschungszentrum Karlsruhe GmbH, Eggenstein-Leopoldshafen (R. Hedderich, S. Dierig)

Saarland University, Department of Biopharmaceutics and Pharmaceutical Technology, Saarbrücken (C.-M. Lehr, U. F. Schäfer, C. Schulze)

Solvay Infra Bad Hönningen GmbH, Hannover (K. H. Kampmann, F. Hardinghaus, S. Thun-Battersby)

University of Bielefeld, Institute for Biophysics and Nanoscience (BINAS), Bielefeld (D. Anselmetti, K. Tönsing, D. Wesner, S. Zünkeler)

University of Münster, Gastroenterological Molecular Cell Biology (GMZ), Department of Medicine B, Münster (J. Schnekenburger, D. Hahn, A. Kroll, M. H. Pillukat)

VDI Technologiezentrum GmbH (VDI-TZ), Düsseldorf (N. Malanowski, W. Luther)

## Annex A: Nano Material Data Sheets

Material

Titanium dioxide (TiO<sub>2</sub>)

**Charge description /  
NanoCare product number**

CH-000231  
1.1

**Provider**

ItN Nanovation AG

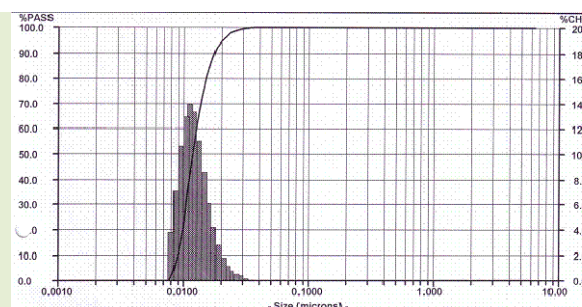
**Available form**

aqueous suspension

**Primary particle size [d<sub>90</sub> in nm]**

17 nm

**Particle size distribution**



**pH**

4.04 (in water)

**BET Surface area**

117 m<sup>2</sup>/g

**Particle morphology**

Irregular spheres

**Crystal phase and crystallinity**

mixed phase anatase (95%)/rutile (5%)

**Stabilisation**

Polyoxa acid

**Solubility in water**

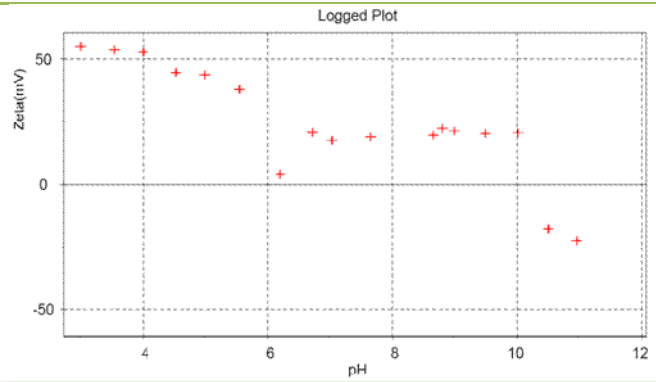
10 ppm

**Purity/contamination**

O 58 %  
Ti 41 %  
Cl <1 %

**REM/TEM**

**Zeta potential  
(in water)**



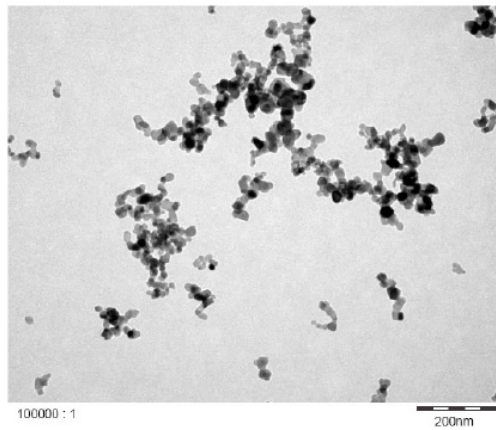
**Surface area chemistry**

O	53 %
Ti	21 %
C	25 %
Cl	0.6 %

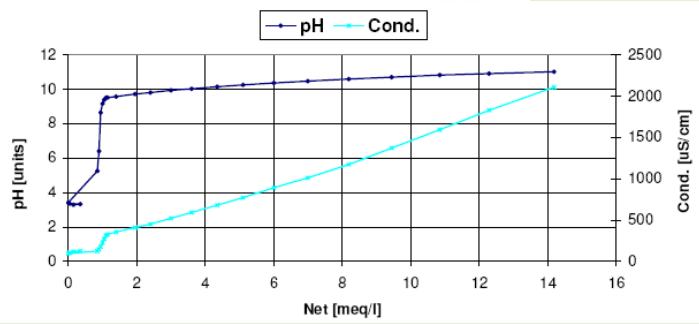
**Material** Titanium dioxide (TiO<sub>2</sub>)

<b>Charge description/ NanoCare Product number</b>	CH-000002 / CH-000003 1.2
<b>Provider</b>	Evonik Degussa GmbH
<b>Available form</b>	Powder
<b>Primary particle size [d<sub>50</sub> in nm]</b>	27.2 nm
<b>Particle size distribution</b>	
<b>pH</b>	3.62
<b>BET Surface area</b>	52 m <sup>2</sup> /g
<b>Particle morphology</b>	crystalline
<b>Crystal phase and crystallinity</b>	TiO <sub>2</sub> Tetragonal Rutile TiO <sub>2</sub> Tetragonal Anatase
<b>Stabilisation</b>	none
<b>Solubility in water</b>	TiO <sub>2</sub> 130 ppm (µg/g)
<b>Purity/contamination</b>	TiO <sub>2</sub>

REM/TEM



Zeta potential



Surface area chemistry

**Material** **TiO<sub>2</sub>\_40**

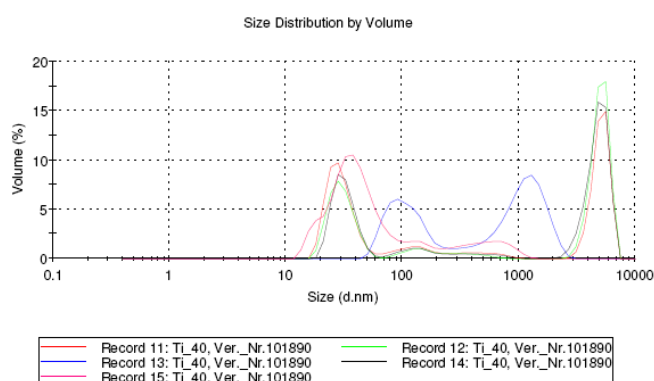
**Charge description/  
NanoCare Product number** CH-000696  
1.3

**Provider** Evonik Degussa GmbH

**Available form** Powder

**Primary particle size [d<sub>50</sub> in nm]** 42.3 nm

**Particle size distribution**



**pH** 3.42

**BET Surface area** 38 m<sup>2</sup>/g

**Particle morphology** crystalline

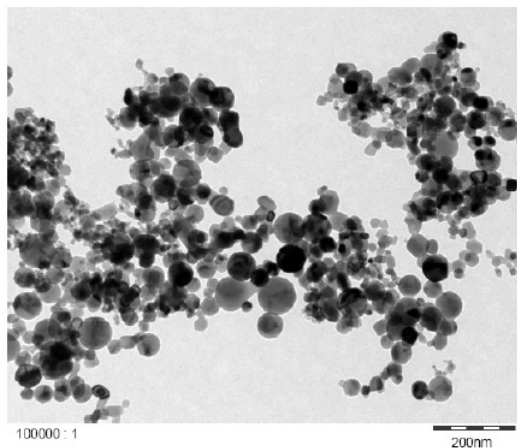
**Crystal phase and crystallinity** TiO<sub>2</sub> Tetragonal Rutile  
TiO<sub>2</sub> Tetragonal Anatase

**Stabilisation**

**Solubility in water**

**Purity/contamination** TiO<sub>2</sub>

REM/TEM



Zeta potential

At pH 3.3: 49.5mV  
IEP at pH 5.8

Surface area chemistry

**Material** TiO<sub>2</sub>\_70

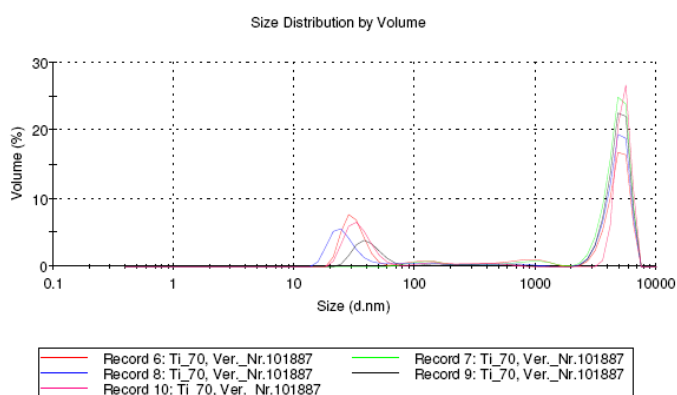
**Charge description/  
NanoCare Product number** CH-000697  
1.4

**Provider** Evonik Degussa GmbH

**Available form** Powder

**Primary particle size [d<sub>50</sub> in nm]** 33.4 nm

**Particle size distribution**



**pH** 3.5

**BET Surface area** 63 m<sup>2</sup>/g

**Particle morphology** crystalline

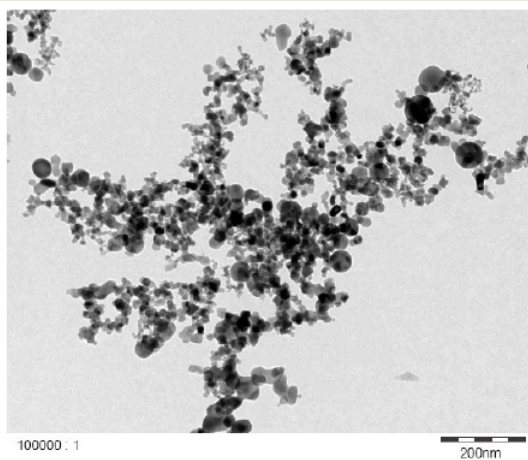
**Crystal phase and crystallinity** TiO<sub>2</sub> Tetragonal Rutile  
TiO<sub>2</sub> Tetragonal Anatase

**Stabilisation**

**Solubility in Water**

**Purity/contamination** TiO<sub>2</sub>

REM/TEM



Zeta potential

At pH 3.5: 48mV  
IEP at pH 5.6

Surface area chemistry

**Material** **TiO<sub>2</sub>\_120**

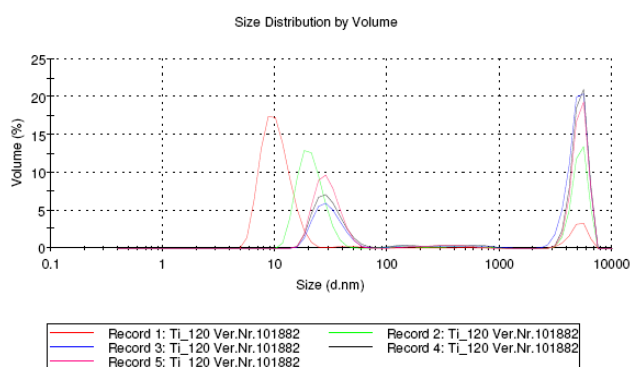
**Charge description/  
NanoCare Product number** CH-000698  
1.5

**Provider** Evonik Degussa GmbH

**Available form** Powder

**Primary particle size [d<sub>50</sub> in nm]** 12.5 nm

**Particle size distribution**



**pH** 3.3

**BET Surface area** 115 m<sup>2</sup>/g

**Particle morphology** crystalline

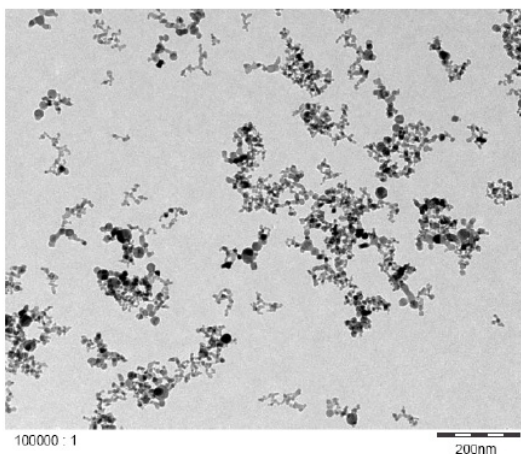
**Crystal phase and crystallinity** TiO<sub>2</sub> Tetragonal Rutile  
TiO<sub>2</sub> Tetragonal Anatase

**Stabilisation**

**Solubility in water**

**Purity/contamination** TiO<sub>2</sub>

**REM/TEM**



**Zeta potential**

at pH 3.2: 52mV  
IEP at pH 5.8

**Surface area chemistry**

**Material** Cerium oxide (CeO<sub>2</sub>) modification A

**Charge description/  
NanoCare Product number** CH-000440  
3.1

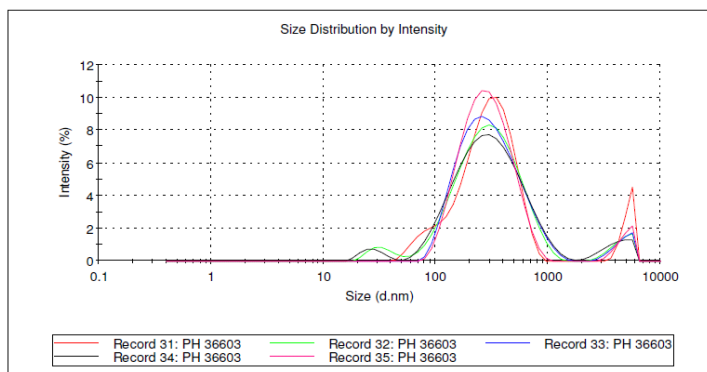
**Provider** Evonik Degussa

**Available form** Powder

**Primary particle size  
[d<sub>50</sub> in nm]** 14 nm

**Particle size distribution**

	Diam. (nm)	% Intensity	Width (nm)
<b>Z-Average (d.nm):</b> 237,0	<b>Peak 1:</b> 305,3	94,2	150,8
<b>Pdl:</b> 0,423	<b>Peak 2:</b> 4785	5,8	732,9
<b>Intercept:</b> 0,856	<b>Peak 3:</b> 0,000	0,0	0,000
<b>Result quality</b> Good			



**pH** 6.2

**BET Surface area** 63 m<sup>2</sup>/g

**Particle morphology** Aggregate

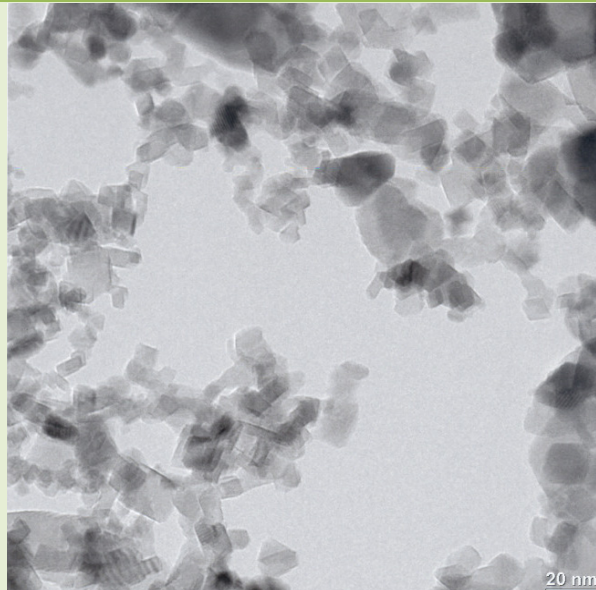
**Crystal phase and  
crystallinity** Crystalline (100 % fcc)

**Stabilisation** HNO<sub>3</sub>

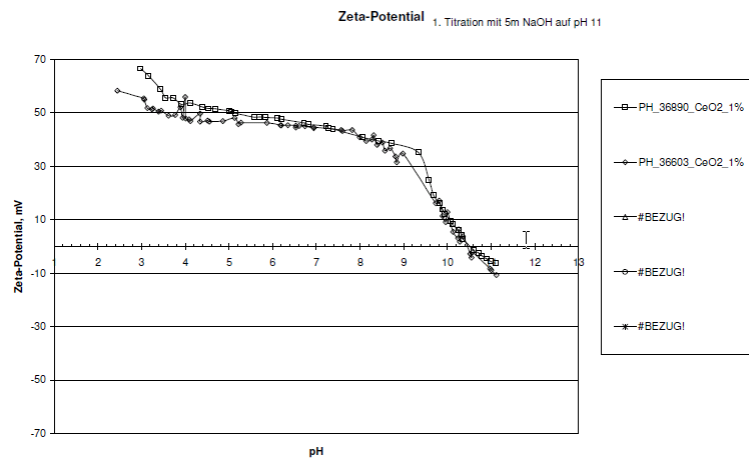
**Solubility in water** -

**Purity/contamination** > 99.97 %

REM/TEM



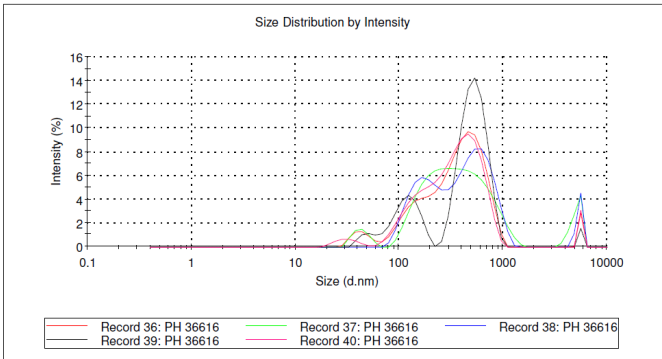
Zeta potential



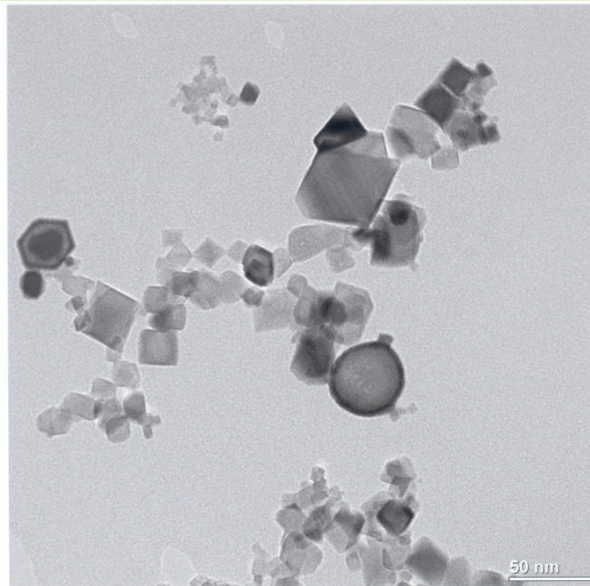
Surface area chemistry

O	56.8 %
Ce	25.0 %
C	18.2 %

**Material** Cerium oxide (CeO<sub>2</sub>) modification B

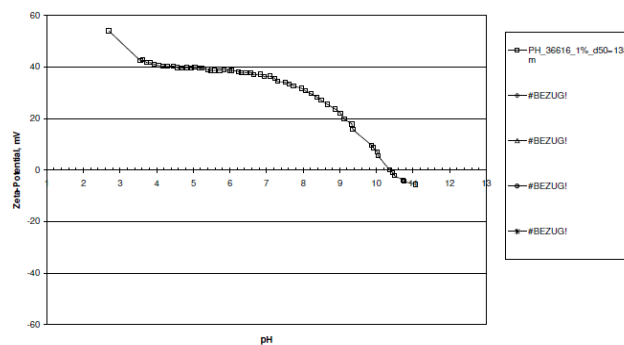
<b>Charge description/ NanoCare Product number</b>	CH-000441 3.2																
<b>Provider</b>	Evonik Degussa																
<b>Available form</b>	Powder																
<b>Primary particle size [d<sub>50</sub> in nm]</b>	20 nm																
<b>Particle size distribution</b>	<p><b>Results</b></p> <table border="1"> <thead> <tr> <th></th> <th>Diam. (nm)</th> <th>% Intensity</th> <th>Width (nm)</th> </tr> </thead> <tbody> <tr> <td><b>Z-Average (d.nm):</b> 496,0</td> <td><b>Peak 1:</b> 364,1</td> <td>93,8</td> <td>195,0</td> </tr> <tr> <td><b>Pdl:</b> 0,548</td> <td><b>Peak 2:</b> 31,79</td> <td>3,1</td> <td>7,707</td> </tr> <tr> <td><b>Intercept:</b> 0,733</td> <td><b>Peak 3:</b> 5560</td> <td>3,1</td> <td>6,104e-5</td> </tr> </tbody> </table> <p><b>Result quality</b> Refer to quality report</p> 		Diam. (nm)	% Intensity	Width (nm)	<b>Z-Average (d.nm):</b> 496,0	<b>Peak 1:</b> 364,1	93,8	195,0	<b>Pdl:</b> 0,548	<b>Peak 2:</b> 31,79	3,1	7,707	<b>Intercept:</b> 0,733	<b>Peak 3:</b> 5560	3,1	6,104e-5
	Diam. (nm)	% Intensity	Width (nm)														
<b>Z-Average (d.nm):</b> 496,0	<b>Peak 1:</b> 364,1	93,8	195,0														
<b>Pdl:</b> 0,548	<b>Peak 2:</b> 31,79	3,1	7,707														
<b>Intercept:</b> 0,733	<b>Peak 3:</b> 5560	3,1	6,104e-5														
<b>pH</b>	5.4																
<b>BET Surface area</b>	44 m <sup>2</sup> /g																
<b>Particle morphology</b>	Aggregate																
<b>Crystal phase and crystallinity</b>	Crystalline (100 % fcc)																
<b>Stabilisation</b>	HNO <sub>3</sub>																
<b>Solubility in water</b>	-																
<b>Purity/contamination</b>	> 99.97 %																

REM/TEM



Zeta-Potential 1. Titration mit 5m NaOH auf pH 11

Zeta potential

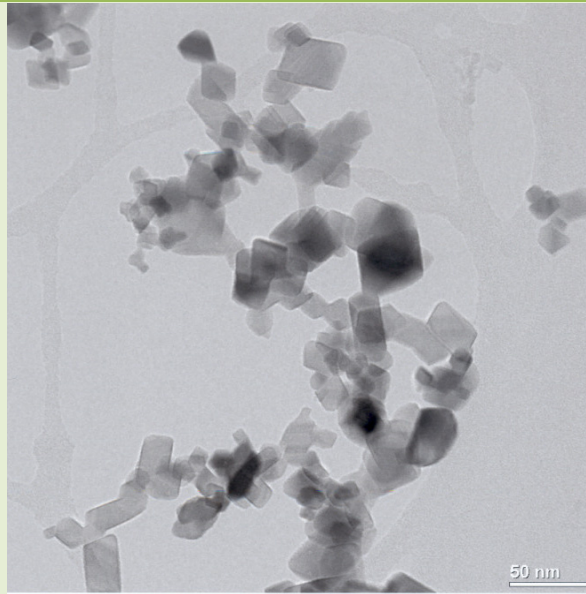


Surface area chemistry	O	56.1 %
	Ce	21.8 %
	C	22.1 %

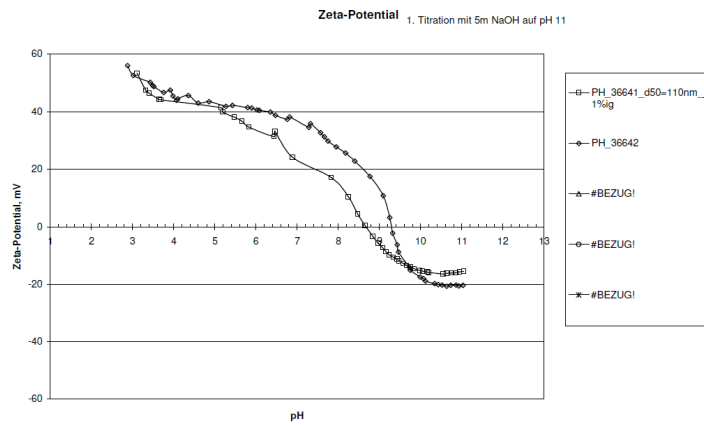
**Material** Cerium oxide (CeO<sub>2</sub>) modification C

<b>Charge description/ NanoCare Product number</b>	CH-000442 3.3																
<b>Provider</b>	Evonik Degussa																
<b>Available form</b>	Powder																
<b>Primary particle size [d<sub>50</sub> in nm]</b>	23 nm																
<b>Particle size distribution</b>	<p><b>Results</b></p> <table border="1"> <thead> <tr> <th></th> <th>Diam. (nm)</th> <th>% Intensity</th> <th>Width (nm)</th> </tr> </thead> <tbody> <tr> <td><b>Z-Average (d.nm):</b> 232,7</td> <td><b>Peak 1:</b> 270,9</td> <td>75,9</td> <td>186,5</td> </tr> <tr> <td><b>PdI:</b> 0,614</td> <td><b>Peak 2:</b> 4605</td> <td>18,2</td> <td>834,5</td> </tr> <tr> <td><b>Intercept:</b> 0,776</td> <td><b>Peak 3:</b> 24,66</td> <td>5,9</td> <td>5,387</td> </tr> </tbody> </table> <p><b>Result quality</b> Refer to quality report</p>		Diam. (nm)	% Intensity	Width (nm)	<b>Z-Average (d.nm):</b> 232,7	<b>Peak 1:</b> 270,9	75,9	186,5	<b>PdI:</b> 0,614	<b>Peak 2:</b> 4605	18,2	834,5	<b>Intercept:</b> 0,776	<b>Peak 3:</b> 24,66	5,9	5,387
	Diam. (nm)	% Intensity	Width (nm)														
<b>Z-Average (d.nm):</b> 232,7	<b>Peak 1:</b> 270,9	75,9	186,5														
<b>PdI:</b> 0,614	<b>Peak 2:</b> 4605	18,2	834,5														
<b>Intercept:</b> 0,776	<b>Peak 3:</b> 24,66	5,9	5,387														
<b>pH</b>	3.4																
<b>BET Surface area</b>	38 m <sup>2</sup> /g																
<b>Particle morphology</b>	Aggregate																
<b>Crystal phase and crystallinity</b>	Crystalline (100 % fcc)																
<b>Stabilisation</b>	HNO <sub>3</sub>																
<b>Solubility in water</b>	-																
<b>Purity/contamination</b>	> 99.97 %																

REM/TEM



Zeta potential



CH 000442 = PH 36641

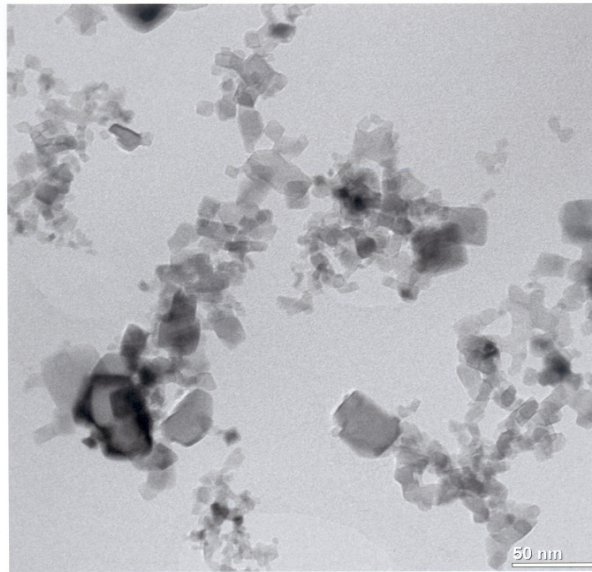
Surface area chemistry

O	56.5 %
Ce	22.1 %
C	21.5 %

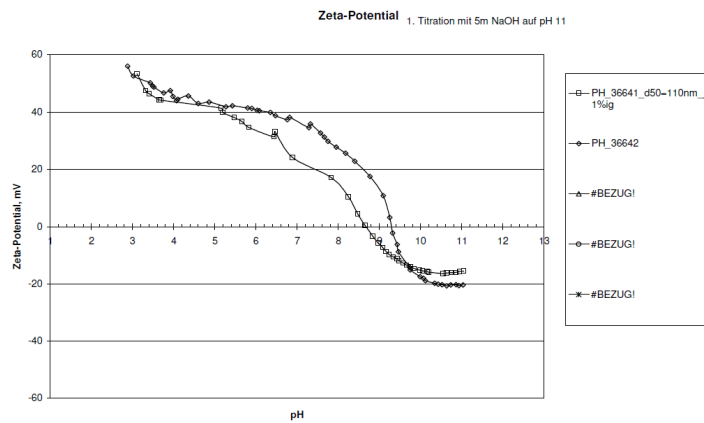
**Material** Cerium oxide (CeO<sub>2</sub>) modification D

<b>Charge description/ NanoCare Product number</b>	CH-000443 3.4																
<b>Provider</b>	Evonik Degussa																
<b>Available form</b>	Powder																
<b>Primary particle size [d<sub>50</sub> in nm]</b>	14 nm																
<b>Particle size distribution</b>	<p><b>Results</b></p> <table border="1"> <thead> <tr> <th></th> <th>Diam. (nm)</th> <th>% Intensity</th> <th>Width (nm)</th> </tr> </thead> <tbody> <tr> <td><b>Z-Average (d.nm):</b> 353,5</td> <td><b>Peak 1:</b> 223,1</td> <td>52,6</td> <td>90,46</td> </tr> <tr> <td><b>Pdl:</b> 0,838</td> <td><b>Peak 2:</b> 921,7</td> <td>25,4</td> <td>347,8</td> </tr> <tr> <td><b>Intercept:</b> 0,785</td> <td><b>Peak 3:</b> 4739</td> <td>21,9</td> <td>766,4</td> </tr> </tbody> </table> <p><b>Result quality</b> Refer to quality report</p>		Diam. (nm)	% Intensity	Width (nm)	<b>Z-Average (d.nm):</b> 353,5	<b>Peak 1:</b> 223,1	52,6	90,46	<b>Pdl:</b> 0,838	<b>Peak 2:</b> 921,7	25,4	347,8	<b>Intercept:</b> 0,785	<b>Peak 3:</b> 4739	21,9	766,4
	Diam. (nm)	% Intensity	Width (nm)														
<b>Z-Average (d.nm):</b> 353,5	<b>Peak 1:</b> 223,1	52,6	90,46														
<b>Pdl:</b> 0,838	<b>Peak 2:</b> 921,7	25,4	347,8														
<b>Intercept:</b> 0,785	<b>Peak 3:</b> 4739	21,9	766,4														
<b>pH</b>	3,4																
<b>BET Surface area</b>	63 m <sup>2</sup> /g																
<b>Particle morphology</b>	Aggregate																
<b>Crystal phase and crystallinity</b>	Crystalline (100 % fcc)																
<b>Stabilisation</b>	HNO <sub>3</sub>																
<b>Solubility in water</b>	-																
<b>Purity/contamination</b>	> 99.97 %																

REM/TEM



Zeta potential

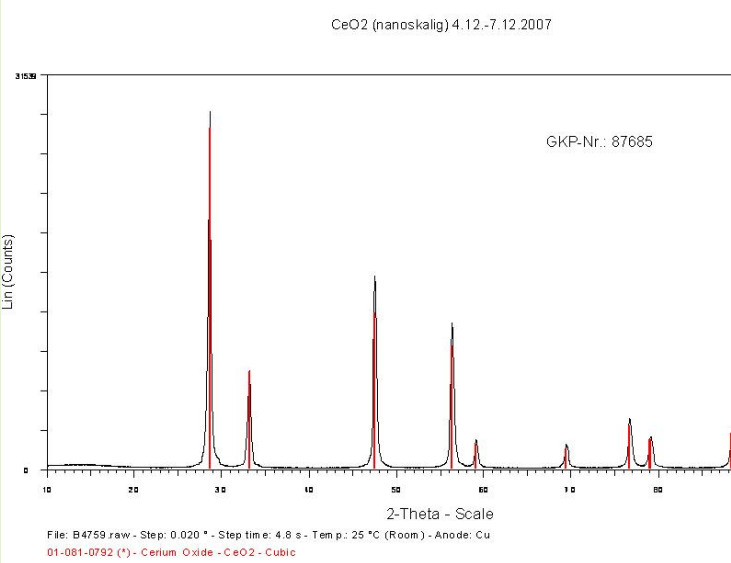


CH 000443 = PH 36642

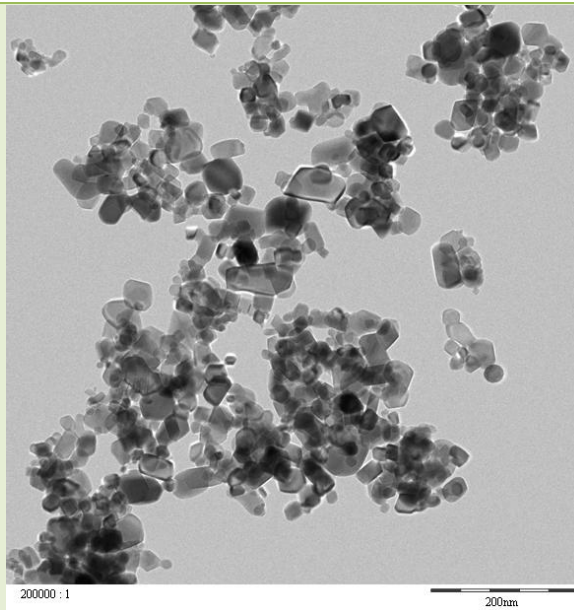
Surface area chemistry

O 56.0 %  
 Ce 22.3 %  
 C 21.7 %

**Material** Cerium oxide (CeO<sub>2</sub>)

<b>Charge description/ NanoCare Product number</b>	CH-000380 3.5
<b>Provider</b>	BASF SE
<b>Available form</b>	Powder
<b>Primary particle size [d<sub>50</sub> in nm]</b>	70 nm
<b>Particle size distribution</b>	10 - 200 nm, see TEM; D <sub>50</sub> of primary particles according to TEM and XRD at 40 nm
<b>pH</b>	n/a (Powder)
<b>BET Surface area</b>	33 m <sup>2</sup> /g
<b>Particle morphology</b>	Irregular spherical
<b>Crystal phase and crystallinity</b>	<p>Cerium oxide cubic</p> 
<b>Stabilisation</b>	no
<b>Solubility in water</b>	In H <sub>2</sub> O and DMEM/FCS below detection limit of 1 ppm  Protocol: initial concentration 10 mg/ml, 24h agitation at 900 rpm; centrifugation and analysis of supernatant
<b>Purity/contamination</b>	Purity 99% see XRD above

REM/TEM



Zeta potential

Surface area chemistry

XPS-results:  
impurities C and Cl on the surface  
O 53 %  
Ce 26 %  
C 20 %  
Cl 0.6 %

**Material** **Boehmite I (AlOOH)**

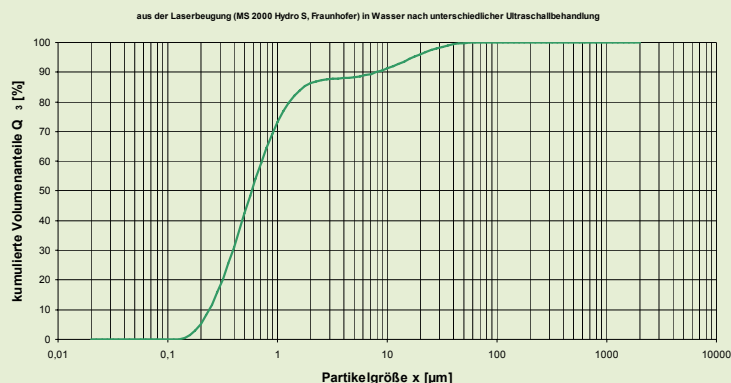
**Charge description/  
NanoCare Product number** CH-000083  
5.1

**Provider** Bayer MaterialScience AG

**Available form** Powder

**Primary particle size [d<sub>50</sub> nm]** 40 nm

**Particle size distribution**



**pH** -

**BET Surface area** 47 m<sup>2</sup>/g

**Particle morphology** irregular spherical

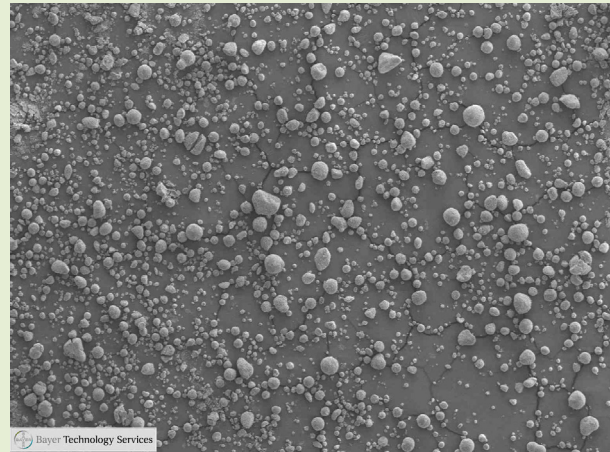
**Crystal phase and crystallinity** Boehmite

**Stabilisation** -

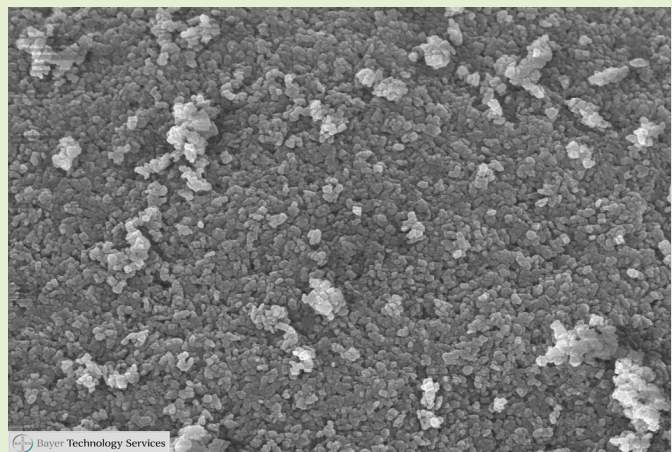
**Solubility in water** -

**Purity/contamination** Purity: 82.7%  
impurities using SIMS:  
Tracer of C, Na, Fe, Si, Li, B

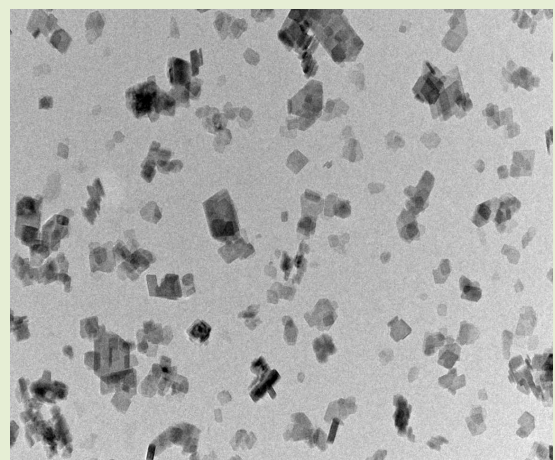
REM/TEM



200µm



2µm



200nm

Zeta potential /IEP  $34.0 \pm 1.1$  mV (in 1mmolarer potassium chloride suspension)

<b>Surface area chemistry</b>	O	61.6 At. %
	Al	31.7 At. %
	C	6.7 At. %

**Material** Boehmite II (AlOOH)

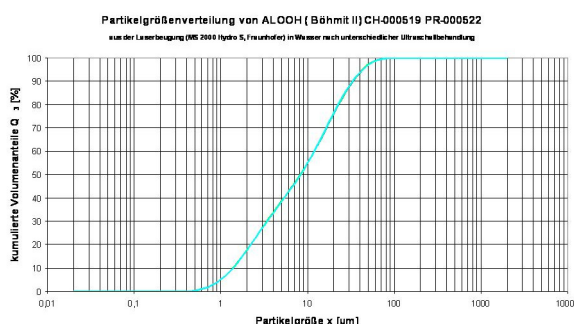
**Charge description/  
NanoCare Product number** CH-000519  
5.2

**Provider** Bayer MaterialScience AG

**Available form** Powder

**Primary particle size** 70 nm

**Particle size distribution**



**pH** -

**BET Surface area** 159 m<sup>2</sup>/g

**Particle morphology** irregular spherical

**Crystal phase and crystallinity** Crystalline Boehmite

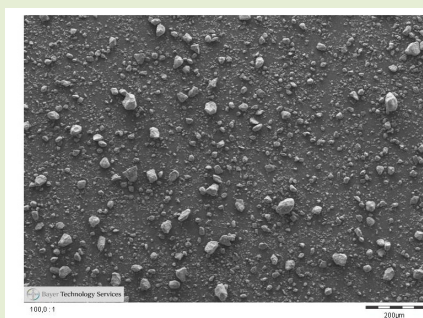
**Stabilisation** -

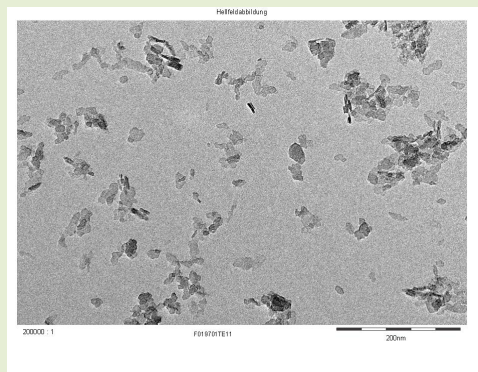
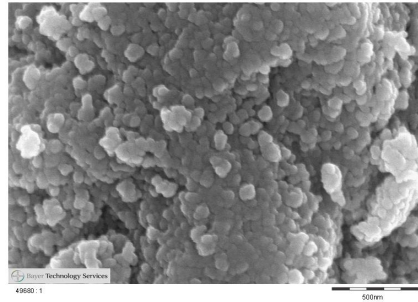
**Solubility in water** -

92.5 At. % Aluminium oxide - 7.5 At. % C

**Purity/contamination** impurities using SIMS:  
Traces of C, Na, Mg, K, Cl, S

**REM/TEM**





**Zeta potential /IEP**

26.4 ± 2.4 mV ( in 1mmolarer potassium chloride suspension)

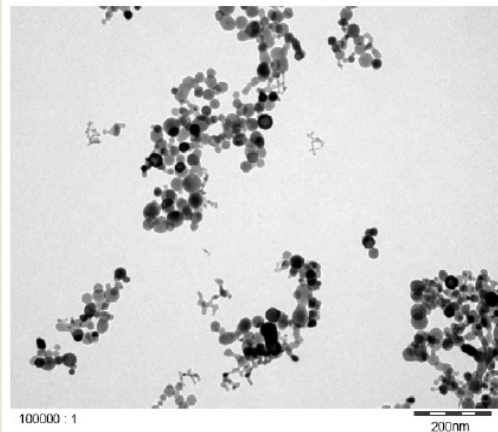
**Surface area chemistry**

O	65.0 At. %
Al	32.1 At. %
C	2.0 At. %
Cl	0.9 At. %

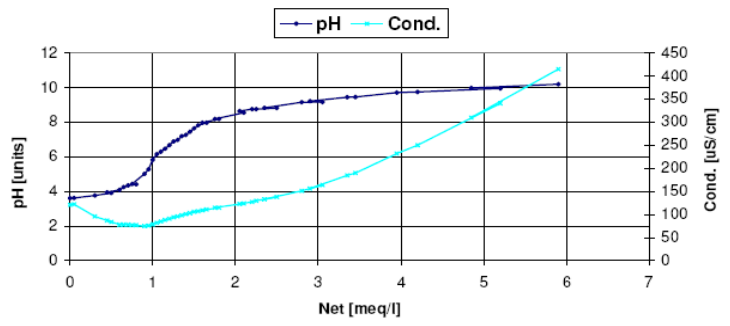
**Material** Ti-Zr\_10/50

<b>Charge description/ NanoCare Product number</b>	CH-000004 6.1
<b>Provider</b>	Evonik Degussa GmbH
<b>Available form</b>	Powder
<b>Primary particle size [d<sub>50</sub> in nm]</b>	28.2 nm
<b>Particle size distribution</b>	
<b>pH</b>	3.5
<b>BET Surface area</b>	44 m <sup>2</sup> /g
<b>Particle morphology</b>	Crystalline
<b>Crystal phase and crystallinity</b>	ZrO <sub>2</sub> Tetragonal / Baddeleyite ZrO <sub>2</sub>
<b>Stabilisation</b>	No
<b>Solubility in water</b>	Ti 15 ppm(µg/g) Zr 36 ppm(µg/g) Ni 31 ppm(µg/g)
<b>Purity/contamination</b>	ZrO <sub>2</sub> 86.57 % TiO <sub>2</sub> 13.15 %

**REM/TEM**

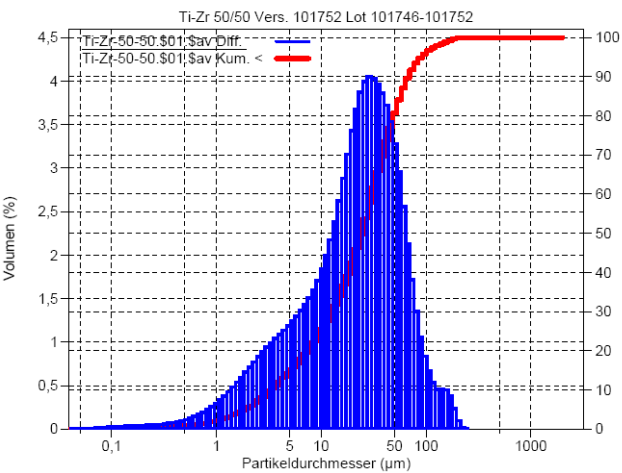


**Zeta potential**

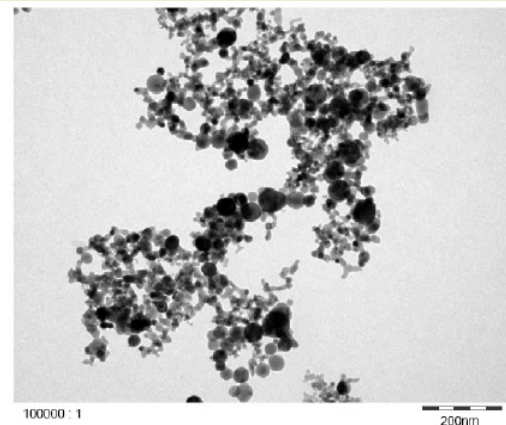


**Surface area chemistry**

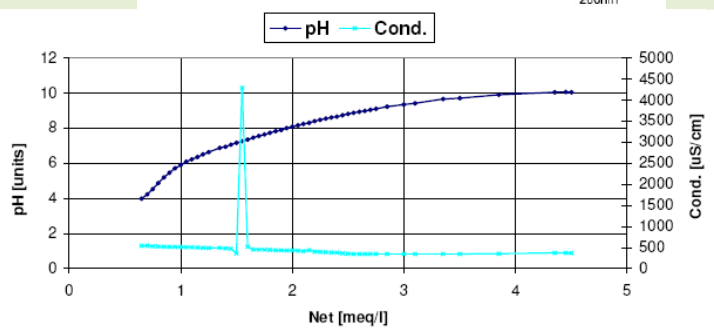
**Material** Ti-Zr\_50/50

<b>Charge description/ NanoCare Product number</b>	CH-000006 6.2
<b>Provider</b>	Evonik Degussa GmbH
<b>Available form</b>	Powder
<b>Primary particle size [d<sub>50</sub> in nm]</b>	36.8 nm
<b>Particle size distribution</b>	
<b>pH</b>	3.74
<b>BET Surface area</b>	54 m <sup>2</sup> /g
<b>Particle morphology</b>	Crystalline
<b>Crystal phase and crystallinity</b>	ZrO <sub>2</sub> Srilankite Orthorhombic TiO <sub>2</sub> maybe Rutile
<b>Stabilisation</b>	No
<b>Solubility in water</b>	Ti 28 ppm (µg/g) Zr 10 ppm (µg/g) Ni 17 ppm (µg/g)
<b>Purity/contamination</b>	ZrO <sub>2</sub> 45.64% TiO <sub>2</sub> 54.12%

REM/TEM



Zeta potential

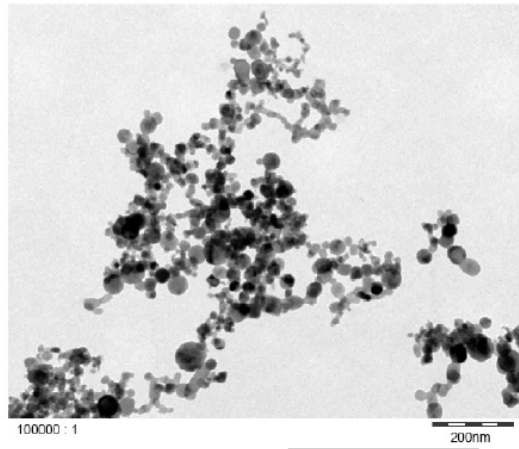


Surface area chemistry

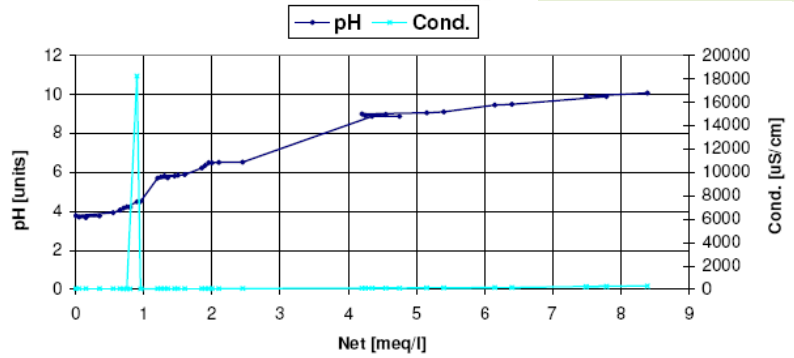
**Material** Ti-Zr\_95/50

<b>Charge description/ NanoCare Product number</b>	CH-000008 6.3
<b>Provider</b>	Evonik Degussa GmbH
<b>Available form</b>	Powder
<b>Primary particle size [d<sub>50</sub> in nm]</b>	37.2 nm
<b>Particle size distribution</b>	
<b>pH</b>	4.00
<b>BET Surface area</b>	51 m <sup>2</sup> /g
<b>Particle morphology</b>	crystalline
<b>Crystal phase and crystallinity</b>	TiO <sub>2</sub> Tetragonal Anatase TiO <sub>2</sub> Tetragonal Rutile
<b>Stabilisation</b>	No
<b>Solubility in water</b>	Ti 21 ppm (µg/g) Zr 1 ppm (µg/g) Ni 16 ppm (µg/g)
<b>Purity/contamination</b>	TiO <sub>2</sub> 94.36 Zr O <sub>2</sub> 5.61

REM/TEM



Zeta potential



Surface area chemistry

**Material** Al-Ti-Zr\_15-10/50

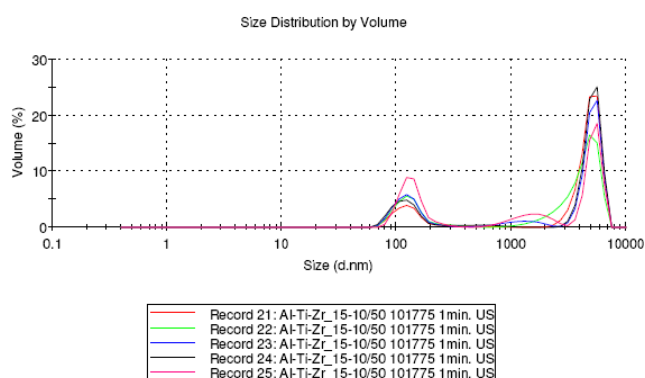
**Charge description/  
NanoCare Product number** CH-000256  
7.1

**Provide** Evonik Degussa GmbH

**Available form** Powder

**Primary particle size [d<sub>50</sub> in nm]** 25.8 nm

**Particle size distribution**



**pH** 4.61

**BET Surface area** 43 m<sup>2</sup>/g

**Particle morphology** crystalline

**Crystal phase and crystallinity** ZrO<sub>2</sub> tetragonal (with changed lattice constant)

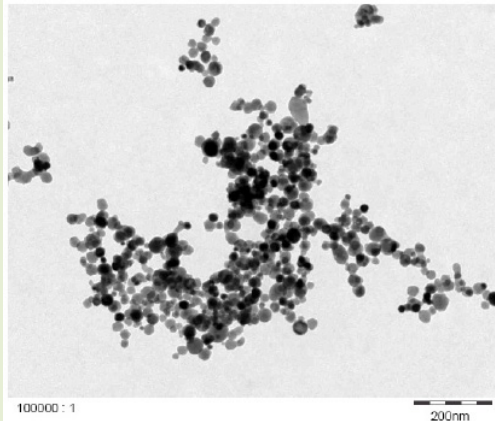
**Stabilisation**

**Solubility in water**

**Purity/contamination**

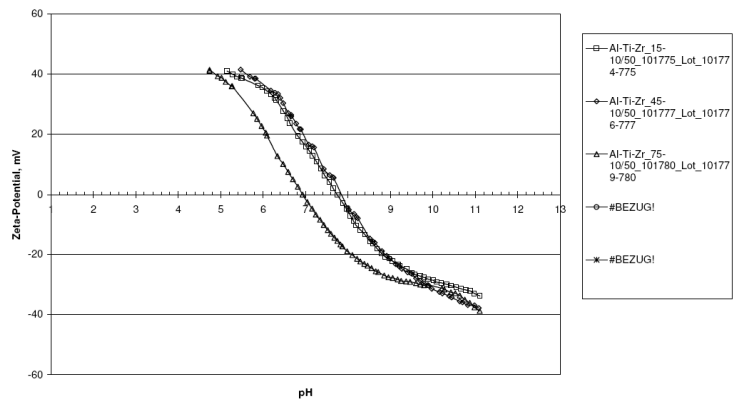
ZrO <sub>2</sub>	68.39 %
Al <sub>2</sub> O <sub>3</sub>	18.51 %
TiO <sub>2</sub>	12.76 %

REM/TEM



Zeta-Potential 1. Titration mit 5m NaOH auf pH 11

Zeta potential



46.4 mV at pH 4.7

Zeta potential  
Surface area chemistry

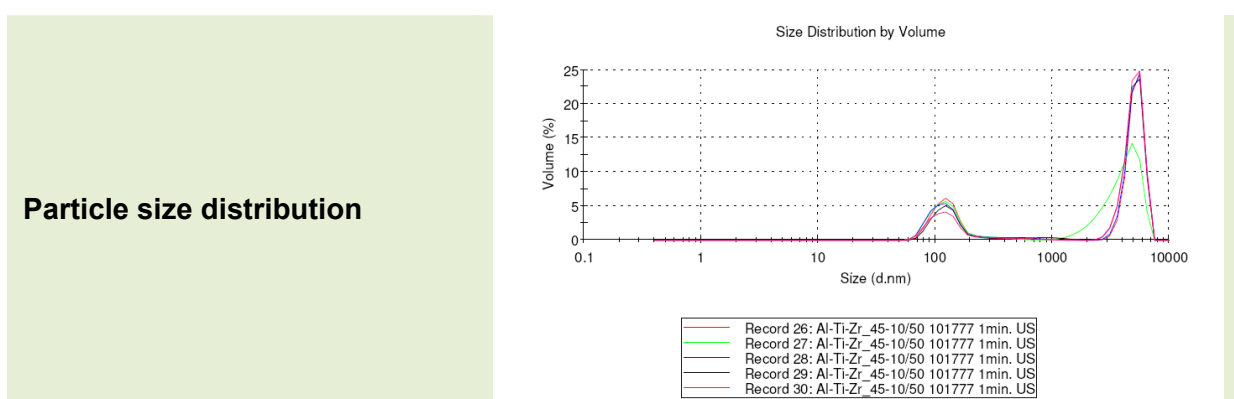
**Material** Al-Ti-Zr\_45-10/50

**Charge description/  
NanoCare Product number** CH-000257  
7.2

**Provide** Evonik Degussa GmbH

**Available form** Powder

**Primary particle size [d<sub>50</sub> in nm]** 34.7 nm



**pH** 4.93

**BET Surface area** 45 m<sup>2</sup>/g

**Particle morphology** Crystalline

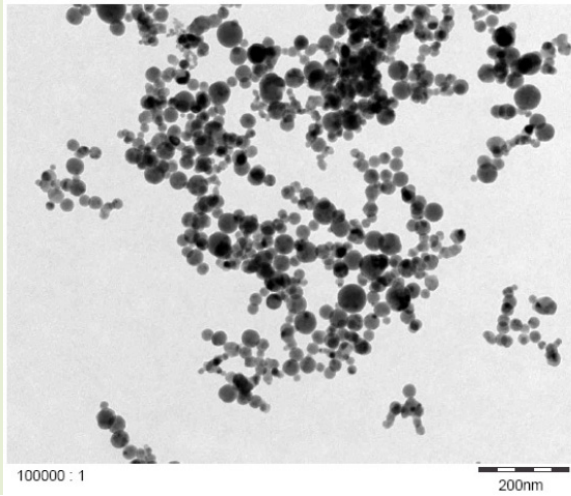
**Crystal phase and crystallinity** Al<sub>0.18</sub>Zr<sub>0.82</sub>O<sub>1.91</sub> Tetragonal  
ZrO<sub>2</sub> Orthorhombic (with changed lattice constant)  
possibly TiO<sub>2</sub> cubic

**Stabilisation**

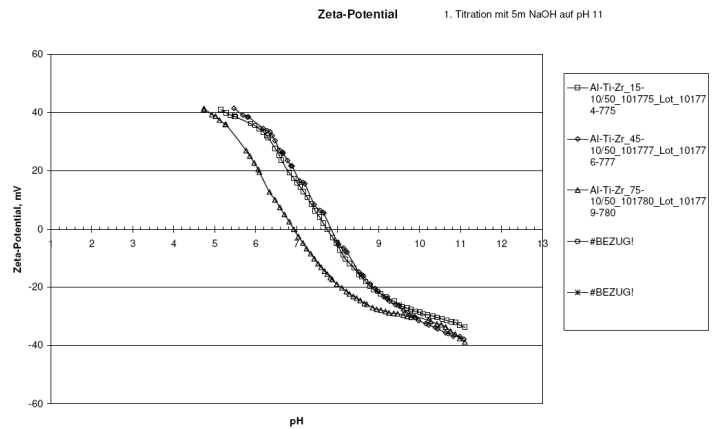
**Solubility in water**

**Purity/contamination** ZrO<sub>2</sub> 40.89 %  
Al<sub>2</sub>O<sub>3</sub> 47.73 %  
TiO<sub>2</sub> 11.19 %

REM/TEM



Zeta potential



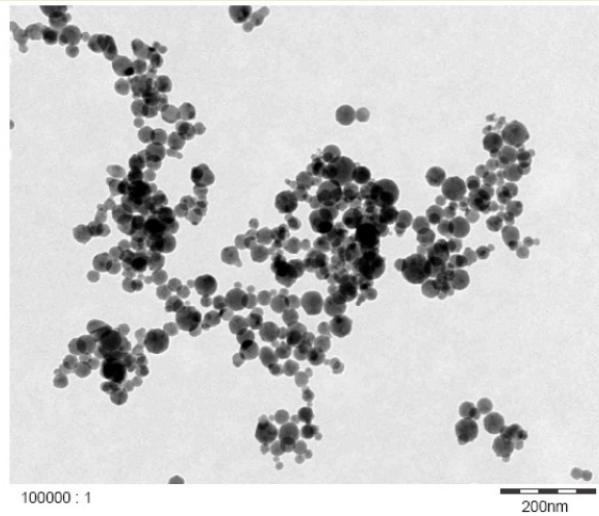
49.1 mV at pH 5.0

Surface area chemistry

**Material** Al-Ti-Zr\_75-10/50

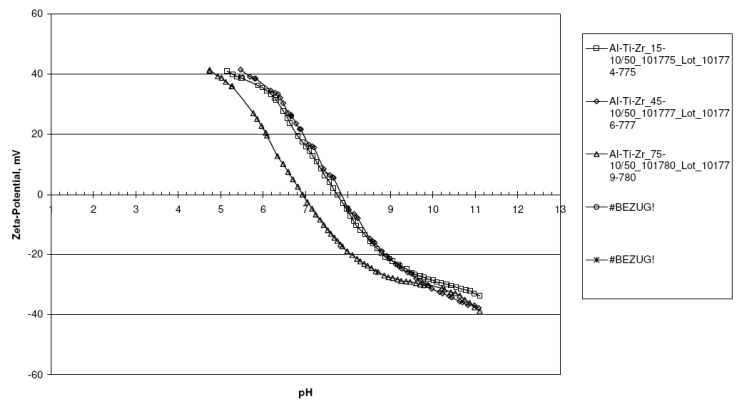
<b>Charge description/ NanoCare Product number</b>	CH-000258 7.3
<b>Provide</b>	Evonik Degussa GmbH
<b>Available form</b>	Powder
<b>Primary particle size [d<sub>50</sub> in nm]</b>	34.7 nm
<b>Particle size distribution</b>	<p>Size Distribution by Volume</p> <p>Volume (%)</p> <p>Size (d.nm)</p> <p>Record 31: Al-Ti-Zr_75-10/50 101780 1min. US          Record 32: Al-Ti-Zr_75-10/50 101780 1min. US          Record 33: Al-Ti-Zr_75-10/50 101780 1min. US          Record 34: Al-Ti-Zr_75-10/50 101780 1min. US          Record 35: Al-Ti-Zr_75-10/50 101780 1min. US</p>
<b>pH</b>	4.57
<b>BET Surface area</b>	48 m <sup>2</sup> /g
<b>Particle morphology</b>	Crystalline
<b>Crystal phase and crystallinity</b>	Al <sub>0.18</sub> ZrO <sub>0.82</sub> O <sub>1.91</sub> Tetragonal Al <sub>2</sub> O <sub>3</sub> Cubic
<b>Stabilisation</b>	
<b>Solubility in water</b>	
<b>Purity/contamination</b>	ZrO <sub>2</sub> 12.40% Al <sub>2</sub> O <sub>3</sub> 76.68% TiO <sub>2</sub> 10.82%

REM/TEM



Zeta-Potential 1. Titration mit 5m NaOH auf pH 11

Zeta potential



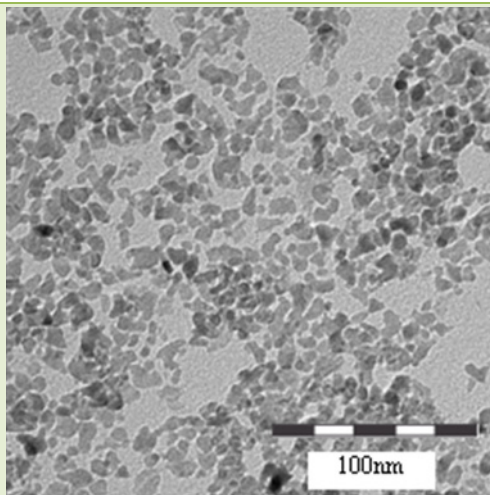
48.8 mV at pH 4.8

Surface area chemistry

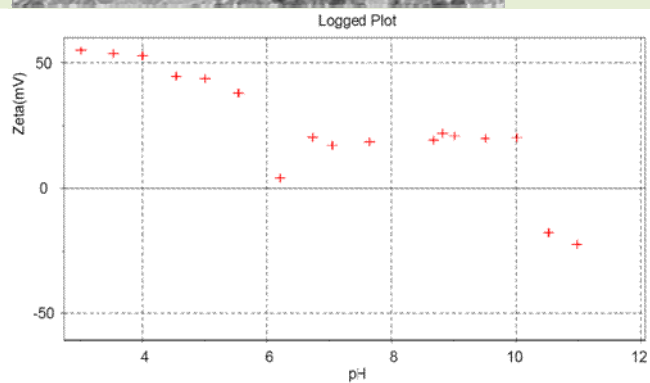
**Material** Zirconium dioxide (ZrO<sub>2</sub>)

<b>Charge description/ NanoCare Product number</b>	CH-000217/421 8.1
<b>Provider</b>	ItN Nanovation AG
<b>Available form</b>	Suspension in water
<b>Primary particle size [d<sub>50</sub> in nm]</b>	36.8 nm
<b>Particle size distribution</b>	<p>The graph displays the particle size distribution of Zirconium dioxide. The x-axis represents particle diameter in nanometers (nm) on a logarithmic scale, and the y-axis represents volume percentage. The distribution is unimodal and centered around 36.8 nm. Key values are d<sub>10</sub>: 12 nm, d<sub>50</sub>: 36.8 nm, and d<sub>90</sub>: 29 nm.</p>
<b>pH</b>	4.06 (in water)
<b>BET Surface area</b>	122 m <sup>2</sup> /g
<b>Particle morphology</b>	Irregular spherical
<b>Crystal phase and crystallinity</b>	Mixed phase monocline (75%)/ tetragonal (25%)
<b>Stabilisation</b>	Organic Polyoxa-acid
<b>Solubility in water</b>	190 ppm (according to SOP)
<b>Purity/contamination</b>	O 60 % Zr 37 % Cl 3 %

**REM/TEM**



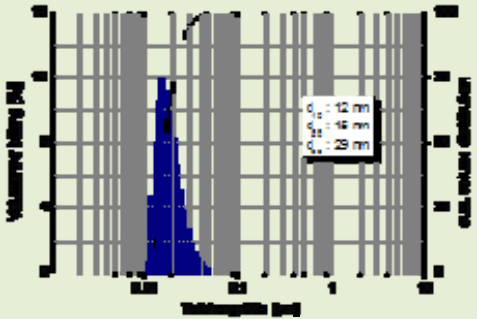
**Zeta potential  
(in water)**



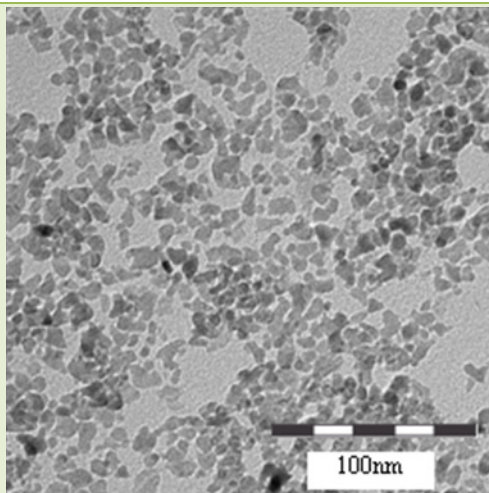
**Surface area chemistry**

O	55 %
Zr	21 %
C	24 %
Cl	0.6 %

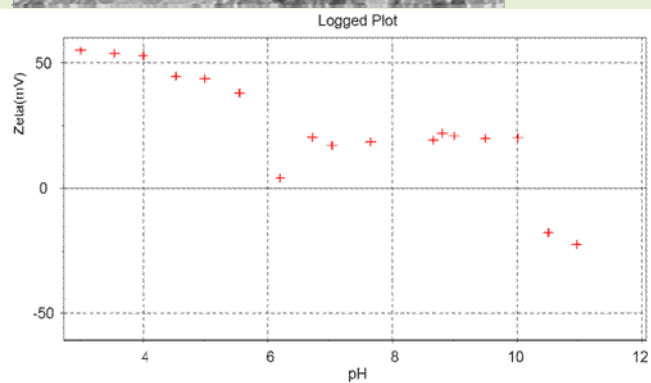
**Material** **Zirconium dioxide (ZrO<sub>2</sub>)**

<b>Charge description/ NanoCare Product number</b>	CH-000218 8.2						
<b>Provider</b>	ItN Nanovation AG						
<b>Available form</b>	Suspension in water						
<b>Primary particle size [d<sub>50</sub> in nm]</b>	31.0 nm						
<b>Particle size distribution</b>							
<b>pH</b>	3.68 (in water)						
<b>BET Surface area</b>	122 m <sup>2</sup> /g						
<b>Particle morphology</b>	irregular spherical						
<b>Crystal phase and crystallinity</b>	mixed phase monocline (75%)/ tetragonal (25%)						
<b>Stabilisation</b>	Acetic acid						
<b>Solubility in water</b>	190 ppm						
<b>Purity/contamination</b>	<table border="0"> <tr> <td>O</td> <td>60 %</td> </tr> <tr> <td>Zr</td> <td>37 %</td> </tr> <tr> <td>Cl</td> <td>3 %</td> </tr> </table>	O	60 %	Zr	37 %	Cl	3 %
O	60 %						
Zr	37 %						
Cl	3 %						

**REM/TEM**



**Zeta potential  
(in water)**

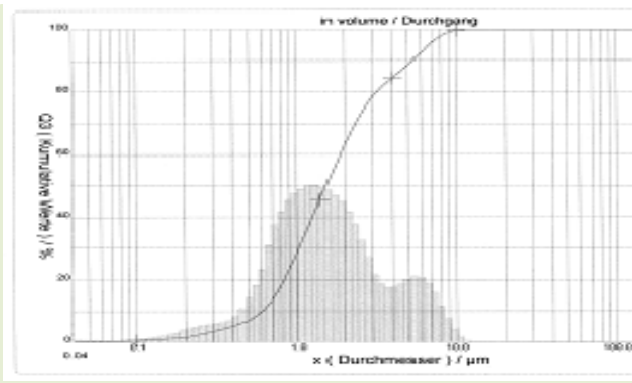
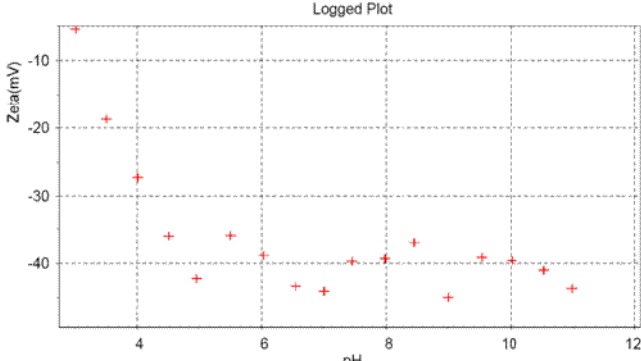


**Surface area chemistry**

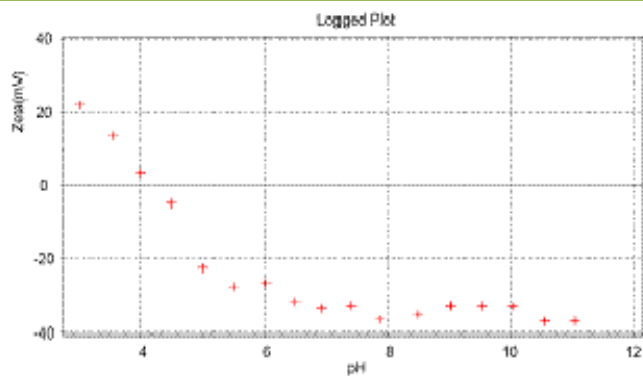
O	55 %
Zr	21 %
C	24 %
Cl	0.6 %

## Material

## Zirconium dioxide (ZrO<sub>2</sub>)

<b>Charge description/ NanoCare Product number</b>	CH-000216 8.3
<b>Provider</b>	ItN Nanovation AG
<b>Available form</b>	Suspension in water
<b>Primary particle size [d<sub>50</sub> in nm]</b>	460.7 nm
<b>Particle size distribution</b>	
<b>pH</b>	9.45 (in water)
<b>BET Surface area</b>	96 m <sup>2</sup> /g
<b>Particle morphology</b>	Irregular spherical
<b>Crystal phase and crystallinity</b>	Mixed phase monocline (75%)/ tetragonal (25%)
<b>Stabilisation</b>	Ammoniumpolyacrylate
<b>Solubility in water</b>	190 ppm
<b>Purity/contamination</b>	O 60 % Zr 37 % Cl 3 %
<b>REM/TEM</b>	
<b>Zeta potential (in water)</b>	

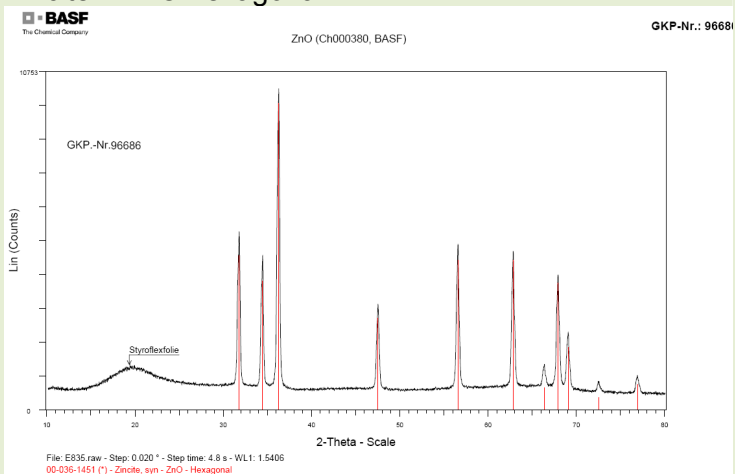
**Zeta potential  
(in DMEM + FCS)**



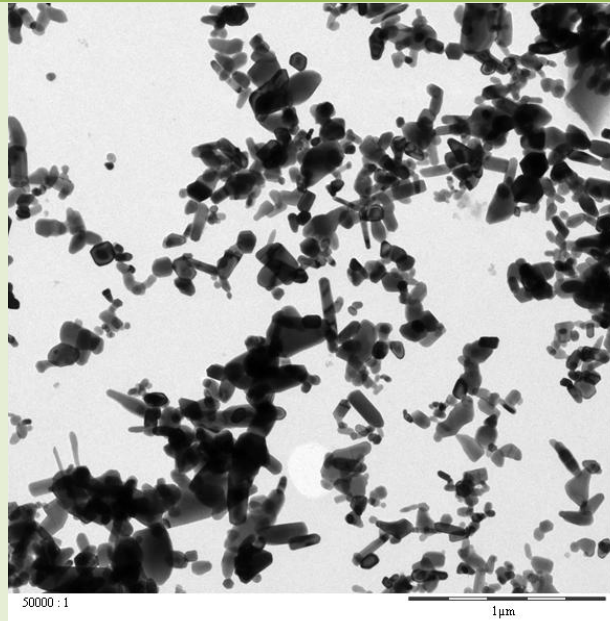
**Surface area chemistry**

O	48 %
Zr	21 %
C	18 %
N	12%
Cl	0.6 %

**Material** Zinc oxide (ZnO)

<b>Charge description/ NanoCare Product number</b>	CH-000380 9
<b>Provider</b>	BASF SE
<b>Available form</b>	Powder
<b>Primary particle size [d<sub>50</sub> in nm]</b>	150 nm
<b>Particle size distribution</b>	20 to 400 nm, see TEM
<b>pH</b>	n/a (Powder)
<b>BET Surface area</b>	
<b>Particle morphology</b>	Nearly isometric, rod and needle like particles
<b>Crystal phase and crystallinity</b>	<p>Zincite – ZnO hexagonal</p>  <p>File: E835.raw - Step: 0.020 ° - Step time: 4.8 s - WL: 1.5406 00-036-1451 (*) - Zincite, syn - ZnO - Hexagonal</p>
<b>Stabilisation</b>	No
<b>Solubility in water</b>	3 ppm // in DMEM/FCS: 37 ppm
<b>Purity/contamination</b>	Protocol: Initial concentration 10 mg/ml, 24h agitation at 900 rpm; centrifugation and supernatant analysis by ICP-MS Impurities of C and Cl in %-level on the surface, see XPS below; Purity of material 99% see XRD above.

REM/TEM



Zeta potential

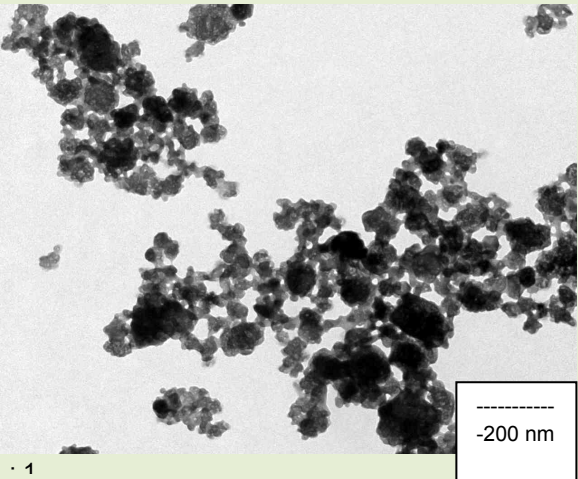
XPS-results:  
Impurities of C and Cl in %-level on the surface

Surface area chemistry

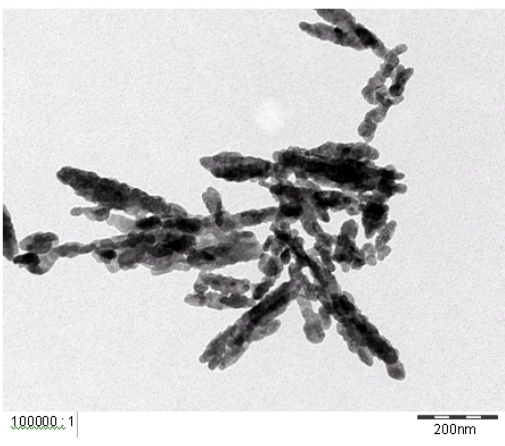
Probe	Nr.	Bez.	C			Cl			Na			O			Zn		
Element		GKP 96686															
Interpretation/				CH,	C-O	O=C-								ZnO	org.	ZnO	
Literaturwerte				CC	O												
Core level [eV]				284,8	+1,5	+4,3								530,5	532,3	1022,3	
Auger [eV]																988,3	
	2	ZnO (Ch000380, BASF)	20,7	0,5	16	2	2	3,4	0,2	3,1	0,2	39,0	0,2	34	4	34,8	0,0

Die Angaben sind in at%  
- Signal nicht nachweisbar  
Die Fehlerangaben geben die laterale Heterogenität von zwei Messstellen wieder

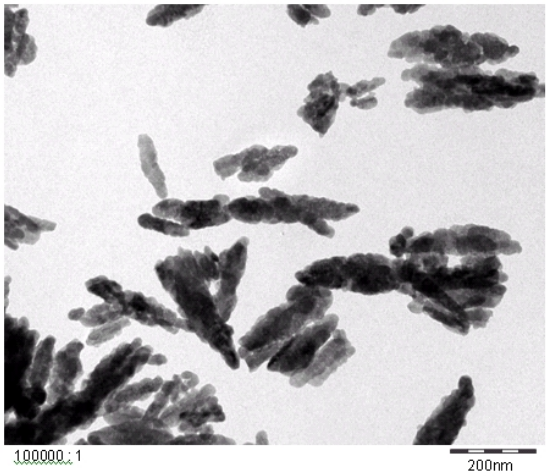
**Material** **Barium sulphate (BaSO<sub>4</sub>)**

<b>NanoCare Product number</b>	10
<b>Charge description</b>	CH-000090
<b>Provider</b>	Solvay Infra Bad Hönningen GmbH
<b>Available form</b>	Powder
<b>Primary particle size (XRD)</b>	37.5 nm
<b>Particle size distribution (Laser diffraction)</b>	d <sub>90</sub> = 35 µm    d <sub>50</sub> =17 µm
<b>pH in water (10 % solids)</b>	9.7
<b>BET Surface area</b>	41.4 m <sup>2</sup> /g
<b>Particle morphology</b>	Spherical primary particles, strongly agglomerated
<b>Crystal phase and crystallinity</b>	Crystalline, orthorhombic, like Baryt
<b>Stabilisation</b>	Organically modified
<b>Solubility in water (NanoCare Method)</b>	6 mg Ba-Ion per litre
<b>Purity/contamination</b>	93.8 % Remaining fraction: Water and org. additive
<b>Microscopy (TEM)</b>	
<b>Zeta potential: 15 % suspension in water</b>	- 33 mV      isoelectric point at pH 4
<b>Surface area chemistry (XPS)</b>	Ba 12.7 At% S 10.8 At% O 51.7 At% C 17.2 At%

## Material Strontium carbonate (SrCO<sub>3</sub>)

<b>NanoCare Product number</b>	11.1
<b>Charge description</b>	CH-000438
<b>Provider</b>	Solvay Infra Bad Hönningen GmbH
<b>Available form</b>	Powder (hydrophilic)
<b>Primary particle size (XRD)</b>	18.5 nm
<b>Particle size distribution (Laser diffraction)</b>	d <sub>90</sub> = 23.7 µm    d <sub>50</sub> = 5.9 µm
<b>pH in water (10 % solids)</b>	7.8
<b>BET Surface area</b>	33 m <sup>2</sup> /g
<b>Particle morphology</b>	rod like primary particles strongly agglomerated
<b>Crystal phase and crystallinity</b>	Crystalline, orthorhombic, like Strontianit
<b>Stabilisation</b>	organically modified, hydrophilic
<b>Solubility in water (NanoCare method)</b>	28 mg Sr-Ion per litre
<b>Purity/contamination</b>	96.4 % Remaining fraction: Water and org. additive
<b>Microscopy (TEM)</b>	
<b>Zeta potential: 15 % suspension in water</b>	- 10 mV                      isoelectric point < pH 7
<b>Surface area chemistry (XPS)</b>	Sr 21.1 At% C 27.1 At% O 51.3 At%

**Material** **Strontium carbonate (SrCO<sub>3</sub>)**

<b>NanoCare Product number</b>	11.2
<b>Charge description</b>	CH-000439
<b>Provider</b>	Solvay Infra Bad Hönningen GmbH
<b>Available form</b>	Powder (hydrophobic)
<b>Primary particle size (XRD)</b>	17 nm
<b>Particle size distribution (Laser diffraction)</b>	d <sub>90</sub> = 18.6 µm    d <sub>50</sub> = 5.9 µm
<b>pH in water (10 % solids)</b>	7.6
<b>BET Surface area</b>	8.9 m <sup>2</sup> /g
<b>Particle morphology</b>	rod like primary particles strongly agglomerated
<b>Crystal phase and crystallinity</b>	Crystalline, orthorhombic, like Strontianit
<b>Stabilisation</b>	Organically modified, hydrophobic
<b>Solubility in water (NanoCare method)</b>	53 mg Sr-Ion per litre
<b>Purity/contamination</b>	85 % Remaining: Water and org. additive
<b>Microscopy (TEM)</b>	
<b>Zeta potential in 15 % suspension in water</b>	- 66 mV      isoelectric point < 7 pH
<b>Surface area chemistry (XPS)</b>	Sr 11.7 At% C 50.6 At% O 37.0 At% P 0.7 At%



**ISBN: 978-3-89746-108-6**